Simulation-based optimization of solar thermal systems

Dissertation zur Erlangung des akademischen Grades
Doktor der Ingenieurwissenschaften (Dr. -Ing.)

Vorgelegt im Fachbereich Maschinenbau
der Universität Kassel von

Oleh Kusyy

Kassel 2017

Die vorliegende Arbeit wurde vom Fachbereich Maschinenbau der Universität Kassel als Dissertation zur Erlangung des akademischen Grades eines Doktors der Ingenieurwissenschaften (Dr.-Ing.) angenommen. Die Forschungsarbeiten erfolgten am Fachgebiet Solar- und Anlagentechnik, Institut für Thermische Energietechnik.

Erstgutachter: Prof. Dr. Klaus Vajen, Universität Kassel

Zweitgutachter: Prof. Dr. Wolfgang Streicher, Universität Innsbruck

Tag der mündlichen Prüfung: 10. November 2017

Abstract

In this PhD thesis application of numerical methods to simulation-based optimization of solar thermal systems both in the planning process and in operation is investigated. The optimization process starting from definition of a target function and specification of optimization parameters, moving forward with application of an optimization algorithm and ending up by sensitivity analysis at the found optimum, is described in detail. A hybrid genetic CHC – binary search algorithm is proposed and applied. As a combination of reliable global genetic algorithm with fast local binary search, the hybrid algorithm is computationally efficient, especially due to good parallelization, and reliable in finding the global optimum. Application of the algorithm to design optimization of the solar heating combisystem shows optimization potential of around 13% in terms of solar energy costs or 19 percent points in terms of extended fractional energy savings when compared to the system configuration planned by the experts. Pareto front is built showing the optimal solar energy costs for desired energy savings of the system, or vice versa. Influence of variation of domestic hot water and space heating demand as well as geographical location on Pareto front and optimal combisystem configuration is investigated. To determine the most important parameters and quantify their influence on the solar energy costs function, three methods of the global sensitivity analysis: multiple linear regression, Morris method and extended Fourier amplitude sensitivity test are applied in two parameter spaces around the optimum.

To overcome dimensionality problem when optimizing solar heating system in operation, splitting long year optimization into many short ones is proposed and applied to optimization of flow rates on hourly basis. Only negligible potential of 0.3 per cent points in terms of extended fractional energy savings is determined. A significant potential is shown in another way for dynamic optimization of the auxiliary heater control settings.

In the last part of the thesis a control-based anti-stagnation approach consisting of induced inefficient daily collector operation and nightly cooling is proposed and theoretically investigated. Minimal specific store volume required for stagnation-free operation of the solar heating system is calculated for ten sunniest days in a row without heat consumption. Influence of location, collector thermal loss coefficient, solar radiation, day and night ambient temperature is analysed. Practical implementation of the approach reduces the excess thermal energy by 33% during the induced inefficient collector operation compared to the usual control strategy.

Zusammenfassung

In Rahmen dieser Dissertation wurde Anwendung numerischer Methoden auf simulationsbasierte Planung- sowie Betriebsoptimierung solarthermischer Anlagen untersucht. Der detailliert beschriebene Optimierungsprozess beinhaltet die Definition der Zielfunktion, die Auswahl zu optimierender Parameter und des Optimierungsalgorithmus sowie die Methoden zur Sensitivitätsanalyse in der Umgebung des Optimums. Für solarthermische Anlagen wurde ein hybride Algorithmus, bestehend aus einem genetischen CHC und einem binären Suchalgorithmus, vorgeschlagen und angewendet. Der hybride Algorithmus ist sehr effizient hinsichtlich des Rechenaufwands besonders aufgrund guter Parallelisierungseigenschaften und zuverlässig bei der Identifizierung eines globalen Optimums. Die Anwendung des Algorithmus auf die Planungsoptimierung solarer Kombianlagen zeigt ein Optimierungspotenzial von 13% niedrigere Gestehungskosten solarer Wärme bei gleicher solarer Deckungsrate ($f_{sav,ext}$) oder 19 Prozentpunkte höhere solare Deckungsrate ($f_{sav,ext}$) bei gleichen Wärmegestehungskosten. Weiterhin wurde eine Pareto Front ermittelt, die die niedrigsten solaren Wärmegestehungskosten für eine gewünschte solare Deckungsrate zeigt und vice versa. Um die Stabilität der optimalen Systemkonfiguration zu bewerten, wurden Warmwasserverbrauch, Raumheizung und Standort variiert und ihr Einfluss auf die optimale Systemkonfiguration und das Optimierungspotential untersucht. Darüber hinaus wurden Methoden globaler Sensitivitätsanalyse herangezogen, um die einflussreichsten Parameter in der Umgebung des Optimums zu identifizieren und deren Einfluss zu quantifizieren.

Betriebsoptimierung solarer Kombianlagen zu jeder Stunde des Jahres wurde ermöglicht durch eine Teilung der jährlichen Optimierung in mehrere kürzere Dauer. Es wurde festgestellt, dass durch die optimalen Massenströme in einer Solaranlage eine vernachlässigbare Verbesserung von 0.3 Prozentpunkten für solare Deckungsrate erreicht werden kann. Dynamische Optimierung von Reglereinstellungen der Nachheizung zeigt hingegen wesentlich höheres Optimierungspotenzial.

Abschließend wurde eine Methode zur regelungsbasierten Vermeidung von Stagnation in solaren Kombianlagen entwickelt. Diese Methode beinhaltet eine Reduktion der Überschusswärme durch einen bewusst verschlechterten Kollektorbetrieb tagsüber und eine Nachtsauskühlung des Speichers. Für zehn sonnenreichste Tage in Reihe ohne Wärmeabnahme wurde das minimale spezifische Speichervolumen bestimmt, der für einen stillstandsicheren Betrieb mit der entwickelten Betriebsmethodik benötigt wird. Weiterhin wurde der Einfluss von dem Standort, der Kollektoreigenschaften, der solaren Einstrahlung und den Umgebungstemperaturen ermittelt. Praktische Anwendung der Methode zeigt, dass im Vergleich zu einer üblichen ΔT Regelung durch den bewussten ineffizienten Kollektorbetrieb der Eintrag von Überschusswärme in den Speicher um 33% reduziert werden konnte.

Contents

1. Introduction

1.1. Background and motivation

It is obvious that the energy is crucial for the mankind. Evolution of human beings implies not only evolution of capabilities but also evolution of needs which enable and facilitate their lives. With industrial progress human needs evolved tremendously and increased the energy consumption. As I was finishing my school in Ukraine in the middle of 90-th my mother bought me a personal computer and I was the only one in my class who had a computer. Now, only two decades later, it is hard to imagine.

Growing consumption of energy mostly supplied by fossil fuels causes environmental problems with unpredictable consequences. Since it is not likely to reduce human needs, the technologies come enabling efficient use of clean renewable energy and in this way reducing environmental impact. However, existence of even the best renewable technology does not necessarily mean its good dissemination. Especially for those who do not have “saving environment” high on their priority list, the new renewable technology must be not only efficient and affordable but also profitable to gain their acceptance. Although the environmental awareness is a key factor and it is encouraging that more and more private households behave accordingly, the governmental incentives are being developed and implemented in Germany and other countries in order to facilitate dissemination by making renewable technologies more attractive. It is especially important in times when fossil fuels prices are low.

Having the main focus on numerical optimization of solar thermal combisystems designed for preparing domestic hot water and space heating in households, this thesis makes an attempt to contribute to better dissemination of solar thermal technology. Since operation of a solar thermal combisystem consisting of many components connected together, is not simple, dynamic system simulations are often required to investigate the system behaviour. Proper dimensioning of the system components as well as efficient controller settings depend on changing boundary conditions as weather, domestic hot water and space heating demand. In addition to energetic performance, the dimensioning of combisystem must be justified economically. All this makes finding the combisystem configuration optimally designed in terms of lowest solar energy costs for a given location and demand rather challenging.

1.2. Objectives and outline

Three main objectives are formulated and pursued within this study:

1. Estimation of potential of design optimization of solar heating combisystems with numerical algorithms. How sensitive is the obtained optimum to changes of boundary conditions or optimized parameters themselves?
2. Development of an approach for estimating potential of optimization of the combisystem in operation
3. Development of the control based approach to avoid stagnation in solar combisystems

As it is seen from the objectives, the focus of this thesis is on methodology development and application. The present study is based on earlier research conducted by Michael Krause at University of Kassel and described in his thesis (Krause, 2003). However, the method applied for design optimization of the solar combisystem as well as those for sensitivity estimations are different. Different approach is also developed and applied to optimization of the flow rates in operation.

Numerical model of the solar heating combisystem already developed for the TRNSYS simulation environment (Klein at al., 2009) in the framework of the IEA Task 32 is used throughout the thesis.

The thesis is structured as follows.

In Chapter 2 the investigated combisystem is presented and described in detail together with the boundary conditions and performance indicators, following the IEA Task 32 report (Heimrath and Haller, 2007).

Chapter 3 gives a brief overview of optimization methods, their strong and weak sides. Structure and general scheme of genetic algorithm are described in more detail. Three global sensitivity methods are introduced here as well.

In Chapter 4, an optimization problem is formulated for design optimization of the IEA Task 32 solar thermal combisystem and a hybrid CHC – binary search algorithm is proposed and applied for its solving. Pareto front between solar energy costs and extended fractional savings of the combisystem is built basing on results of several optimization runs. Influence of boundary conditions as weather (geographic location of the combisystem), domestic hot water and space heating demand on both the optimal combisystem configurations and Pareto front itself, is shown and analysed. In the second part of the chapter, introduced sensitivity

analysis methods are applied in the space around the optimum point to investigate influence of single optimization parameters and two boundary conditions on the solar energy costs. Special attention is paid to computational aspects such as parallelisation potential of the methods. Convergence and reliability are addressed as well.

In Chapter 5 a method is proposed enabling time-consuming hourly optimization of the combisystem. It is based on an idea of separation of the whole year optimization into many short ones. The presented method is applied to the estimation of potential of dynamic flow rate optimization. Potential of the dynamic optimization of the boiler controller settings is estimated in different way, by replacing the boiler heating up the auxiliary part of the store by two electrical instant heaters placed in domestic hot water and space heating loops.

In Chapter 6 a control-based anti-stagnation approach is proposed and theoretically investigated consisting of inefficient daily collector operation and nightly cooling of the store. Minimal specific store volume is determined which is required for stagnation-free operation of the solar thermal system during ten modelled sunniest days in a raw without heat consumption. Influence of the boundary conditions such as solar radiation, collector heat loss coefficient, ambient day and night temperatures, night cooling duration, on the minimal specific store volume is theoretically estimated. Difficulties in practical implementation of the inefficient daily collector operation, possible solution and results from field tests are addressed as well.

In Chapter 7 the results of the thesis are summarized and limitations are discussed.

2. Description of investigated reference solar thermal combisystem

In this Chapter the reference solar thermal combisystem investigated throughout the thesis is briefly described following (Heimrath and Haller, 2007). The reference combisystem was proposed within a framework of the IEA Task 32 project. The reference conditions and reference simulation environment were defined for simulation of solar thermal comibsystems intended for domestic hot water preparation and heating of the building. Figure 2.1 shows simplified schematics of the solar heating combisystem consisting of water storage tank, solar collector, auxiliary heater, two external heat exchangers, pumps, etc.

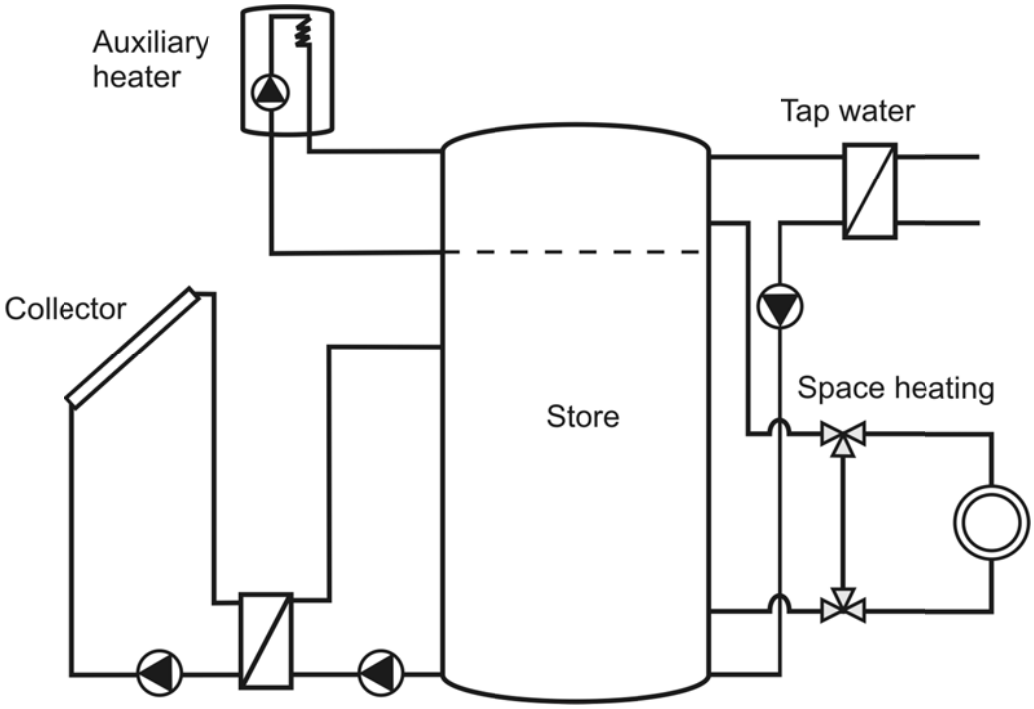

Figure 2.1: *Schematics of reference solar combisystem with auxiliary heating loop*

A numerical model of the combisystem was built in the TRNSYS (Transient System Simulation Tool) simulation program allowing user to perform numerical simulations on the system under various boundary conditions. Each component of the system modelled in TRNSYS (so-called Type) is a mathematical model of a real component, consisting of mathematical equations describing its physical behaviour. In the following section, main components of the IEA Task 32 reference combisystem are described in more details.

2.1. Main components of IEA Task 32 combisystem

2.1.1. Storage

As the solar insulation profile usually does not match the load profile, in solar thermal applications a short-term or seasonal thermal storage tank is needed to store the energy delivered from solar collector. In the Task 32 combisystem the storage tank filled with water as a store medium is the central component. It is modelled by Type 340 "Multiport store model for TRNSYS" developed by Drück (Drück, 2006) the present version of which describes a stratified fluid storage tank with up to four immersed heat exchangers, an internal electrical auxiliary heater and a maximum of ten double ports (inlet/outlet couples) used for direct charge or discharge of the storage. Up to five temperature sensors can be implemented for control purpose.

There are four loops attached to the storage tank in the Task 32 combisystem. Since the working fluid in the collector loop is a mixture of water and antifreeze, solar collector loop charges the storage tank via a heat exchanger, external in our case. Charging by auxiliary heater (boiler) is done directly through one of the double ports. On the consumption side the storage tank is directly attached to the space heating loop of the building using the water of the space heating as a store medium. The domestic hot water preparation loop discharges the store via fresh water station.

None of the heat exchangers immersed into the storage tank is used in the Task 32 combisystem; the store is charged and discharged via the double ports (or external heat exchangers and double ports) only. A study conducted at University of Kassel shows only a little benefit of charging and discharging the store via internal heat exchangers comparing to the external ones (Zass et al., 2007).

The stratified storage tank is modelled by N_{max} completely mixed segments (nodes) of equal volume. The higher N_{max}, the better the stratification of the store can be modelled. $N_{max} = 1$ represents a fully mixed store. If for a double port the stratified charging is chosen then the water enters the store at the node with the temperature closest to the inlet temperature. Otherwise the inlet positions are fixed and the incoming water is mixed up with the water in the respective node of the store.

Temperatures of the nodes are calculated by solving the system of differential equations. For each node of the store the energy balance equation is written, describing the change of its internal energy with the time as the sum of heat transfer

caused by mass flows, heat transfer between the internal heat exchanger and the node, conductivity with the neighbour nodes and the heat loss to the ambient.

The equation system is solved numerically in an iterative manner. The accuracy is specified explicitly and the higher it is, the more iterations and calculation time is required for the equation system to converge.

The energy balance of the whole store is calculated for each time step and the error is summed up and printed out at the end of the simulation. The high error values might indicate the convergence problems during simulation.

Heat loss capacity rate from the store to the ambient can be separately specified for the bottom and top of the tank as well as for up to four different zones of the store mantle. A correction factor is introduced (Heimrath, 2004) dependent on the store volume to describe the imperfect insulation.

Auxiliary heated volume inside the store is fixed to 200 liters.

In Chapter 4, several store parameters are subject to optimization. They are the store volume, auxiliary heated volume, thickness of the insulation, positions of the double ports (if not stratified), position of the temperature sensor used for the collector pump control.

2.1.2. Collector loop

On days with high solar insolation, the working fluid in the solar collector usually warms up enough to be able to charge the store via the collector loop consisting of solar thermal collector, external heat exchanger, collector pipes, pumps and controller.

For simulation of the solar collector, the model (Type 832) developed by Perers and Bales is used. It is a dynamical model which accounts for beam and diffuse solar radiation, heat losses to the ambient and effective thermal capacitance of the collector. Most collectors can be described by this model. For more information on the model refer to (Perers and Bales, 2002)

Three reference collector types are defined in the IEA Task 32 with parameters summarized in Table 2.1.

Table 2.1: *Reference collector parameters. Source: (Heimrath and Haller, 2007)*

Collector	η_0, -	a_1, W/m^2K	a_2, W/m^2K^2	C_p, J/m^2K	K_d, -	b_0, -	Optical mode
Flat-plate, selective	0.80	3.50	0.015	7000	0.90	0.18	1
Flat-plate, nonselective	0.75	5.46	0.021	7000	0.88	0.18	1
Evacuated tube	0.77	1.09	0.009	44400	0.95		4

For calculation of the incident angle modifier (IAM) for the flat plate collectors the parameter b_0 is used (optical mode 1). For the evacuated tube collector the IAM is calculated with use of an external data table (optical mode 4).

The counter flow external heat exchanger (Type 5) separates the collector loop with mixture of the polypropylene and water as the working fluid from the water used as the medium in the storage tank. On the primary side the heat exchanger is connected to the collector pipes and on the secondary side directly to the double port of the store. The UA-value of the collector heat exchanger is calculated dependent on the collector area using an equation from (Heimrath 2004):

$$UAHX_c = 88.561 * A_{col} + 328.19, [W/K] \quad (2.1)$$

In Chapter 4 the optimal UA-value of the collector heat exchanger is found for the specific combisystem.

The specific flow rate on the primary side of the heat exchanger is set by the user. On the secondary side it is calculated from the equality of the capacitance flow rates on the primary and secondary sides as

$$\dot{m}_{sec} = \dot{m}_{pri} * C_{bri} / C_{wat}, [kg/h] \quad (2.2)$$

The heat losses are not taken into account by the heat exchanger model. To simulate the heat losses in the collector loop, two 15 meter long copper pipes are introduced connecting the heat exchanger with the solar collector. Diameter of the pipes and their insulation are calculated based on the flow rate so that the velocity of the fluid in the pipe is about $0.6\,m/s$. Pipe diameter and flow rate are optimized independently in Chapter 4.

Primary and secondary pumps in the collector loop are controlled by a Type 2 hysteresis ΔT controller. The pumps are turned on by the controller when the difference between readings of the temperature sensors mounted at the collector output and at the bottom of the tank exceeds the upper dead band setting of the

controller and switched off when this difference becomes smaller than the lower dead band. Another two controller rules are implemented to prevent overheating in the collector loop in case of collector stagnation and to protect the storage tank. The primary and secondary pumps are switched off when either threshold fluid temperature of $110\,℃$ at the collector output is reached or the temperature sensor at the top of the storage tank shows the temperature higher than $95\,℃$. The pumps are turned on again only after the above temperatures fall $15\,K$ and $5\,K$ below the corresponding threshold values, respectively. All the control preferences can be easily changed by the user. The lower and upper dead bands of the ΔT hysteresis controller are optimized in Chapter 4.

2.1.3. Auxiliary loop

When there is not enough thermal energy delivered by collector to fully cover the consumption needs, the conventional auxiliary boiler turns on and charges the auxiliary volume in the top of the store to fill the gap. In Task 32 combisystem the auxiliary boiler is modelled by Type 370. To control the boiler a separate auxiliary controller is introduced. It starts the boiler whenever the auxiliary temperature sensor shows 8°C below the auxiliary set temperature $T_{\mathrm{aux,set}}$ and runs it until the temperature $T_{\mathrm{aux,set}} + 2°\mathrm{C}$ is reached. The auxiliary boiler is connected with the storage tank by a 10 meter long pipe which helps to avoid some instability problems in simulation. Heat losses in the pipe are calculated with respect to the constant ambient temperature of $15\,℃$. The boiler set temperature, lower and upper dead bands of the auxiliary controller are to be optimized in Chapter 4.

2.1.4. DHW preparation loop and load profile

Hot water stored in the storage tank is used both for the domestic hot water preparation and for the space heating. The yearly profile for the domestic hot water demand with a 6 minute time resolution is constructed using the DHWcalc tool developed by Jordan (Jordan and Vajen, 2005). According to the profile, the consumption of the domestic hot water is stochastically distributed over the days having main loads in the morning and late afternoon. Daily hot water demand for a single family house is supposed to be $200\,l/d$ and for a multi-family house – $1000\,l/d$.

Preparation of the domestic hot water in Task 32 combysystem is performed via the external heat exchanger Type 805 which delivers the required amount of hot water

to the user, according to the consumption profile. When the consumption occurs, the flow rate in the primary loop is adjusted in the way that the specified set temperature $45\,℃$ is held constant on the exit of the heat exchanger. Temperature of the cold water coming into the heat exchanger varies on a seasonal basis as a sinus curve with an average value at $11\,℃$ and amplitude of $5\,℃$. If the domestic hot water demand cannot be fully covered by the combisystem on specific days, then the penalties are applied. Similarly as in collector loop, a 15 meter long pipe is introduced to account for the heat losses. Overall heat transfer coefficient of the DHW heat exchanger is set to $5333\,W/K$ and subject to optimization in Chapter 4. Influence of the DHW consumption on the optimum of the solar combisystem is investigated there as well.

2.1.5. Space heating loop

Heating of the building is provided by the space heating loop with the radiator Type 362 simulating the room radiators. Before entering the radiator, the hot water which comes from the store is mixed up in the mixing valve with the cold water returning from the radiator to achieve the required temperature. The flow rate in the radiator is determined by the PID controller keeping the air temperature inside the building over the set temperature of $19.5\,℃$. At the time steps at which the air temperature inside the building drops below $19.5\,℃$, a numerical penalty is applied.

2.2. Reference climates and buildings

The weather conditions are the most sensitive input data for simulation of solar heating systems, that is why careful preparation of the climate data is required. For simulation of the Task 32 combisystem the locations of Stockholm, Zurich and Madrid are chosen representing a wider range of the European climates. The weather data profiles of statistical meteorological years for these locations are generated based on the commercial database Meteonorm (Meteotest, 2016).

For simulation of the building, a two-storey free standing single family house with the effective floor area of $70\,m^2$ per store, and glazed area mostly on the south façade ($12\,m^2$, 25% of the south façade) is chosen. The building is simulated as a single thermal zone. For more detailed information on wall and windows construction elements as well as on internal gains, ventilation, electricity consumption, thermal comfort, etc., refer to (Heimrath and Haller, 2007).

Three building types with the same architectural design but different wall insulation and window thermal quality resulting in different heating loads (30, 60 and 100 kWh/m^2a for Zurich climatic conditions) are defined within Task 32 and simulated along with the thermal heating system. Influence of the heating demand on the optimum of the solar combisystem is shown in Chapter 4 below.

2.3. Performance indicators

Different indicators are used to measure the performance of the solar thermal heating systems. In the Task 32 reference TRNSYS model the fractional energy savings indicators developed in the previous IEA Task 26 and described in (Streicher and Heimrath, 2002) are used.

The fractional thermal energy savings $f_{sav,therm}$ measures in percentage the reduction of the auxiliary energy input to the heating system due to utilization of the solar energy:

$$f_{sav,therm} = 1 - \frac{Q_{aux}}{Q_{ref}} \tag{2.3}$$

This indicator does not take into account the electricity use. The extended fractional energy savings $f_{sav,ext}$ is defined in a similar way but it also includes the electricity consumption of the system components like pumps, controllers, etc.

$$f_{sav,ext} = 1 - \frac{Q_{aux}/0.85 + W_{el}/0.4}{Q_{ref}/0.85 + W_{el,ref}/0.4} = 1 - \frac{E_{sol}}{E_{ref}} \tag{2.4}$$

As it is possible to reach high $f_{sav,ext}$ and $f_{sav,therm}$ but meanwhile not to meet the comfort criteria for space heating or domestic hot water preparation, another fractional solar savings indicator, f_{si} is introduced in Task 32 reference system. This indicator includes the penalty term $F_{penalty}$ which is added when the evaluated system configuration does not meet the comfort criteria.

$$f_{si} = 1 - \frac{Q_{aux}/0.85 + W_{el}/0.4 + F_{penalty}}{Q_{ref}/0.85 + W_{el,ref}/0.4} = 1 - \frac{E_{sol} + F_{penalty}}{E_{ref}} \tag{2.5}$$

As already mentioned above, the penalty functions are applied when either the required domestic hot water temperature (45 ℃) cannot be supplied or the room temperature drops below the desired set temperature (19.5 ℃). They are defined as follows:

$$F_{penalty} = F_{pen,DHW} + F_{pen,SH}, \quad (2.6)$$

$$F_{pen,DHW} = \dot{m} \cdot c_p \cdot (\Delta T_{DHW} + [\Delta T_{DHW} + 1]^4 - 1)/3600, \text{[kWh]} \quad (2.7)$$

$$F_{pen,SH} = UA \cdot (\Delta T_{SH} + [\Delta T_{SH} + 1]^2 - 1)/1000, \text{[kWh]} \quad (2.8)$$

where $\Delta T_{DHW} = \max(0, 45 - T_{DHW})$, $\Delta T_{SH} = \max(0, 19.5 - T_{air})$ and $UA = 165\ W/K$ is the UA-value of the building.

Since it is not really reasonable to refer to $f_{sav,ext}$ and $f_{sav,therm}$ indicators without satisfying the comfort criteria, the indicators are modified to include the penalty function $F_{penalty}$ so that $f_{sav,ext} = f_{si}$ in simulations below.

2.4. Simulation in TRNSYS environment

A well investigated model of the reference combisystem in form of a TRNSYS input (deck) file ready for simulation by TRNSYS software was created as one of the outcomes of the IEA Task 32. To get accurate simulation results and to avoid convergence errors during the simulation, settings of the simulation environment, in particular, those of the TRNSYS solver, must be properly chosen. In (Heimrath and Haller, 2007) dependency of the simulated performance indicators $f_{sav,therm}$, $f_{sav,ext}$ and f_{si} on simulation time step and tolerance settings (convergence and integration accuracy) is shown. The performance indicators show stronger dependency on tolerance settings for smaller time steps (1 or 2 minutes). To obtain consistent simulation results for Task 32 combisystem it was recommended to use simulation time steps of 2 or 3 minutes and tolerances of 0.002 or 0.003 both for convergence and integration.

The computational time needed for a one-year simulation of the combisystem grows exponentially with simulation time step decreasing. From this reason a larger time step of 6 minutes is used in optimization calculations below. Although the accuracy is slightly worse than for 3 minutes time step, it seems to be a good trade off in sake of computational time. For simulation time step of 6 minutes a one-year simulation takes around 4 minutes on a computer with 2.2 GHz CPU.

In order to facilitate making changes to Task 32 deck file and to follow the connections between system components more easily, a visualized studio version of the text deck file was developed at University of Kassel (Wilhelms et al., 2008). Simulations carried out in this thesis are to much extent facilitated by this version.

3. Introduction to numerical optimization and sensitivity analysis

In this Chapter a brief introduction to the theory of numerical optimization and sensitivity analysis with their application to engineering problems is given.

Despite the first works on optimization theory are dated back to the 18th century, significant development of the most numerical optimization algorithms took place in the second half of the last century and was closely connected with rapid development of computational devices. The problems of calculating optimal trajectories of space rockets, optimal control of robots, traffic jam prediction and finding the best route are only few examples to solving of which the optimization methods have been applied.

Optimization is literally around us. In everyday life we face the problems of the optimal choice: when we buy something we look for the highest quality at moderate price, when we play a game we try to find the best strategy, when we have too much to do we try to plan our time in most efficient way, etc. In all cases we have a plenty of choices and look for the best one.

In general words, task of the optimization theory might be defined as follows: to identify the best solution from a vast collection of alternatives without having to evaluate all of them. To achieve this, an optimization algorithm is needed which performs a clearly defined sequence of logical steps, usually done in an iterative manner, leading, step by step, to the optimal solution being sought. Quality of the algorithm might be seen as a combination of two criteria: reliability with which the optimal solution is found and cost in form of number of evaluations (or computational time) needed for this. These criteria are controversial meaning that the more reliable algorithm most probably needs more system evaluations and, other way around, only a rough estimation of the optimal solution might be possible with only a few evaluations of the target function. In the limiting cases, the most reliable algorithm is to evaluate all possible candidates what is also the most time-consuming or, on the other side, to pick up only one candidate and call it the optimal solution with a reliability of only 1/(number of all candidates). Both efficient and reliable algorithm lies somewhere in between. In practice, reliability of the algorithm is difficult to measure, as the optimal solution is normally not known in advance. It could be benchmarked on a series of test optimization problems

having, for example, analytical solutions. As a result one might say that a particular algorithm is doing well on some target functions and worse on others.

When choosing an appropriate algorithm for a given optimization problem, it is advantageous to know the shape of the target function, optimum of which the algorithm is going to find. More complicated target functions with many parameters might demand more sophisticated algorithms.

3.1. Local and global optimization algorithms. Overview

Assuming that in a chosen parameter space a target function may have not only one optimum point but several local ones, it could be difficult to say if the optimum found by a certain optimization algorithm is the sought global one. It might be a case that the algorithm is getting stuck in one of the local optimum points which is, however, not the best one. The optimization algorithms able to find the global optimum of a target function among all the local optima it has in a chosen parameter space are called global optimization algorithms. The algorithms which start at a certain given point of the parameter space and find an optimum usually nearest to this point by following a certain path, are called the path-oriented optimization algorithms or local optimization algorithms. There are also hybrid algorithms which usually are combination of the above two.

In the following sections representatives of local, global and hybrid algorithms are described in more detail.

3.1.1. Path-oriented optimization algorithms

The path oriented algorithms build in a stepwise manner a path along which they follow to the optimum point. They start at a chosen point of the parameter space which is called the initial point. At each step of the algorithm a direction is chosen and an optimum of the target function in this direction is found. Steps are repeated until no improvement of the target function in any direction is possible. In this way the optimization of a complex multidimensional target function is reduced to the series of searches along single dimensions (one-dimensional functions) each of which is a slice of the target function in a chosen direction.

Steepest descent and coordinate descent methods, Hook-Jeeves method, gradient methods, etc., (e.g., Nocedal and Wright, 2006), belong to the path oriented optimization algorithms.

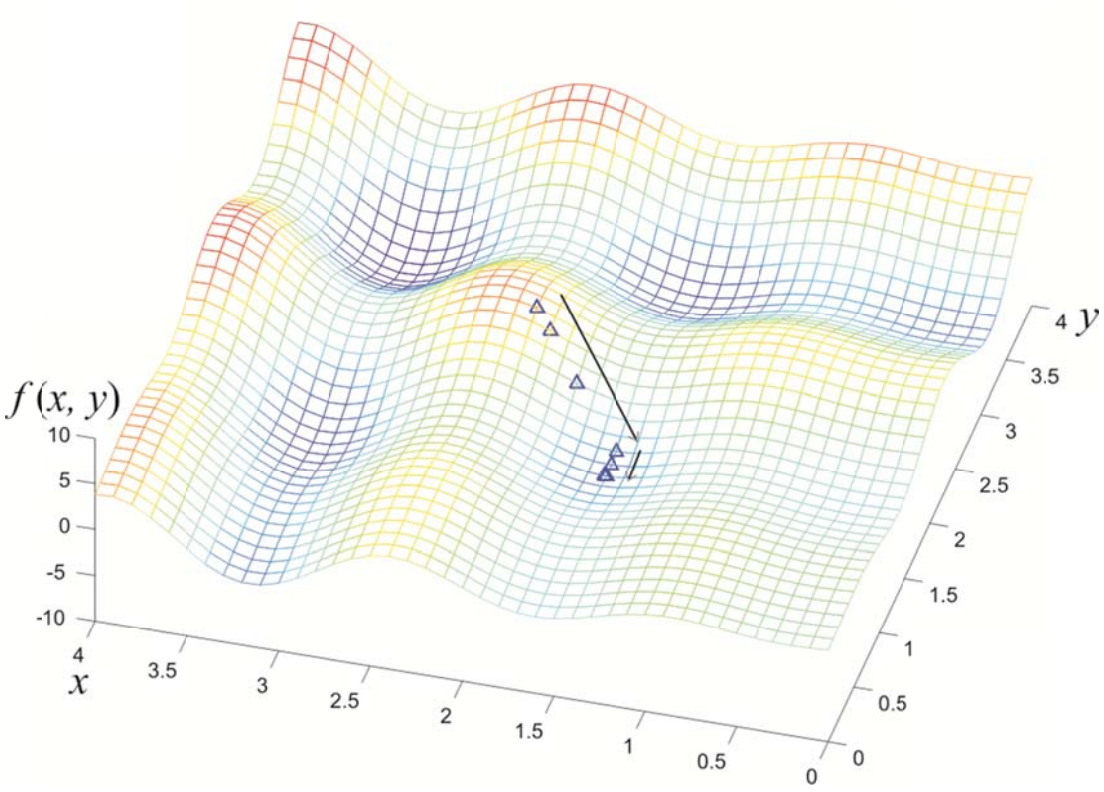

Figure 3.1: *Example of search trajectory of the steepest descent local optimization method minimizing two-dimensional target function* $f(x,y) = xsin(3.5x) - ycos(4y)$ *from initial point* $(x = 2.3, y = 2.3)$

In Figure 3.1 the path to a local minimum of the two-dimensional function $f(x,y) = xsin(3.5x) - ycos(4y)$ built by the steepest descent optimization method is shown. The algorithm starts at the chosen initial point $(x = 2.3, y = 2.3)$. At this point the steepest descent direction is determined as an opposite to the gradient of the target function. The algorithm finds the minimum point in this direction and continues from this point in a new steepest descent direction. The path of descent built by this method looks like a trajectory of a ball rolling down a hill to the next lowest point. Just like a ball having normally not enough inertia to roll over to the deeper valley, the algorithm may stuck in the nearest minimum.

3.1.2. Heuristic optimization algorithms. Evolutionary algorithms

Another class of the optimization algorithms called heuristic algorithms is inspired by the processes occurring in the nature. Evolutions of species, behaviour of the ant colony, hunting of grey wolves, swarm intelligence are only a few to mention.

Heuristic algorithms implicitly comprise of exploratory and focusing stages. In the early stage of the algorithm the exploratory features of the algorithm dominate, the

algorithm explores the parameter space in order to find the promising regions where the sought global optimum might be located. In the later stage the focusing is of more importance; the algorithm tries to converge to the global optimum, region of which is roughly located in the previous stage.

As it was previously shown in works at University of Kassel (Krause, 2003) the heuristic algorithms perform better than their path-oriented counterparts when applied to optimization of solar heating systems. In comparison to path-oriented methods they are more robust to small perturbations of the target functions and usually find the global optimum. In Chapter 4 the CHC genetic algorithm is applied to optimization of the solar heating combisystem.

A simple genetic algorithm is an example of the evolutionary algorithms (Goldberg, 1998). It mimics evolution of a species population which in natural environment undergoes processes of selection, recombination (pairing) and mutation. Each individual of the population is a parameter vector which belongs to the search space of the optimization problem. Each single parameter of the parameter vector describes an individuals´ characteristic. For example, an individual of the animal's population is a bunch of its characteristics like height, eye or skin color, etc. An "individual" of the solar heating systems´ "population" is a system with its collector size, solar thermal storage volume, flow rates, etc., as single characteristics (parameters) which comprise a parameter vector.

By analogy to genetics, in genetic algorithms the population individuals are first encoded to the so-called chromosomes consisting of genes representing single characteristics of the individual. Usually the binary encoding by zeros and ones is used but other encodings are possible as well. An example of an encoded population individual is shown in Figure 3.2.

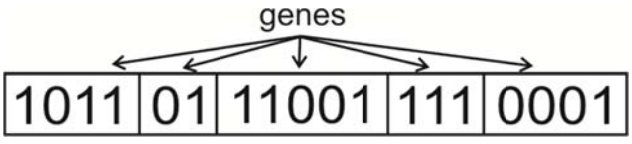

Figure 3.2: *Example of binary encoding of a population individual (chromosome) consisting of 5 characteristics (genes)*

As the length of the whole chromosome as well as each of its genes is finite and fixed, the encoding of an optimization parameter automatically means its discretization. In the case of binary encoding the number of sampling points per parameter (i.e. resolution of discretization) is 2^N where N is a length of the gene representing this parameter. This length is specified for each parameter before the

algorithm starts. For example, if for the parameter "Collector area" the encoding length $N = 2$ and the variation range $[11; 14]$ are specified, then the sampling points which the algorithm may choose for calculation of the target function are $11, 12, 13$ and $14\ m^2$. In genetic algorithms all "genetic" operations are performed on encoded strings. To calculate the target function the parameter vector must be decoded, as calculation (simulation of the solar heating system) can be carried out only if decimal values are assigned to optimization parameters.

The genetic algorithm starts by choosing an initial population of N individuals (parameter vectors) randomly distributed within the parameter space. For each individual the performance, i.e. value of the target function is assessed. The individuals who have better performance, that is, represent better solutions to the target problem are favoured when selecting for reproduction. There exists a wide variety of selection rules according to which the better individuals are being picked up for recombination. The probability to be picked up directly depends on the performance of the individual. Once selected, the pairs of individuals are recombined, that is, certain genes are exchanged between them. In Figure 3.3 an example of the one-point recombination is shown.

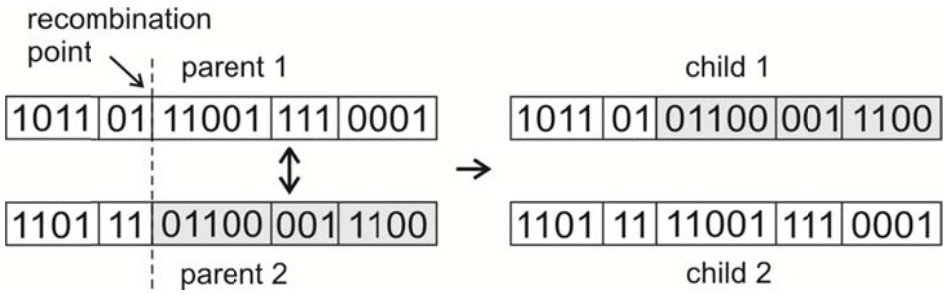

Figure 3.3: *Example of one-point recombination of two individuals*

After recombination is complete, a new population of children called also as a new "generation" of the individuals is created. In the last step of the genetic algorithm the individuals' genes are mutated in the way that their bits are inverted with specified small probability.

Application of selection, recombination and mutation operators is repeated until a predefined termination condition is reached, that is, the algorithm converges (see Figure 3.4). In present implementation, this happens if no improvement of the target function was recorded during last N generations.

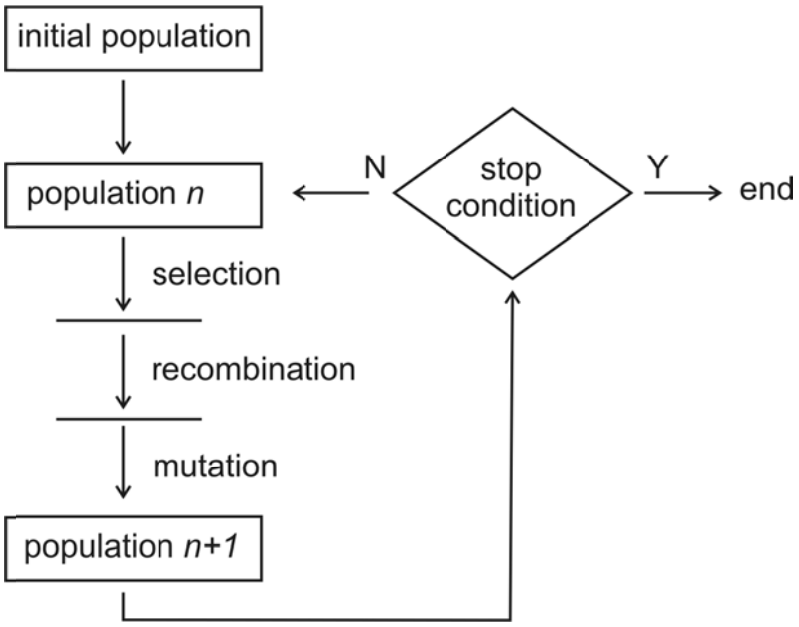

Figure 3.4: *General scheme of simple genetic algorithm*

3.1.3. Hybrid algorithms

As already noticed above, the hybrid optimization algorithms are the combinations of global and local optimization algorithms. Having taken the advantages of both of them, the hybrid algorithms are an attempt to build a reliable and at the same time fast optimization algorithm. They normally start with the global optimization algorithm running in the exploratory mode to locate one or a few promising regions in the parameter space, where the sought global optimum might be found. After this part is finished, the algorithm switches to a faster local optimization algorithm which starts from the best solution found by the previous global algorithm and converges faster to the optimum. In other words, the global algorithm is used to roughly locate the valley of the global optimum; fine search is done at the second stage by the local algorithm.

The challenge for the hybrid algorithm is choosing the point at which the optimization by global algorithm switches to the local one. If it happens too early, before the region where the sought global optimum is located, was found by global algorithm, then the consequent optimization by the local algorithm might lead to a local optimum and miss the global one. If it happens too late, then the computation time might be wasted as the faster local algorithm was not started in time.

The hybrid algorithms are less reliable than the pure global optimization algorithms; they are normally used to speed up the optimization process in the cases when saving the computational time is crucial.

3.2. Sensitivity analysis methods. Overview

Sensitivity analysis (SA) is a bunch of mathematical techniques used to assess the relative importance of the input parameters for the output of a numerical model, that is, the target function. The qualitative SA methods answer the questions like “which input parameter influences the target function the most?” or what is similar: “which of the uncertain inputs brings the most uncertainty to the target function”. Ranking of the input parameters in order of their importance is also a task of the qualitative SA. Quantification of the variation of the target function due to variation of the input parameters is done by the quantitative SA.

Another principal division of the SA methods is based on their application domain, whether they are applied locally at certain points of the input parameters space, or they estimate parameters importance globally by exploring the whole space. In this sense, the global and local SA are distinguished.

In the following subsections the global SA methods are described in more detail. For introduction to SA methods and their application refer to (Saltelli, 2004).

3.2.1. Multiple linear regression

This subsection shortly introduces the multiple linear regression (MLR) and describes its applicability to estimation of the influence of the parameters on the target function around optimum.

MLR attempts to model the relationship between k independent variables $x_j, j = 1, .., k$ (system parameters) and dependent variable y (target function) in the form:

$$y_i = \beta_0 + \sum_{j=1}^{k} \beta_j x_{ij} + \varepsilon_i, \qquad i = 1, .., n, \tag{3.1}$$

where y_i are n measurements of the target function for corresponding parameter vectors $(x_{i1}, \dots x_{ik})$, that is, system configurations x_i; ε_i denote the model errors. The estimates of the coefficients β_j, denoted as $b_j, j = 0, \dots, k$, are calculated by finding the least-squares error, that is, from $\sum_{i=1}^{n} \varepsilon_i^2 \rightarrow min$. The coefficient b_0 is called intercept and it estimates the value of the target function when all the parameters equal zero. The coefficients $b_j, j = 1, \dots, k$ are called slopes. They represent the change in the mean of the target function y due to the unit increase in the corresponding parameters x_j when all other parameters are fixed. The fit values

of the target function are obtained as $\hat{y}_i = b_0 + \sum_{j=1}^{k} b_j x_{ij}$ and the residuals between measured and fitted target function are $e_i = y_i - \hat{y}_i$.

To determine the quality of the model, that is, to check how well the measured values y_i are described by the fit, the determination coefficient or squared multiple correlation R^2 is introduced as:

$$R^2 = \frac{SSM}{SSTO} = 1 - \frac{SSE}{SSTO}, \tag{3.2}$$

where $SSM = \sum_{i=1}^{n}(\hat{y}_i - \bar{y})^2$ is the sum of squares of the model quantifying how far is $\hat{y}$ estimated by the model from "no relationship" simple mean $\bar{y}$ of measured data, $SSE = \sum_{i=1}^{n}(y_i - \hat{y}_i)^2$ is squared sum of errors telling how much the modelled target function differs from the measured one, and $SSTO = \sum_{i=1}^{n}(y_i - \bar{y})^2$ is the total sum of squares describing how much the measured data vary around their mean. $SSTO = SSM + SSE$.

The determination coefficient R^2 is a proportion of the variation due to the regression model (SSM) in the whole variation of the measured data $SSTO$ and therefore it varies between 0 and 1. Small values of R^2 mean poor fit of the measured data by the MLR model, whereas the values close to 1 show the good quality of the model. In other words, $R^2 \cdot 100\%$ shows how many percent of the variation in the target function y can be explained by the model, that is, by the parameters $x_1, \dots, x_k$.

Besides the fit coefficients b_j and determination coefficient R^2, the statistical software calculate the p – values which are the measures for statistical significance of the parameters. More precisely the p – value shows how compatible the measured data are with the so-called null hypothesis $H_0: \beta_j = 0$ stating that the fit coefficient is zero, that is, the parameter x_j has no impact on the target function. The p – value is the probability of obtaining effect of the parameter at least as strong as in the measured data sample when assuming that the null hypothesis is true. For example the p value of 0.01 means that if assume the null hypothesis to be true, at least the observed impact can be obtained in only 1% of samples due to random sampling error. If the p value is small then one of the following is true: either the null hypothesis is true but the measured data sample is so unusual or the null hypothesis is false. Testing with other data might be useful for rejecting the null hypothesis that is, stipulating the significance of the influence of the parameter on the target function with more confidence. The levels of the p value smaller than

0.001 and 0.01 indicate very strong and strong significance of the corresponding parameter.

The $n\%$ confidence interval can be calculated for each regression coefficient β_j as well. It tells that other estimates of the regression coefficient which can be obtained using different randomly sampled measurement data lie within this confidence interval $n\%$ of time. In this study usual 95% confidence intervals are obtained for the regression coefficients.

The MLR method is applied to estimating the portion of the influence of the solar combisystem parameters on the chosen target function near the previously found optimum. It is applied because the regression coefficients of the MLR model can be easily interpreted and, in fact, they are the sought portion of the influence. Another advantage of the method is that in contrast to the differential analysis in which the influences are estimated only at the selected points, the MLR model is valid over the space made up by variation ranges of the parameters. The method also allows self-verification in the form of the coefficient of determination R^2 telling how much variation in target function is explained by the linear model. If R^2 is relatively small, in our case smaller than 80%, then other methods of the sensitivity analysis should be applied.

3.2.2. Morris method

In contrast to the MLR, the Morris method can be successfully applied to the problems having significantly non-linear relationships between the target function and parameters. However, the Morris method can identify the parameter importance only qualitatively providing no reliable quantification of its influence. Another drawback is lack of the self-verification indicator similar to the MLRs coefficient of determination R^2.

Identification of the most important input parameters of the model is commonly used for simplifying the existing model or rethinking its structure by eliminating the parameters which have almost no influence on the target function. Ranking of the parameters might also be beneficiary when choosing them for optimization of the target function because exclusion of the unimportant parameters from optimization process saves valuable computation time. After the optimal configuration of the parameters is found another importance ranking in the vicinity of the optimal point can be applied to determine uncertainty of which input parameter has the most influence on the uncertainty of the target function and therewith lessens the

optimization potential the most. In practical implementation these important parameters must be handled particularly carefully.

In the case when a large number of parameters are to be ranked and, at the same time, the number of model evaluations must be keep as small as possible, an efficient experimental design is crucial. The screening SA methods fulfil this requirement. They efficiently perform the qualitative analysis of the parameters importance without really quantifying how much is one parameter more important than another. Several screening SA methods have been proposed in the literature. In this subsection the method proposed by Morris at (Morris, 1991) is described in more details.

In the Morris method two quantities are used as sensitivity measures for each parameter; the measure μ estimates the overall, linear effect of the parameter on the target function, and the measure σ accounts for the second and higher order effects, including interaction effects in which the parameter is involved. The Morris method varies one parameter at a time. Each parameter may take only a set of discrete values, the so-called levels, fixed within the parameter variation range.

The Morris method is simple in implementation and efficient at the same time as it requires small number of model evaluations which grows only linearly with respect to the number of investigated parameters. The drawback of the method is that it analyses the so-called elementary effects defined below in (3.3), which are the sensitivity measures at selected local points. As seen from the definition, the elementary effect is similar to the derivative. The final sensitivity measure μ, however, is obtained by averaging the elementary effects calculated at a number of local points and therefore can be regarded as the global measure over the whole parameter space, not dependent on the specific point especially when the number of points is large enough.

Basing on the sensitivity measures μ and σ, the method of Morris determines which of the input parameters can be considered as negligible, which have mostly linear impact on the target function and which have nonlinear effect or are involved in interactions with other parameters.

To describe the way, in which the sensitivity measures are calculated for each input parameter, assume that the k input parameters take the discrete values from the unit p-level set $\{0, 1/(p-1), 2/(p-1), \dots, 1\}$ which must be appropriately rescaled for calculation of the target function. By assuming such discretization of the input parameters, the input space Ω as the k -dimensional p-level grid is generated.

The elementary effect of the i-th parameter at any selected local point x from Ω, is defined as follows:

$$d_i(x) = \frac{y(x_1, \dots x_{i-1}, x_i + \Delta, x_{i+1}, \dots, x_k) - y(x)}{\Delta} \tag{3.3}$$

where Δ is a predetermined multiple of $1/(p-1)$ and the point x is selected such that the shifted point $x + e_i \times \Delta$ (e_i is the unit transformation vector having one at the i-th position and zeros at all others) remains within Ω.

For each i, $i = 1, .., k$, the elementary effects are calculated at a number of randomly chosen points x from Ω and their distribution is denoted by F_i. In (Campagnolo et al., 2007) it is proposed to consider the distribution G_i of the absolute values of the elementary effects along with F_i. Here we follow it and take μ^*, the mean of the distribution G_i and σ, the standard deviation of the distribution F_i, as the sensitivity measures upon which the importance of the input parameter is determined. The mean value μ of the distribution F_i is less informative than μ^* of G_i because the elementary effects having opposite signs cancel each other in F_i, and, therefore, μ may underestimate the parameters linear effect on the target function y. Despite of this, μ might be used in no extra computational costs to identify if the parameter has only positive or only negative effect ($|\mu|$ and μ^* are nearly the same) or the effect has different signs depending on the point at which the effect is calculated (μ^* is large and $|\mu|$ is noticeably smaller than μ^*).

The standard deviation σ of the distribution F_i is considered as a measure detecting the nonlinearity of the parameters effect or the degree of its interactions with other parameters. The value of σ is large when the elementary effects of the parameter are significantly different at different points (values of other parameter), where they are calculated. In contrast, the small value of σ indicates that the considered parameter is not involved in the interactions with other parameters (or this interaction is negligible) and that its effect on the target function is linear.

3.2.3. Fourier amplitude sensitivity test

The Morris screening method described in the above subsection cannot be used for quantifying the effect of the input parameter on the model output. For this the methods of quantitative SA should be applied. These methods evaluate the “main effect” also called “first order effect” S_i, that is, the contribution of the parameter x_i to the variation of the target function defined in Bayesian notation as

$$S_i = \frac{var_X[E(y/x_i)]}{var(y)}, \tag{3.4}$$

where y is the target function, $E(y/x_i)$ is the expectation of y taken over the whole parameter space $x_j, j = 1, \dots, k, j \neq i$ but at the fixed value of the parameter x_i, and the variance var_X is taken over all possible values of x_i. The sum of main effects describes how much variance in the target function is described by all parameters. This value must be close to 1 if the FAST analysis is successful.

Another measure quantified by the quantitative SA is the total sensitivity index which estimates the total effect of the parameter. For the model with three parameters it is calculated as follows:

$$S_{T1} = S_1 + S_{12} + S_{13} + S_{123}, \tag{3.5}$$

where S_{T1} is the total effect of the parameter 1, S_1 is the first-order sensitivity index of this parameter, its main effect, S_{12} is the second-order sensitivity index for the two parameters 1 and 2, showing the two-way interaction between them, and so on.

In this subsection the Fourier amplitude sensitivity test (FAST) method for estimation of main effect indices of the input parameters is described in more details, following (Saltelli et al, 1999). To calculate the total effect indices the extension of the FAST method was proposed in (Saltelli et al, 1999).

The FAST method appears to be efficient for estimating the sensitivity indices for models with many input parameters, as it requires relatively small sample size, that is, less model evaluations comparing to other quantitative SA methods, however, still much more than it is required for the qualitative Morris method.

Let the target function y depend on the parameters $x_1, \dots, x_n$ by means of the model f, $y = f(x)$. Let also assume that vector $x(x_1, \dots, x_n)$ lie within the unit hypercube $K^n(x| \, 0 \leq x_i \leq 1; \; i = 1, .., n)$.

Calculation of the main effects and interactions between the parameters is based on the calculation of the following integral, denoted as the r_{th} moment of y:

$$y^{(r)} = \int_{K^n} f^r(x) dx \tag{3.6}$$

This presentation of $y^{(r)}$ is true under the assumption that the input parameters are identically and uniformly distributed in K^n.

In the FAST method, in order to avoid calculation of the multidimensional integrals, the one-dimensional Fourier decomposition is suggested which is performed along a search curve, exploring the hypercube K^n. The curve is defined as follows:

$$x_i(s) = G_i\big(sin(w_i \times s)\big), \qquad i = 1,..,n, \tag{3.7}$$

where s is a scalar variable, $-\infty < s < +\infty$, G_i are the transformation functions, and w_i are the frequencies associated with corresponding parameters x_i. Choice of the transformation functions G_i determines how uniformly the unit hypercube K^n is explored by the search curve.

By varying the point s, values of input parameters x_i(s) oscillate periodically and independent of each other, with their own frequencies w_i. The investigated target function y will also show different periodicities connected with different frequencies w_i. The stronger the effect of the parameter x_i on the target function y is, the higher the amplitude of oscillations of y at the corresponding frequency w_i.

The search curve completely fills the hypercube K^n if and only if the frequencies w_i are selected according to the rule that none of the frequencies can be obtained by the linear combination of the others, that is

$$\sum_{i=1}^{n} r_i w_i \neq 0 \tag{3.8}$$

for any integer $r_i: -\infty < r_i < +\infty$. In this case the integral over the hypercube K^n in (3.6) can be replaced with the one-dimensional integral along the curve. With account of (Cukier et al., 1978) and denoting $f(x_1(s), \dots, x_1(s))$ as $f(s)$, the r_{th} moment of y can be then computed as follows:

$$y^{(r)} = \frac{1}{2\pi} \int_{-\pi}^{\pi} f^r(s) ds \tag{3.9}$$

By definition of the variance D of the model y and after omitting some intermediate assumption:

$$D = y^{(2)} - \left(y^{(1)}\right)^2 = \frac{1}{2\pi} \int_{-\pi}^{\pi} f^2(s) ds - \left[\frac{1}{2\pi} \int_{-\pi}^{\pi} f(s) ds\right]^2 \tag{3.10}$$

Further, the target function $f(s)$ is expanded in the Fourier series:

$$y = f(s) = \sum_{j=-\infty}^{+\infty} \{A_j \cos(js) + B_j \sin(js)\} \tag{3.11}$$

with Fourier coefficients A_j and B_j:

$$A_j = \frac{1}{2\pi} \int_{-\pi}^{\pi} f(s)\cos(js)ds \tag{3.12}$$

$$B_j = \frac{1}{2\pi} \int_{-\pi}^{\pi} f(s)\sin(js)ds \tag{3.13}$$

The power spectrum of the Fourier series expansion of y is defined as

$$\Lambda_j = A_j^2 + B_j^2 \tag{3.14}$$

where j is an integer frequency, $j \in Z$.

Summing up all Λ_{pw_i}, $p \neq 0$ corresponding to each frequency w_i and its higher harmonics pw_i, we get estimation of the portion of the variance D_i in the total variance D of the output y, which is due to the variation of the i_{th} factor x_i.

$$D_i = \sum_{p \neq 0} \Lambda_{pw_i} = 2 \sum_{p=1}^{+\infty} \Lambda_{pw_i} \tag{3.15}$$

because $\Lambda_{-pw_i} = \Lambda_{pw_i}$.

The total variance D is then the sum of all Λ_j ($j \neq 0$) and $\Lambda_{-j} = \Lambda_j$

$$D = \sum_{j \neq 0} \Lambda_j = 2 \sum_{j=1}^{+\infty} \Lambda_j \tag{3.16}$$

The ratio D_i/D calculated in this way estimates the main effect of the i_{th} parameter x_i on the target function y.

The minimum sample size for calculation of the main effects was shown to be

$$N_s = 2Mw_{max} + 1 \tag{3.17}$$

where M is the interference factor, usually chosen to be 4 or higher, w_{max} is the largest frequency among w_i.

Suggestions on the appropriate choice of the transformation functions G_i, frequencies w_i as well as the optimal sample size are given in (Saltelli et al., 1999).

4. Numerical optimization of solar thermal combisystems in planning process. Application of sensitivity analysis around optimum

In this Chapter, the methods of numerical optimization and sensitivity analysis are applied to the solar thermal combisystem described in Chapter 2. Choice of the target function and parameters of the combisystem that might have influence on it has been discussed along with construction of the optimization algorithm.

An optimization process of the solar heating system can be seen as an improvement of the system as a whole, improvement of its single component, connections between the components in the system, the way in which the system operates, etc.

Before the numerical optimization can be performed on the system the following questions must be cleared:

What should be optimized?

The boundary of the system to be optimized must be clearly defined in advance and an approved mathematical model of the system as long as possible validated by measurements must be provided. These are the prerequisites to successful optimization.

What is the purpose of optimization?

We try to improve the system so that it becomes optimal in some reasonable sense. It is not always easy to define this "reasonable sense" appropriately because often controversial criteria must be taken into account, for example, energy output of the system and its costs.

What should be adjusted on the existing system?

Optimization is only possible if there is a degree of freedom, that is, it is possible to adjust some parameters of the system as, for example, dimensions of single components, controller settings, etc. All parameters which seem to have impact on the purpose of optimization and can be varied in specified variation ranges are reasonable to optimize.

What optimization algorithm should be used?

Among plenty of algorithms already successfully applied to solving other optimization problems, the one must be chosen to carry out optimization of the solar heating combisystem. The reliability and computationally efficiency of the algorithm are of key importance.

Numerical optimization has already been successfully applied to optimization of solar combisystems. (Fiedler et al., 2006) applied Hook-Jeeves algorithm to optimization of auxiliary heater settings. (Bornatico et al., 2012) used Particle Swarm optimization algorithm to optimization of main components of solar thermal system and compared with results of genetic algorithm. (Cheng and Zmeureanu, 2014) applied a hybrid Particle Swarm – Hook Jeeves algorithm to optimization of solar combisystem with respect to life cycle cost, energy use and exergy destroyed. (Rey and Zmeureanu, 2016) used multi-objective particle swarm optimization algorithm to build a Pareto front between life cycle costs and life cycle energy.

In the following the target function is defined, optimization parameters and optimization algorithm are selected for optimization.

4.1. Target function

During design of solar thermal systems or their single components the important compromise between the energetic performance and costs must be found. It is almost always possible to construct a huge solar heating system which will cover user heating demand to 100% but will be so expensive that it becomes not economically reasonable. Vice versa, with no investments there is no system what can be an optimal choice at certain boundary conditions, for example, when fossil fuel prices are low enough. As it is easily seen, energetic performance and costs are controversial criteria: maximization of the energetic output mostly leads to increase of the costs. However, in certain cases when the investment costs do not change with changing the system configuration, it is possible to come up with energetic criterion only. For example, decision on the heights of inlets and outlets of the solar store may be made basing on the energy output of the system unless putting the inlets or outlets in some definite positions requires additional material or labour efforts. The same is true for optimization of the controller settings, altering of which is usually not connected with additional costs, unless the adjusted controller settings lead to, for example, more electric consumption of the pumps.

In the planning process of the solar thermal system, the dimensions of the system components or their type are relatively free to choose with some natural restrictions (house roof area for the collectors, cellar volume for the storage, etc.). Obviously, the costs for the whole system will vary with changing the dimensions of its components and these costs must be reflected in the target function.

The target function for design optimization of the solar heating systems usually consists of energetic and economic parts. The both parts, however, are not easy to estimate. Calculation of each of them has different sources of uncertainties.

As already mentioned in Chapter 2, the energetic performance of the solar heating systems can be estimated by several performance indicators. In this study the solar combisystem is optimized for minimum cost per kWh of saved auxiliary final energy. The target function dependent on the set of the optimization parameters $X = \{x_1, \dots, x_N\}$ which are listed in Table 4.1 in the following section, installer margin m and interest rate r (both explained in subsection 4.1.2), is constructed as follows:

$$F_{target}(X, c, m, r) = \frac{F_{cost}(X, m, r)}{E_{ref} - E_{sol}(X) + \hat{F}_{penalty}\left(f_{save,ext}(X), c\right)} \tag{4.1}$$

having in the numerator economics of the combisystem represented by its annuity costs $F_{cost}(X, m, r)$ and in the denominator the energetic performance in sense of saved auxiliary energy calculated over a year. $\hat{F}_{penalty}$ is the penalty function applied when the required level of extended fractional savings c is not reached.

4.1.1. Energetic performance of the combisystem

As already mentioned above the energetic performance of the combisystem is described by the denominator of the target function (4.1), in which

$$E_{ref} = (Q_{SH} + Q_{DHW} + Q_{loss,ref})/0.85 + E_{par,ref}/0.4 \tag{4.2}$$

is the auxiliary final energy consumption of the reference heating system with Q_{SH} and Q_{DHW} denoting space heating and domestic hot water demands, respectively, $Q_{loss,ref}$ - the heat losses of the reference store and $E_{par,ref}$ – parasitic electrical energy consumption by the reference system, i.e. electrical consumption by the pumps, controller and boiler. Energy consumption of the solar combisystem is defined by

$$E_{sol}(X) = Q_{aux,pen}(X) + E_{par,sol}(X)/0.4\,, \tag{4.3}$$

where $E_{par,sol}$ is the parasitic electrical energy consumption of the solar combisystem. $Q_{aux,pen}$ is the auxiliary energy consumption including penalties for not meeting DHW and SH demands described by $F_{penalty}$ from (2.6). It is defined as follows:

$$Q_{aux,pen}(X) = Q_{aux}(X)/0.85 + F_{penalty}(X) \quad (4.4)$$

Boiler efficiency is set to be constant 0.85 throughout its operation and the electricity is produced with the efficiency of 0.4.

The energetic performance of the combisystem is measured by the amount of saved auxiliary final energy $E_{ref} - E_{sol}(X)$ over a year. The third term $\hat{F}_{penalty}$ in denominator of (4.1) is the penalty added to the target function if the extended fractional energy savings $f_{sav,ext}$, defined being equal to f_{si} from (2.5), are less than a given value c. This term is needed only if the extended fractional energy savings $f_{sav,ext}$ of the optimized combisystem are required to be not smaller than c. $\hat{F}_{penalty}$ describes how much solar gains are missing in order to reach $f_{sav,ext} = c$. It is defined as follows:

$$f_{sav,ext}(X) \geq c \;:\; \hat{F}_{penalty}\big(f_{sav,ext}(X), c\big) = 0 \quad (4.5)$$

$$f_{sav,ext}(X) < c \;:\; \hat{F}_{penalty}\big(f_{sav,ext}(X), c\big) = (1 - c) \cdot E_{ref} - E_{sol}(X) \quad (4.6)$$

To calculate energetic performance, a one-year simulation of the solar heating combisystem is carried out by the TRNSYS simulation software environment.

Calculation of the energetic performance is coupled with uncertainties which are coming from input data (weather conditions, load profiles, building envelope, etc.), the numerical models of the components and from TRNSYS environment itself. In this study, however, the magnitude of uncertainties has not been estimated and, thus, their influence on the optimization results is not taken into account.

4.1.2. Costs of combisystem

To determine the costs of the combisystem described by the numerator of the target function F_{target} defined in (4.1), comprehensive market study is required. It is connected with large uncertainties due to variety of the solar thermal components of different quality present on the market. Furthermore, the prices of the system components, transportation costs, interest rate, etc., are noticeably time dependent, different special offers influence the cost function as well. All this together with non-transparency of the installer price margins makes determination of the cost function quite difficult.

In this study a simple calculation of the prices of single system components is attempted. If any optimization parameters from Table 4.1 below have an impact on the price of a certain system component then the price function for this component

is built which is a dependency of the component price from the magnitude of these parameters.

The price functions are built for each component basing on the offers of online discount suppliers. Dependency of the price on the optimization parameters is chosen in the form of polynomial up to the second degree and the unknown coefficients of the polynomial are determined by performing linear or multi linear regression. Component price functions obtained in this way are listed in Appendix A.

As already mentioned, the prices offered by the online discounters are taken as the regression data. They seem to be the cheapest retail prices on the market accessible for the end user and probably be the best approximate for the wholesaler prices. The component prices offered by the installers most likely already include their margins which might be different for different components and also vary from installer to installer. For example, one installer might add 30% to the price of collectors and 50% to the store price offered by the wholesaler whereas another installer might do vice versa. From this reason the component prices offered by the discounters and not the installer prices are chosen to be appropriate for building the cost function of the solar combisystem.

On the other hand, however, it seems unlikely that the end user will succeed to hire the installer to build up the combisystem out of the user's own components bought by the discounter. From one side the end user has usually not enough experience to buy the correct components in correct sizes and from the other side, the installer will most probably neither guarantee nor assume the responsibility for the combisystem built up out of such components. From this reason, to estimate the final price for each component $C_i, i = 1, \dots, N$ for the end user, the discounter price $F_{cost,disc}(C_i)$ (see Appendix A) is corrected by the factor m representing expected installer margin, supposed to be the same for all components. To get the final capital costs $F_{cost,cap}$ the installation costs equal to 20% of the price for solar combisystem are added.

$$F_{cost,cap}(X, m) = 1.2 \cdot m \cdot \sum_{i=1}^{N} F_{cost,disc}(C_i) \tag{4.7}$$

The final capital costs $F_{cost,cap}$ depend implicitly (through the functions $F_{cost,disc}(C_i)$) on at least some of the optimization parameters X. In the present implementation the capital costs include German value added tax equal to 19%

Following the annuity method, the annual payments due each year over the lifetime of the solar combisystem at the given interest rate r are calculated as follows:

$$F_{cost}(X, m, r) = \frac{(1+r)^{20} \cdot r}{(1+r)^{20} - 1} \cdot F_{cost,cap}(X, m) + 0.007 \cdot F_{cost,cap}(X, m) \quad (4.8)$$

The lifetime of the combisystem is set to 20 years and it is not varied in any of the following optimizations. Second term in (4.8) describes annual maintenance and insurance costs. These costs discounted to the installation year, equal around 11% of the capital costs $F_{cost,cap}$ for the lifetime of the combisystem and the interest rate of 2.5% ($r = 0.025$).

The cost function $F_{cost}(X)$ with interest rate of 2.5% and $m = 1.5$, meaning that 50% is added to the discount component prices as an installer margin, is used in the target function $F_{target}(X, c)$ from (4.1) in the following optimizations. Other annuities $F_{cost,contr}(X) = F_{cost}(X, 1, 0.025)$ and $F^0_{cost,contr}(X) = F_{cost}(X, 1, 0)$ both representing the costs with different interest rates of 2,5% and 0%, respectively, for the company which installs the solar thermal systems ($m = 1$), are calculated as well. After subtracting the value added tax ($\hat{F}^0_{cost,contr}(X)$) and substituting into (4.1), the costs per kWh of saved auxiliary final energy are obtained for the installation company doing, for example, the energy contracting. The cost function $F^0_{cost}(X) = F_{cost}(X, 1.5, 0)$, that is, the cost function for the end user ($m = 1.5$) investing its own savings ($r = 0$) in a solar combisystem is presented in the results below as well.

After substituting the annuity cost functions into (4.1) the corresponding target functions, are obtained. Since all the cost functions derived here do not change the weighting of the capital costs $F_{cost,disc}(C_i)$ of single components under the sum sign in (4.7) but only modify the sum as the whole, the optimum system configuration $X = X_{opt}$ received for one of the functions is also the optimum for all others.

4.2. Optimization parameters

Before the optimization algorithm may start, the parameters of the system, values of which are believed to be not optimal and are to be changed in order to improve the existing system, must be specified. Not only the parameters themselves, but also the variation ranges in which the parameter values can be varied during optimization are to be chosen. Too wide variation ranges will most likely slow down the optimization whereas too narrow ranges may cause missing the optimum when the

optimal parameter value lies beyond the specified variation range. In this case the optimal value of the parameter found by the optimization algorithm will probably lie exactly on the boundary of the variation range. It is a good indication that for this parameter the variation range must be extended beyond this boundary.

In general, parameters to be optimized as well as their variation ranges can be chosen independently from each other, that is, without taking care about possible correlations between parameters. However, for any two parameters which are involved in interactions with regard to the target function (f.e. flow rate and pipe diameter), the variation ranges should be chosen such that none configuration of the values (f.e. flow rate chosen large and pipe diameter – too small) will cause the system simulation to fail. Large number of such "invalid" configurations may mislead the optimization algorithm.

In this work, 18 parameters of the solar heating combisystem have been adjusted in the process of optimization in order to get the optimal value of the solar energy costs (4.1). They comprise such design parameters as collector area, store volume, insulation thickness, UA-values of the heat exchangers, pipe diameter, inlet/outlet positions, etc., and operational parameters as flow rate, set temperature of the auxiliary heater, dead bands of the collector and auxiliary heater controllers. All the optimization parameters with their variation ranges, discretization steps and corresponding coding lengths used in genetic algorithm, are listed in Table 4.1. In several optimizations below the variation ranges of certain parameters are modified so that the optimum lie within the variations ranges.

Table 4.1: *List of optimization parameters with variation ranges, discretization steps and coding lengths for optimization algorithm. For several optimizations with large extended solar fractional savings in below variation ranges of collector area and store volume are changed in order to include optimum*

Parameter	Variation range	Step	Coding length
1. Collector area, m^2	[5;36]	1	5
2. Store volume, m^3	[0.5;2.0]	0.1	4
3. Number of auxiliary nodes	[5;20]	1	4
4. Insulation thickness, m	[0.05;0.8]	0.05	4
5. Pipe inner diameter, mm	[10;40]	2	4
6. Specific collector flow rate, kg/m^2h	[5;36]	1	5
7. ΔT controller upper dead band, K	[4;11.5]	0.5	4
8. ΔT controller lower dead band, K	[0.1;4.0]	≈ 0.25	4
9. ΔT temperature sensor position in store	[0.01;0.3]	≈ 0.02	4

10. UA value of external solar HX, W/K	[1000;5500]	300	4
11. UA value of external DHW HX, W/K	[1000;10300]	620	4
12. Collector inlet position in store	[0;1]	≈ 0.03	5
13. Space heating outlet position in store	$[1 - V_{aux}/V_{store}; 1]$	≈ 0.06	4
14. Space heating inlet position in store	[0.075;0.3]	≈ 0.02	4
15. Set temperature of auxiliary heater, $°C$	[50;70]	≈ 1.3	4
16. Auxiliary controller upper dead band, K	[4;16]	0.8	4
17. Auxiliary controller lower dead band, K	[0.5;4]	≈ 0.25	4
18. Collector slope,°	[40;71]	1	5

4.3. Hybrid genetic CHC - binary search optimization algorithm

The solution found by the optimization algorithm is the system configuration optimal with regards to a chosen target function. Whether the found solution is really the optimal one and how efficient the performed operations are, are the questions of reliability and efficiency of the algorithm. As already noted, there are global optimization algorithms which are, as a rule, reliable but not really efficient, and the local ones being relative fast but not really reliable. Hybrid optimization algorithms are an attempt to make the reliable global optimization algorithms faster by coupling them with computationally less expensive local algorithms. In this work the CHC genetic algorithm is coupled with the local binary (n-ary) search algorithm.

4.3.1. CHC genetic algorithm

The CHC genetic algorithm, implemented in this work is a modification of the simple genetic algorithm (see Chapter 3). It was developed by Eshelman and described in (Eshelman, 1991). The CHC abbreviation stands for Cross generational elitist selection, Heterogeneous recombination by incest prevention and Cataclysmic mutation. General scheme of CHC algorithm is shown in Figure 4.1.

The CHC algorithm monotonically collects the best individuals found so far. It starts with an initial random parent population similarly as a classical genetic algorithm. The recombination is done by the half uniform crossover called HUX, which swaps each bit with a probability of 0.5 between two individuals chosen randomly from the parent population. In this way both children get approximately a

half of the bits from each parent. An example of the HUX crossover is given in Figure 4.2.

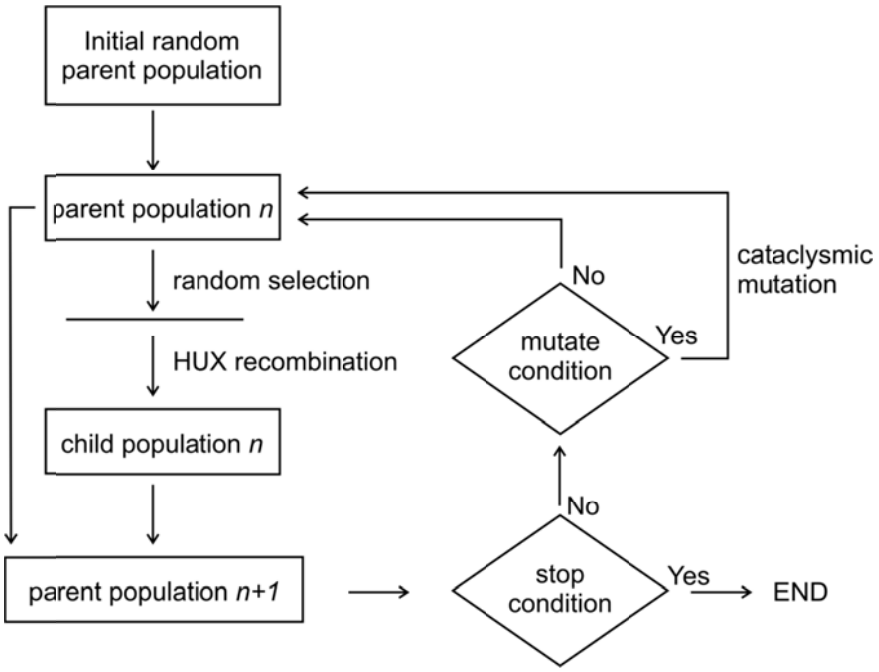

Figure 4.1: *General scheme of CHC algorithm*

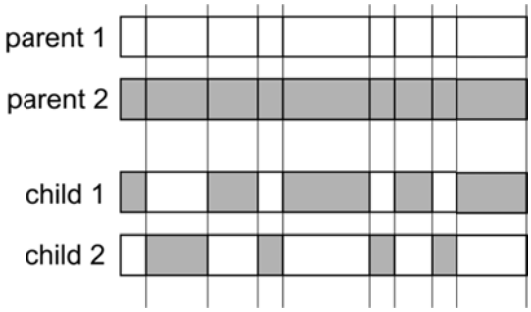

Figure 4.2: *Example of HUX crossover. Children get half of bits from parent 1 and another half from parent 2. Crossover points are chosen randomly*

Selection of the parent individuals for recombination is performed randomly with the restriction, that their binary encodings must be a certain Hamming distance (number of the bits in which the binary encodings differ one from another) apart from one another. For example, two parents with binary encodings "100011100101" and "100100110011", respectively, are not allowed to be chosen for recombination if the required Hamming distance is larger than 6. Such "incest prevention" is designed to promote diversity in the offspring population. However, in progress of optimization the required Hamming distance is being gradually decreased allowing the algorithm to converge to the optimum.

After recombination, the N best individuals are drawn from both the parent and offspring populations to create the next parent generation (see Figure 4.1).

Other than in classical genetic algorithm, in the CHC algorithm no mutation operator is applied to the population individuals. However, when the population converges to the point that it begins to reproduce nearly the same individuals and the best value of the target function does not improve for a specified number of populations, then the cataclysmic mutation is performed. It heavily mutates all the individuals except for the best one, preserving the monotonicity of the best value of the target function. In the proposed implementation 35% of the bits are mutated. The cataclysmic mutation promotes diversity by adding new genetic material to the optimization and is able to kick the algorithm out of the local optimum in which it might be stuck.

The CHC algorithm typically uses small population sizes.

4.3.2. Binary (n-ary) search

The binary (n-ary) search also known as half-interval search is a simple one-dimensional search. It runs along one parameter at a time, while the other parameters remain fixed. Schematic description of the n-ary search with $n = 4$ along the chosen optimization parameter X is shown in Figure 4.3.

First, the variation range of the parameter X is divided by $n + 1 = 5$ equidistant points $x_{1,1}, x_{1,2}, \dots x_{1,5}$ at which the target function F_{target} is calculated. The points $x_{1,1}$ and $x_{1,3}$ nearest to the best point $x_{1,2}$ are then chosen as the boundaries of the new range for the second run. In this run F_{target} must be calculated at only two points $x_{2,2}$ and $x_{2,4}$ because it has already been calculated at the remaining points $x_{2,1}$, $x_{2,3}$ and $x_{2,5}$. The n-ary divisions are repeated until the value of target function does not significantly improve, that is, a given precision or discretization deepness is reached. After that, the n-ary search fixes the optimized parameter X to the obtained optimal value ($x_{3,4}$ in Figure 4.3) and moves to the next optimization parameter. This outer parameter cycle repeats over all parameters so many times until the target function F_{target} cannot be improved any more, that is, the algorithms stops if the best value of the target function in the i-th run $F_{target,i}$ equals the best value $F_{target,i-1}$ of the previous $i - 1$-th run (see Figure 4.4).

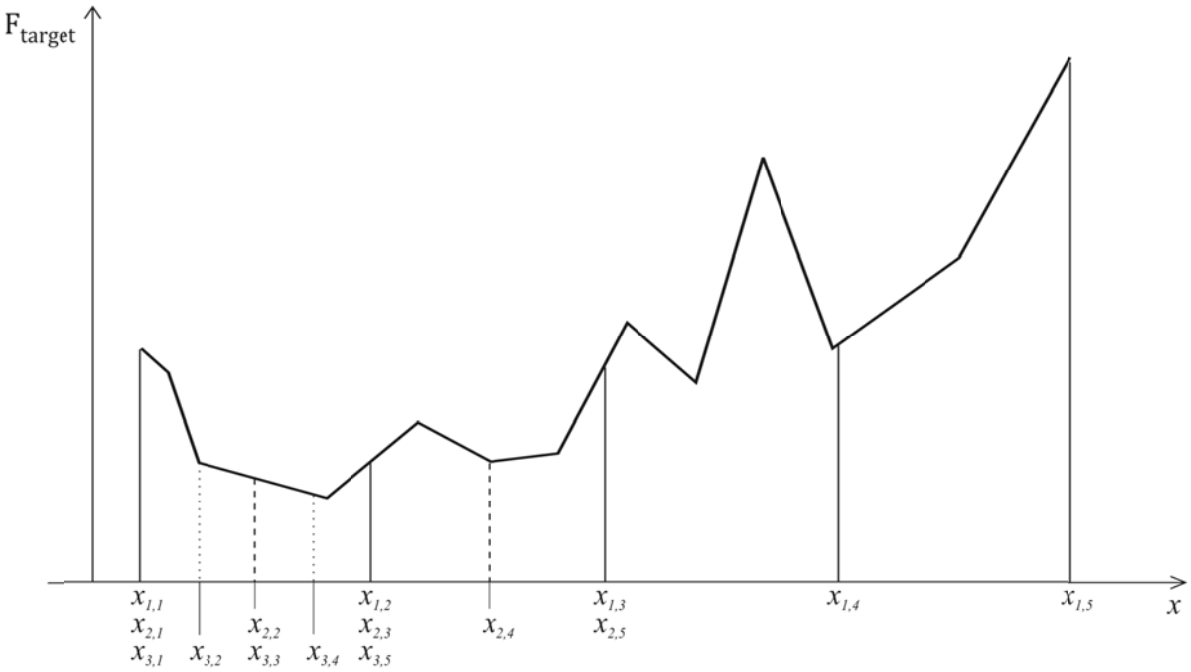

Figure 4.3: *Example of an one-dimensional optimization by the n-ary search with $n = 4$. In each deep run i, $i = 1,..,3$ target function F_{target} is calculated in equidistant points $x_{i,j}$, $j = 1,..,5$ and the point with the best F_{target} is taken as the middle of the interval for the next deep run*

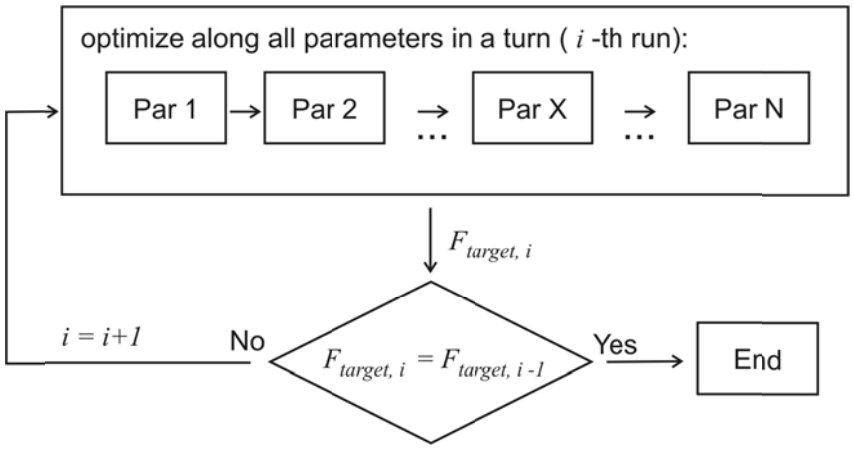

Figure 4.4: *Scheme of outer loop of the n-ary search. In each i–th run target function F_{target} is optimized along all parameters in a turn as shown in Figure 4.3. and then the optimal $F_{target,i}$ is compared with optimal $F_{target,i-1}$ from the previous run*

The n-ary search is the local optimization method as it optimizes only one parameter in a turn. However, on the contrary to the path-oriented methods which start from the initial point and move only in the direction where the target function can be locally improved, the n-ary search algorithm checks the function at n points

and it is therefore more robust and may avoid local optima as shown in an example (Figure 4.3).

4.3.3. Coupling CHC and binary (n-ary) search algorithms

Switching from the CHC algorithm to the n-ary search occurs when the best individual of the CHC has not been significantly improved for a given number of population generations. If the target function is expected to have not a very complex surface and the CHC algorithm hits the basin of the global optimum relatively fast, then it could be reasonable to switch to the n-ary search before the cataclysmic mutation of the CHC algorithm takes place. Otherwise it is better to sacrifice more computational time to the CHC algorithm and switch to the n-ary search after mutation.

The pure CHC algorithm is, in general, more reliable in finding the global optimum as it widely explores the searching space. But even this algorithm might stuck in the local optimum in the case if the population size is chosen too small or restriction on the Hamming distance between two mating individuals is too weak. It is possible in this situation that the n-ary search hits out of the local optimum and reaches if not the global optimum then at least a better local one. The results below show exactly such a case.

The proposed hybrid algorithm should be carefully tuned with a closer look onto the complexity of the target function. To ensure the reliability, it is recommended to run the same optimization several times each time starting with different initial population, that is, different parameter values and running different ways to the optimum. If the optimization results are (nearly) the same in all runs, then it is more likely that the global optimum has been reached.

4.3.4. Implementation in GenOpt. Coupling with TRNSYS

The proposed hybrid algorithm was coded in Java programming language and implemented in generic optimization software (GenOpt) (Wetter, 2008). GenOpt provides standard routines for input/output, interaction with the simulation software, error handling, etc., what lets the developer to fully focus on the algorithm implementation. GenOpt software can be easily coupled with any simulation environment like TRNSYS, input/output of which can be done via usual ASCII-coded text files. The information flow between GenOpt and simulation program is shown in the Figure 4.5.

GenOpt starts with reading the initialization, configuration and command text files through which it gets the locations of the files needed for simulation, description of the optimization parameters and settings of the chosen optimization algorithm. The optimization algorithm prepares the input file for TRNSYS, by assigning the values to the optimization parameters in the so-called simulation template file which describes the model to be optimized. GenOpt starts TRNSYS simulation and after it is successfully completed, reads the value of the calculated target function from the specified simulation output file. Based on it, the optimization algorithm decides on new values which are to be assigned to the optimization parameters, prepares next input file and runs the simulation again. This loop repeats until the terminating condition of the optimization algorithm occurs. If the TRNSYS simulation terminates with an error then an appropriate error message appears in the GenOpt graphical user interface and the optimization algorithm is informed about it. It is up to the algorithm to decide how the simulation errors shall be handled. In the implementation of the hybrid algorithm, a large value of target function is assigned to such an “invalid” parameter configuration to possibly skip it in successive populations, but the optimization does not terminate, it continues running.

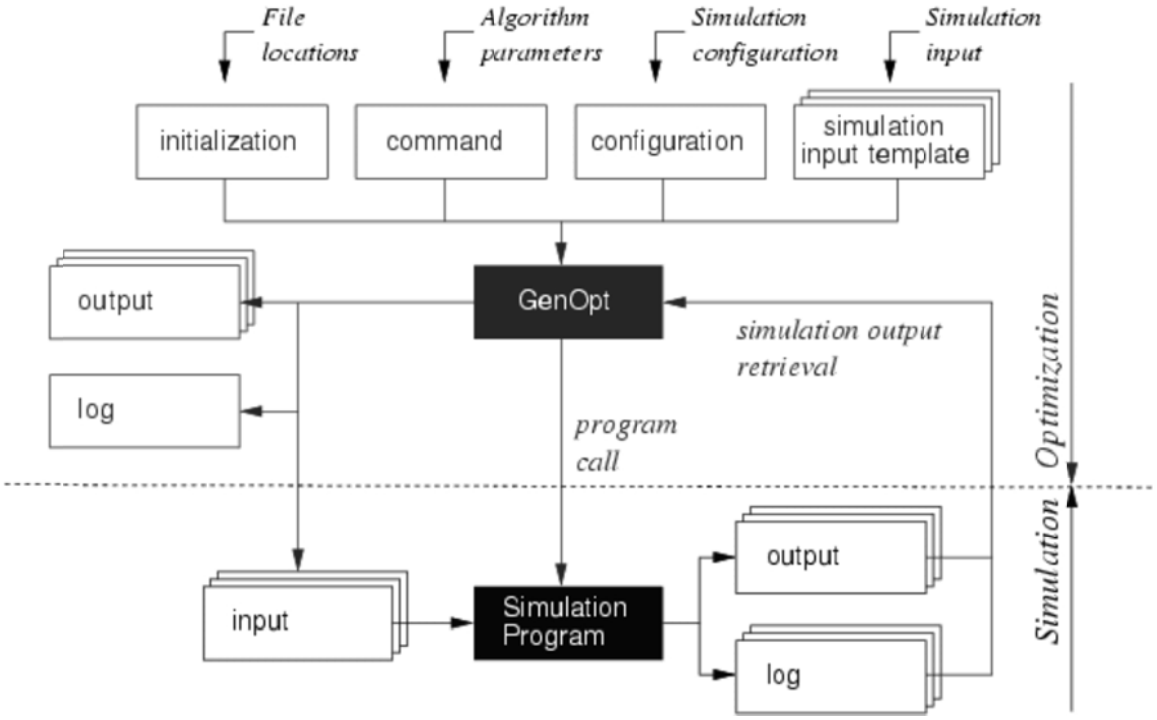

Figure 4.5: *Coupling GenOpt with a simulation program, information flows. Source: (Wetter, 2008)*

For more detailed description of coupling GenOpt with TRNSYS refer to the GenOpt manual (Wetter, 2008).

4.3.5. Potential of Parallelization

Genetic algorithms in common and the proposed hybrid algorithm in particular can be easily parallelized on multi-core CPUs to decrease the computation time of the algorithm and achieve the efficient use of the hardware. Simulations done by the genetic algorithms to calculate the target function for each individual in a certain generation may run in parallel as they do not exchange any information and do not depend on each other. Let the population size be N, and at least the same number of CPUs is available. Consider an ideal case when simulation runtime is the same for calculating the target function for all individuals, that is, it does not depend on system parameter configuration. Then the simulation of the whole genetic algorithm may be decreased in N times by means of parallelization. In practice, runtimes of single simulations are unequal not only because TRNSYS simulations for some system configurations last longer than for others but also because it might be the case that some of N available CPUs must be shared with other applications running on the same machine. Some CPUs will stay idle after finishing their simulations

waiting for other CPUs which still calculate. From this reason for genetic algorithm with population size N the parallelization potential will be less than N.

In general, potential of parallelization for the hybrid CHC – binary search algorithm is lower than for the pure CHC algorithm because for the binary search algorithm the number of simulations which can be run in parallel is normally less than the population size N of the CHC algorithm. If more than one optimization is to be done it looks reasonable to start them in parallel to use idling CPUs more efficiently.

Parallelization does not necessarily mean the investment into an expensive multi-core server in order to be able to implement it and use its benefits. Distributed computing which is performed on available computational resources in the network might be used as well. The parallelized version of the current implementation of the hybrid algorithm was coded and run on computers in the network by means of open source HTC Condor (High Throughput Computing) distributed computing software. The HTC Condor software performs all the management tasks like monitoring the available computational resources (CPUs) in the network, submitting und running the jobs (simulations) on these CPUs, migrating the job if the CPU is no more available, etc. See the HTC Condor manual (HTCondor, 2017) for further explanations about installation and running jobs within HTC Condor environment.

4.3.6. Reliability

The probability with which the optimization algorithm hits the optimum is one of the most important characteristics of the algorithm and it is called to be the reliability of the algorithm. The optimization algorithms are tested on certain mostly analytical target functions of different complexity for which the optimum points are known in advance. The algorithms are tested for reliability (how often they found the optimum) and benchmark (how fast they found the optimum). After testing one may assert that a particular algorithm works better on some functions and worse on others.

In real applications the complexity of the target function and particularly where its optimum is located are, as a rule, unknown. Thus, the reliability of the algorithm cannot be easily estimated. In this case, the algorithm is run a number of times each time starting with different randomly chosen initial population. If the optimum found after each optimization is the same or nearly the same, then the probability is high that it is the sought global optimum, and that the algorithm is reliable.

Otherwise, the algorithm settings must be tuned up in order to enhance diversity, for example, by increasing the population size, allowing more cataclysmic mutations in CHC algorithm, etc. If this does not work, another algorithm should be chosen.

In this study, to test the reliability, the hybrid CHC – binary (n-ary) search algorithm was started 6 times in a row for chosen optimizations. All the optima found by the algorithm differed less than $1-2\%$ from their mean value, depending on the number of optimization parameters, boundary conditions and system configurations. This means that most probably the global optimum was found each time and the algorithm might be seen as a reliable one.

4.4. Results of optimization

The proposed above hybrid CHC – binary (n-ary) search optimization algorithm is applied to optimization of the solar combisystem described in Chapter 2. The solar combisystem supplying heat to a two-story single family house located in Zurich, Switzerland is to be optimized. The house has $140\,m^2$ of the floor area, space heating demand of $60\,kWh/m^2a$ and domestic hot water consumption is set to $200\,l/d$. List of optimization parameters which are varied during the optimization is given in Table 4.1 and the target function F_{target} is defined by (4.1).

4.4.1. Behaviour of hybrid CHC – binary (n-ary) search algorithm

In Figure 4.6 improvement of the target function F_{target} with $c = 0.3$, that is, with the extended fractional savings $f_{sav,ext}$ of the combisystem required to be not less than 0.3 is shown for one run of the CHC - binary search hybrid optimization algorithm. Overall 3642 calculations of the combisystem are started by the algorithm from which 2180 are unique, that is, for that many combisystem configurations TRNSYS simulations are carried out. The exploratory CHC part of the algorithm (solid line in Figure 4.6) is run up to the simulation number 2261 and then the algorithm switched to local binary (n-ary) search (dashed line). Overall 1511 unique simulations are started by the CHC algorithm and 669 by the binary search. This ratio is rather typical for optimizations presented in this study.

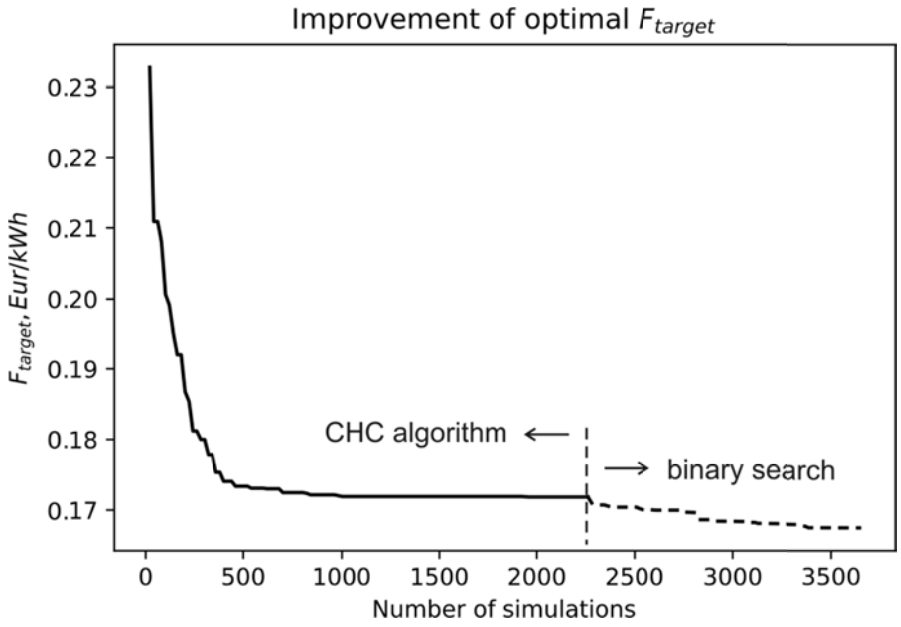

Figure 4.6: *Progress of optimization by CHC - binary search hybrid algorithm for F_{target} with $c = 0.3$ constraint on $f_{sav,ext}$. CHC algorithm (solid line) is switched to binary search (dashed line)*

As it is seen from Figure 4.6 the CHC algorithm converged relatively fast (in around 500 first simulations) to the basin of likely global optimum, but then many simulations were spent by exploring other regions of the parameter space. For this three cataclysmic mutations of the CHC algorithm were applied but they brought no essential improvement to the optimal solution. The binary search which was launched after the CHC algorithm finished, localized the optimal solution with $F_{target} = 0.1675\ Eur/kWh$ and $f_{sav,ext} = 0.30$.

In Figure 4.7, the best values of the target function obtained so far by the proposed hybrid CHC-binary (n-ary) search (dashed lines) and by the pure CHC genetic algorithm (solid lines) versus the number of simulations are presented. This figure is picked out from (Kusyy, 2010). In fact, it is obtained for the target function in the form identical to F_{target} which is used throughout this thesis but having the cost function F_{cost} somewhat differently defined. However, it is irrelevant here because not the absolute values of the target function but the performance of the algorithms is of the main importance.

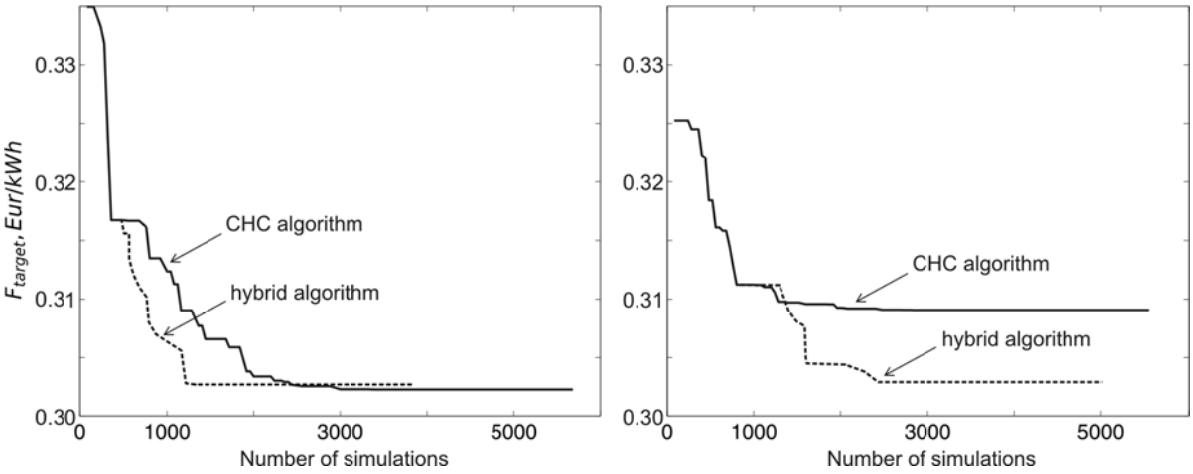

Figure 4.7: *Performance of hybrid CHC - binary search algorithm vs. pure CHC algorithm for two independent runs (Kusyy, 2010). Left figure shows typical pattern of faster convergence of the hybrid algorithm compared to the pure one and both algorithms reach the same optimum. Right figure shows pure CHC algorithm stuck at local optimum whereas hybrid algorithm found probably the global one*

Figure 4.7 shows two independent optimization runs for the both algorithms. The first run (left graph in Figure 4.7) shows the pattern which is frequently observed whereas the second run (graph to the right) is most likely an exception. The results are the same up to the point at which the binary search is launched. In the first run it is seen that the binary search can accelerate the convergence and ends up at the same optimum almost two times faster than the pure CHC algorithm does.

In the second run (right graph in Figure 4.7), the CHC algorithm stuck in a local minimum, whereas the binary search improved the solution up to the (likely) global minimum. Although in the second run the hybrid algorithm needs almost as many calculations as the pure CHC algorithm in the first run, it is more reliable. It is not typical that the pure genetic algorithm is worse in terms of reliability than the hybrid algorithm based on it. It can be explained by not optimally chosen settings of the algorithm such as small population size, rough discretization of the parameter space, weak constraint on the Hamming distance, which might cause fast convergence of the genetic algorithm to the local optimum. In this example, the binary (n-ary) search runs with $n = 4$, the population size of the CHC algorithm is taken as $N = 30$. Switching from the CHC algorithm to the binary search is done early, just before the first cataclysmic mutation of the CHC algorithm, because the study of the target function surface showed that it is quite shallow and relatively smooth in the basin of expected optimum.

In the following optimizations as well as in the optimization from Figure 4.6 above, the hybrid CHC-binary (n-ary) search algorithm is configured with the smaller

population size $N = 20$ and three cataclysmic mutations before switching to the binary (n-ary) search with $n = 4$. Smaller population size is chosen to get more quickly to the basin of global optimum. The reliability of the hybrid algorithm is ensured by three cataclysmic mutations in the CHC algorithm and capability to avoid local optimum by binary search. Another reason to choose the settings so that more simulations are performed by the CHC algorithm than by binary search is better ability of parallelization of the CHC algorithm along with sufficient number of CPU cores available.

In general, when not enough computational resources are available early switching to binary search might noticeably decrease the optimization time but probably at the cost of reliability. To decide on the early switching, a priori information about the complexity of the target function might be helpful. Reliability of the algorithm should be also checked by running the algorithm a number of times on the same problem each time starting with different initial population.

4.4.2. Pareto front

Solar combisystem is optimized for different given extended fractional energy savings $f_{sav,ext}$. Seven optimizations are carried out with respect to F_{target} with different constraints $c, c = 0.3, 0.35, \dots, 0.6$ on the $f_{sav,ext}$, as well as one optimization is started without any constraint, that is, with $c = 0$. The optimization function F_{target} plotted versus $f_{sav,ext}$ shows the Pareto front, that is, minimal costs per kWh of saved auxiliary energy for each given extended fractional energy savings $f_{sav,ext}$. Each point (F_{target}, $f_{sav,ext}$) lying to the left of the Pareto front is not reachable, that means, no combisystem can be built having such properties. On the other hand, each combisystem with the properties (F_{target}, $f_{sav,ext}$) lying to the right of the Pareto front is realizable but not optimal.

The Pareto front for the investigated solar combisystem is shown in Figure 4.8

Optimum of each optimization corresponding to a given constraint $c, c = 0.0, 0.3, 0.35, \dots, 0.6$ is marked by a blue cross. Colored points depict the properties (F_{target}, $f_{sav,ext}$) of intermediate non-optimal system configurations which are calculated by the algorithm before the optimum is reached. Colors of the points correspond to the constraint c, for example, red color means $c = 0.35$, black - $c = 0.5$, etc. Higher density of the points is observed in the vicinity of the crosses where the algorithm converges and performs more calculations. Only the points

corresponding to combisystem configurations with $F_{target} < 0.23\ Eur/kWh$ are shown for better visibility. Blue dashed line connecting the blue crosses shows interpolation of the Pareto front.

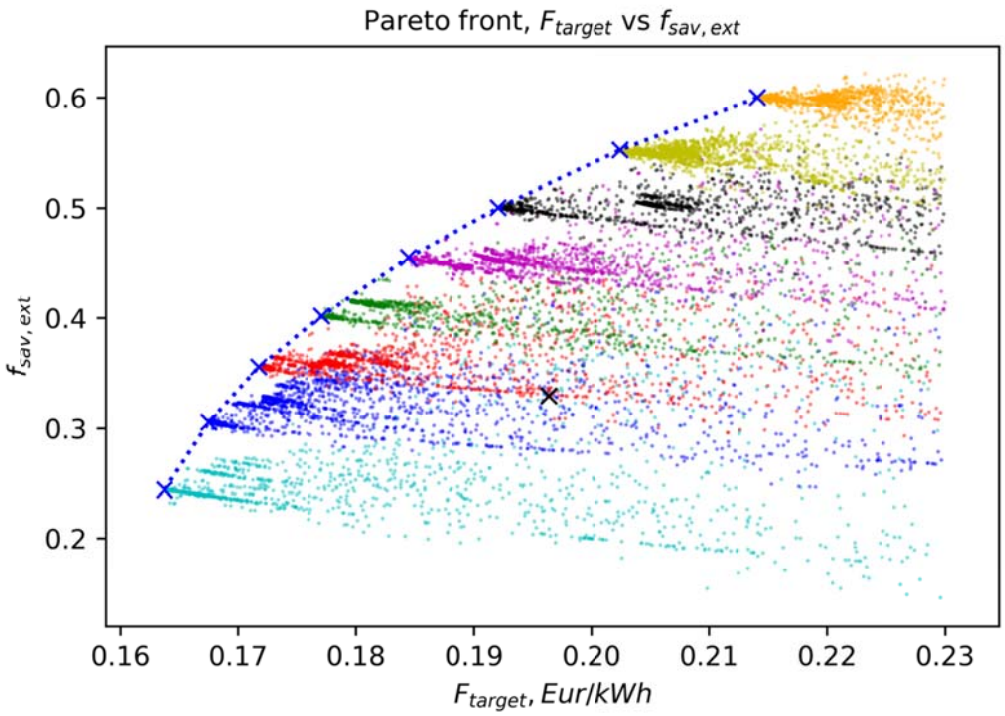

Figure 4.8: *Interpolation of Pareto front: optimal F_{target} versus $f_{sav,ext}$. Results of 8 optimizations are shown by blue crosses. Colored points depict non-optimal configurations (F_{target}, $f_{sav,ext}$) calculated in progress of optimizations. Colors correspond to same optimization, that is same constraint c on $f_{sav,ext}$. Black cross shows properties (F_{target}, $f_{sav,ext}$) of base combisystem*

4.4.3. Optimization potential. Comparison to Task 32 reference combisystem

The base configuration of solar combisystem from IEA Task 32 has the extended fractional energy savings $f_{sav,ext}$ around 0.33 and energy costs of 0.1964 Eur per kWh of saved final auxiliary energy. This point is depicted by the black cross in the Figure 4.8. The costs for kWh of saved final auxiliary energy reachable for the combisystem with the same fixed $f_{sav,ext} = 0.33$, is nearly 0.17 Eur/kWh what is around 13.5% cheaper than that for the base configuration. On the other hand at nearly the same F_{target} as for the base system, it is possible to construct the combisystem with noticeably higher fractional energy savings $f_{sav,ext} = 0.52$.

Optimal values of optimization parameters, target function F_{target}, corresponding $f_{sav,ext}$, energy amounts such as solar yield, auxiliary energy Q_{aux}, store losses Q_{loss}, etc., measured at the store inputs, various capital and annuity costs for end user and installer / energy contractor both with interest rate of 2.5% and when investing own capital, are listed in Table 4.2 for all eight optimized combisystems along with the base case.

Table 4.2: *Properties of solar combisystem optimized for different extended energy savings* $c = 0.0, 0.3, 0.35, \ldots, 0.6$. *Optimal values of parameters being varied, energy demands, solar yield and store losses for both reference heating system and optimized solar combisystems followed by differently defined capital and annuity costs (see subsection 4.1.2) and resulting target functions are showed together with reached fractional energy savings. First column shows properties of base case combisystem defined in framework of the IEA Task 32*

	base case Task 32	opt1, $c = 0.0$	opt2, $c = 0.3$	opt3, $c = 0.35$	opt4, $c = 0.4$	opt5, $c = 0.45$	opt6, $c = 0.5$	opt7, $c = 0.55$	opt8, $c = 0.6$
Optimization parameters									
Collector area, m^2	20	10	14	19	24	30	38	45	54
Store volume, m^3	2	0.8	1.2	1.5	1.9	2	2.1	2.5	3.1
Auxiliary volume, m^3	0.2	0.14	0.16	0.14	0.12	0.2	0.12	0.16	0.18
Store insulation, m	0.15	0.2	0.2	0.2	0.15	0.25	0.2	0.25	0.25
Pipe inner diameter, mm	13	14	10	12	12	14	14	14	16
Specific flow rate, kg/m^2h	15	36	11	10	10	9	10	9	8
ΔT upper dead band, K	7.0	4.5	4.0	4.0	4.0	4.5	9.5	5.5	6.5
ΔT lower dead band, K	4.0	0.7	4.0	1.9	2.1	1.0	2.1	0.7	1.7
ΔT sensor pos. in store, %	0.1	0.15	0.15	0.15	0.15	0.15	0.07	0.13	0.07
UA of solar HX, W/K	2100	1000	1000	1300	1900	2200	2500	3100	3400
UA of DHW HX, W/K	5333	5340	6580	5340	6580	5960	7200	7200	6580
Coll. inlet pos. in store, %	0.4	0.65	0.81	0.84	0.81	0.84	0.87	0.84	0.68
SH outlet pos. in store, %	0.96	0.85	0.88	0.91	0.94	0.91	0.95	0.94	0.95
SH inlet pos. in store, %	0.15	0.28	0.30	0.30	0.27	0.27	0.27	0.26	0.18
Set temp. of aux. heater, $°C$	63	55	52	55	55	54	54	51	51
Aux. upper dead band, K	8	9.6	7.2	7.2	10.4	11.2	10.4	8.0	8.8
Aux. lower dead band, K	2	2.6	2.1	2.8	3.8	2.6	3.8	2.6	3.5
Collector slope,°	45	51	53	56	57	61	60	60	61
Energy quantities, MWh/a									
Aux. energy demand, Q_{aux}	7.82	8.84	8.08	7.45	6.89	6.24	5.68	5.02	4.43
Solar yield, (kWh/m^2a)	5.89 (294)	3.54 (353)	4.51 (322)	5.34 (281)	6.50 (270)	6.68 (222)	7.58 (199)	8.17 (181)	9.09 (168)
Store losses	2.30	1.00	1.22	1.41	1.99	1.50	1.82	1.74	2.05
Ref. store losses, $Q_{loss,ref}$	0.64	0.64	0.64	0.64	0.64	0.64	0.64	0.64	0.64
SH demand, Q_{SH}	8.46	8.44	8.44	8.44	8.45	8.45	8.46	8.45	8.45
DHW demand, Q_{DHW}	2.93	2.93	2.93	2.93	2.93	2.93	2.93	2.93	2.93
Ref. demand, E_{ref}	14.72	14.7	14.7	14.7	14.71	14.71	14.72	14.72	14.72
Ref. el. demand, $E_{par,ref}$	0.23	0.23	0.23	0.23	0.23	0.23	0.23	0.23	0.23
Solar demand, E_{sol}	9.88	11.11	10.21	9.47	8.80	8.02	7.36	6.59	5.88
Solar el. demand, $E_{par,sol}$	0.27	0.28	0.27	0.27	0.27	0.27	0.26	0.26	0.26

Capital costs, $kEur$ (Eur/m^2)									
End user $F_{cost,cap}$	13.3	8.2	10.5	12.5	14.6	17.2	19.7	23.0	26.4
	(663)	(819)	(749)	(659)	(608)	(573)	(519)	(510)	(488)
Contractor $F_{cost,cap}$	8.9	5.5	7.0	8.4	9.7	11.5	13.2	15.3	17.6
	(442)	(546)	(499)	(439)	(405)	(382)	(346)	(340)	(325)
Target function (Annuity costs), Eur/kWh (Eur/a)									
End user, interest rate 2.5%	**0.196**	**0.164**	**0.168**	**0.172**	**0.177**	**0.184**	**0.192**	**0.202**	**0.214**
F_{target}, (F_{cost})	(951)	(587)	(752)	(898)	(1046)	(1234)	(1414)	(1645)	(1891)
End user, own capital	0.158	0.131	0.134	0.138	0.142	0.148	0.154	0.162	0.172
F^0_{target}, (F^0_{cost})	(763)	(471)	(603)	(721)	(840)	(990)	(1134)	(1320)	(1517)
Contractor, int. rate 2.5%	0.131	0.109	0.112	0.115	0.118	0.123	0.128	0.135	0.143
$F_{target,contr}$, $(F_{cost,contr})$	(634)	(391)	(501)	(598)	(697)	(822)	(942)	(1096)	(1260)
Contractor, own capital	0.105	0.088	0.090	0.092	0.095	0.099	0.103	0.108	0.115
$F^0_{target,contr}$, $(F^0_{cost,contr})$	(509)	(314)	(402)	(480)	(560)	(660)	(756)	(880)	(1011)
Contractor, own cap., no tax	0.088	0.074	0.075	0.077	0.080	0.083	0.086	0.091	0.096
$\hat{F}^0_{target,contr}$, $(\hat{F}^0_{cost,contr})$	(427)	(264)	(338)	(403)	(470)	(554)	(635)	(739)	(850)
Extended fractional energy savings									
$f_{sav,ext}$	**0.329**	**0.244**	**0.305**	**0.356**	**0.402**	**0.455**	**0.500**	**0.552**	**0.600**

It is seen from Table 4.2 that the Task 32 reference combisystem is more expensive than the optimal combisystem with approximately the same fractional energy savings. It is mostly due to larger collector area and store volume. The auxiliary heating volume is also slightly larger but the store insulation is thinner. The store losses are with 2.3 MWh/a noticeably larger than by the optimal combisystem (only ca 1.3 MWh/a). The systems significantly differ also in specific flow rates, set temperatures of the auxiliary heater, collector inlet positions, etc. However it is not obvious which parameters except, probably, collector area and store volume, make the most contribution to the difference between target functions of the both combisystems. The results of sensitivity analysis from Section 4.5 might be used for rough estimation.

The optimal combisystem with similar solar energy costs F_{target} as the reference system reaches almost 19% higher $f_{sav,ext}$. It has significantly more solar collectors ($38m^2$ vs $20m^2$) and therefore more solar yield. The store volume remains nearly the same; the store losses are still smaller due to more store insulation and lower auxiliary set temperature.

4.4.4. Profitability of optimized solar combisystem

In order to calculate the profitability of the solar combisystem solar energy costs and reference fuel price, for example, gas price should be at hand for the lifetime period of the system. In Figure 4.9 profit over 20 years compared to reference fuel

price taken constant at 0.16 Eur/kWh is shown versus extended fractional savings of the system for five different solar energy costs functions (see Table 4.2 and definitions from subsection 4.1.2). According to the figure, different size (fractional energy savings) of the combisystem is optimal for each solar energy costs function. For example, for the private person investing its own capital (magenta curve) the solar combisystem with $f_{sav,ext} = 0.35$ would be the most profitable and it would bring around 2.3 $kEur$ over 20 years at this fuel price level. For the contractor investing own capital (no tax), the solar combisystem with $f_{sav,ext} = 0.55$ would be the best, bringing 11.2 $kEur$ profit.

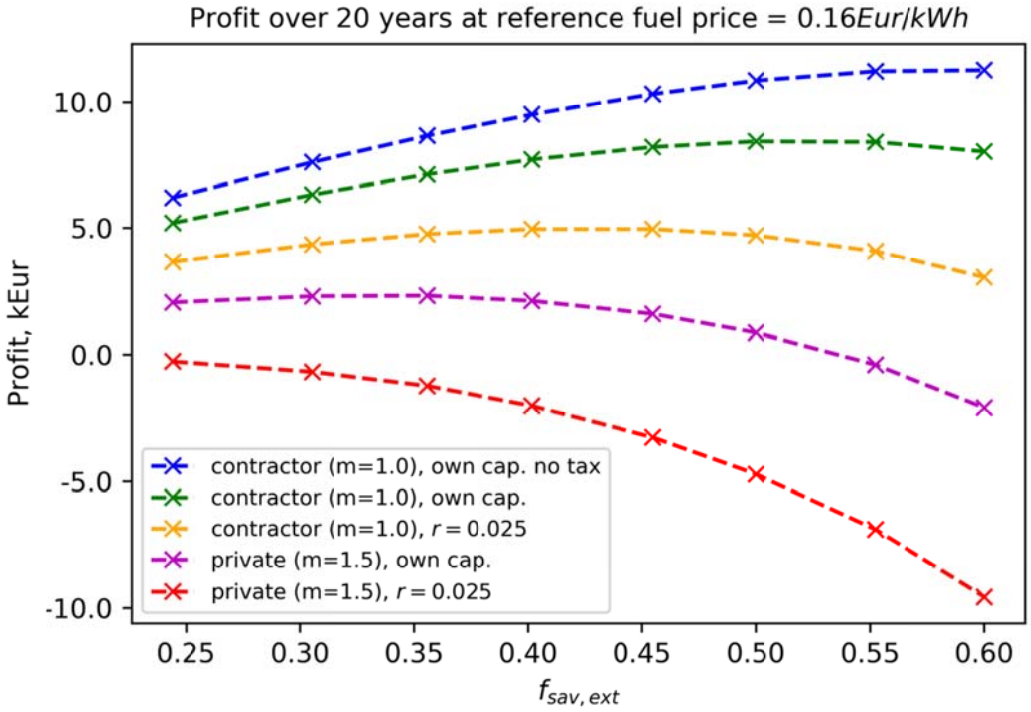

Figure 4.9: *Profit calculation over 20 years lifetime for different extended fractional savings (system size) and five differently defined cost functions (private, contractor). Reference fuel price is set constant to* 0.16 Eur/kWh *for lifetime period*

It is obvious that the profit calculation and consequently the best size of the solar combisystem are influenced by the reference fuel price to much extent. Changing the gas price to 0.10 Eur/kWh makes the combisystem for the three out of five cost functions unprofitable. Only for the contractor investing own money (no tax) the solar combisystem remains bringing small profit with optimum around 2.4 $kEur$ at $f_{sav,ext} = 0.40$ as shown in Figure 4.10.

No governmental or any other subsidies are taken into account in profit calculations.

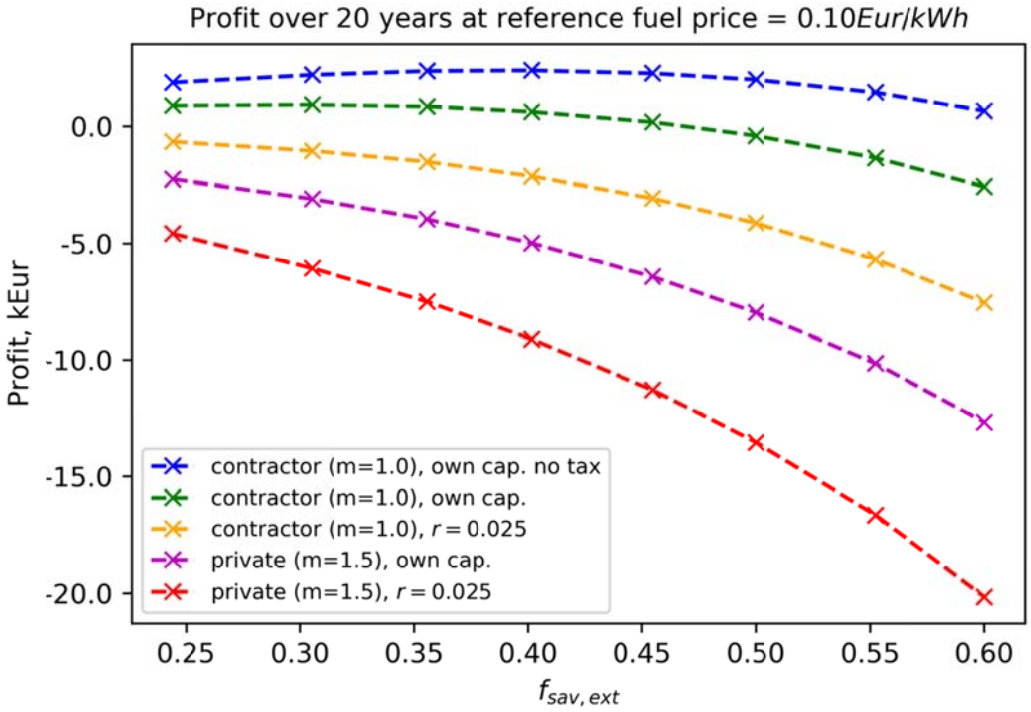

Figure 4.10: *Profit calculation over 20 years lifetime for different extended fractional savings (system size) and five differently defined cost functions (private, contractor). Reference fuel price is set constant to* 0.10 Eur/kWh *for lifetime period*

4.4.5. Influence of boundary conditions on optimization results

The boundary conditions have an influence on the single optimal combisystem configurations, as well as on the Pareto front as the whole. Sensitivity of the optimum to the alternated chosen boundary condition might also depend on the point on the Pareto front. In the following the domestic hot water demand, space heating demand and weather conditions are changed one in a turn and the corresponding Pareto fronts are calculated. Detailed optimization results in the tabular form similar as in Table 4.2 are presented in Appendix B.

Influence of domestic hot water demand

To estimate the influence of DHW demand, the demand is changed proportionally, that is, the DHW profile is simply multiplied by the factor. The combisystem is optimized for $\pm 50\%$ change in DHW consumption, that is, for $100l/d$ and $300l/d$. The corresponding Pareto fronts are shown in Figure 4.11. Grey dotted lines show $-10\%, +10\%$ and $+20\%$ with respect to F_{target} of the Pareto front for the combisystem with the base DHW demand of $200l/d$ (blue curve in Figure 4.11). From Figure 4.11 it is seen that if the DHW consumption decreases by 50% to

$100l/d$ then the solar energy costs F_{target} of the combisystem optimized for this consumption increases by around 15% depending on the point on the Pareto front. On the other hand, the combisystem optimized for 50% larger DHW demand will be around $5-8\%$ cheaper.

The quality of the solar combisystem optimized for the base DHW demand of $200l/d$ but used with reduced demand of $100l/d$ is shown by the magenta curve in Figure 4.11. It is seen that although the energy costs are increased by around $18-20\%$ in comparison to the base demand, the combisystem optimized for the base demand but used with the reduced demand is not significantly worse (only around $1-5\%$) than the combisystem optimized for the reduced demand. Similar comparison with the combisystem optimized for the increased demand of $300l/d$ does not work because of the penalty function applied when DHW demand of the given set temperature cannot be supplied.

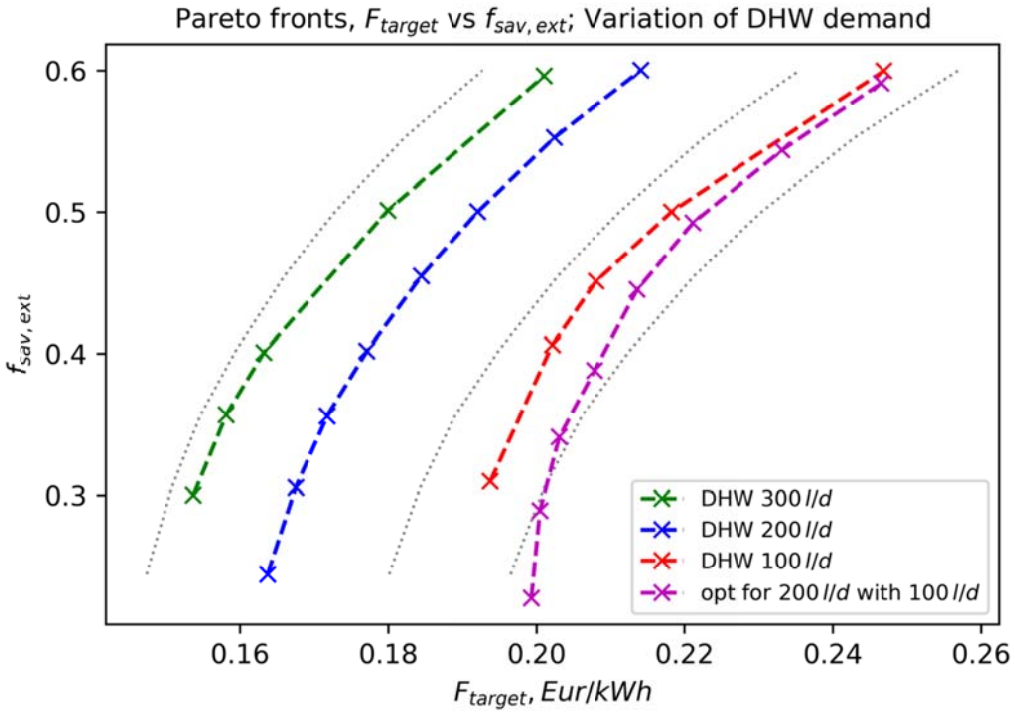

Figure 4.11: *Pareto fronts for combisystem with* $\pm 50\%$ *changed DHW demand. Grey dotted lines show* $-10\%, +10\%, +20\%$ *target function levels with respect to combisystem with base DHW demand of* $200l/d$ *(blue line). Pareto front for combisystem optimized for DHW demand of* $200l/d$ *but then used with* $100l/d$ *is shown in magenta dashed line. Results show significant influence of DHW demand*

Influence of space heating demand

Influence of the space heating demand is estimated in the similar way as that of the DHW consumption. Three building envelopes are defined within IEA Task 32 having space heating demand of $30, 60$ and $100\ kWh/m^2a$. Pareto fronts for the optimal combisystems for all three buildings located in Zurich are shown in Figure 4.12. The curves lie close to each other, differing in less than 5%. A closer look at the data behind the curves reveals more distinctions, for example, to reach $f_{sav,ext} = 0.50$ by the combisystem optimized for the SH demand of $30\ kWh/m^2a$, collector area of $20\ m^2$ is required, for $60\ kWh/m^2a$ - $38\ m^2$ and for $100\ kWh/m^2a$ - $57\ m^2$. The fact that the green curve corresponding to SH demand of $30\ kWh/m^2a$ lies to the right of the blue one can be explained by good house insulation – SH demand is shifted to colder months with less solar yield.

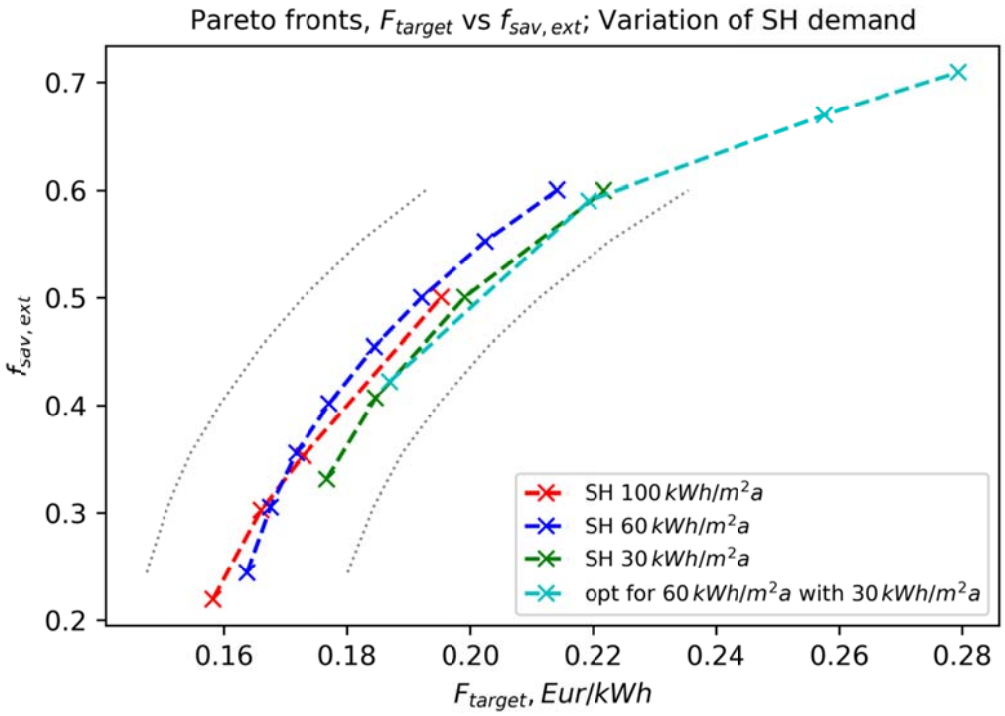

Figure 4.12: *Pareto fronts for combisystem with changed SH demand. Grey dotted lines show $-10\%, +10\%$ target function levels with respect to combisystem with base SH demand of $60\ kWh/m^2a$ (blue line). Pareto fronts for combisystem with changed SH demand lie close to each other, however, system configurations differ significantly. Combisystem optimized for SH demand of $60\ kWh/m^2a$ and then applied to better insulated house with $30\ kWh/m^2a$ (in cyan) remains optimal but each point on base Pareto front is shifted to point located higher on this line*

The combisystem optimized for the SH demand of $60\ kWh/m^2a$ but calculated with $30\ kWh/m^2a$ is almost as good as the combisystem optimized for $30\ kWh/$

m^2a. This is shown by the cyan curve in Figure 4.12 built through only the selected points (cyan crosses) which do not induce large DHW penalty. The curve is shifted up meaning that, for example, the combisystem with $f_{sav,ext} = 0.30$ optimized for the SH demand of $60\ kWh/m^2a$ obviously has significantly higher $f_{sav,ext} = 0.42$ when applied to the house with $30\ kWh/m^2a$ heating demand.

Influence of weather conditions

To estimate influence of the weather condition on the optimum, the combisystem is optimized for two more locations, Stockholm and Madrid. Corresponding Pareto fronts are shown in Figure 4.13.

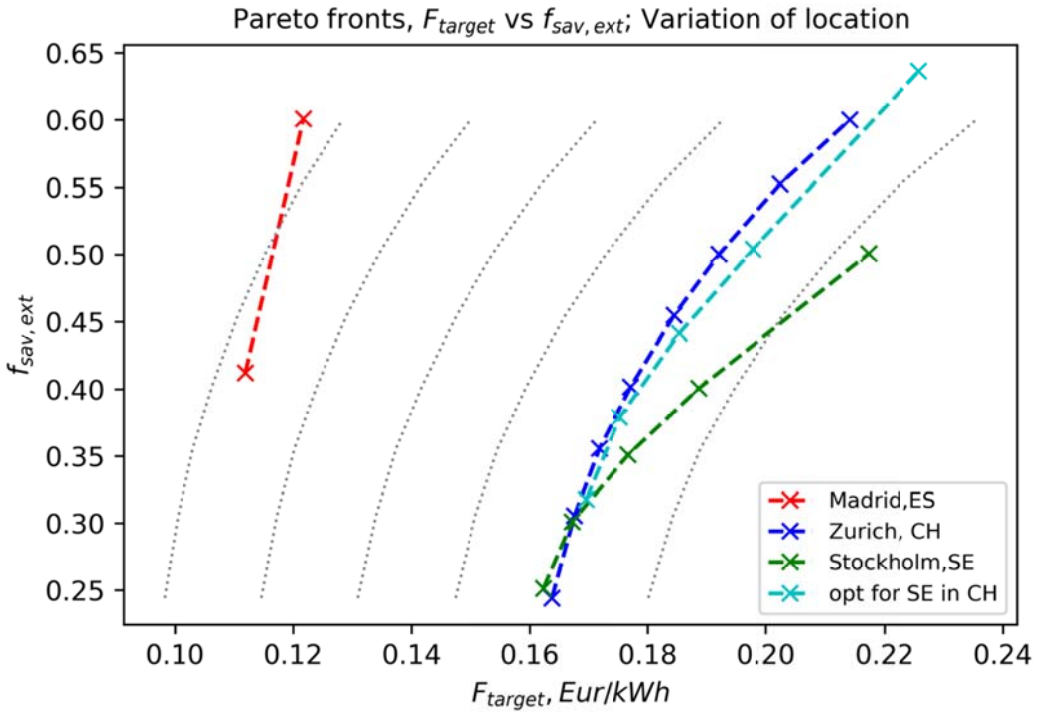

Figure 4.13: *Pareto fronts for combisystem optimized for different locations. Grey dotted lines show in 10% steps target function levels with respect to combisystem located in Zurich. Combisystem built in Madrid is around 40% cheaper. Combisystem built in Stockholm is nearly same expensive as that located in Zurich for $f_{sav,ext} < 0.35$ but it is more expensive for larger $f_{sav,ext}$. Combisystem optimized for Stockholm location and then built in Zurich is almost optimal but with similar shift as for variation of SH demand*

In Madrid location the combisystem is optimized with less insulated house having larger space heating demand of $100\ kWh/m^2a$ if located in Zurich but still with only around $42\ kWh/m^2a$ for Madrid. The solar energy costs are nearly equal for the combisystems built in Stockholm and Zurich for $f_{sav,ext} < 0.35$; For higher

$f_{sav,ext}$ up to 0.50 the comibsystem for Stockholm is up to 12% more expensive whereas the combisystem built in Madrid is around 40% cheaper.

Similarly as in the case of variation of space heating demand above, variation of the location (simultaneous variation of solar gain and space heating demand) leaves the combisystem to be nearly optimal, at least when moving the combisystem from Stockholm to Zurich as it is shown by cyan curve in Figure 4.13.

4.5. Application of sensitivity analysis around the optimum of solar combisystem

In this section the results of application of sensitivity analysis methods theoretically described in Section 3.2 are presented. First influence of selected parameters on the solar energy costs F_{target} is calculated by simple parameter variations (one at a turn) at the optimum point. Estimation of the sensitivity of the solar energy costs F_{target} upon single parameters varied in a larger parameter space containing the optimum point is carried out by global sensitivity analysis methods: Multiple Linear Regression (MLR) method, Morris method and Fourier Amplitude Sensitivity Test (FAST) method. Sensitivity analysis is applied to the solar combisystem already optimized for the reference boundary conditions: Location in Zurich, DHW demand of 200 l/d, SH demand of around 8400 kWh/a (60 kWh/m^2a), and the cost of the system defined as in subsection 4.1.2. No constraints are applied to $f_{sav,ext}$ in calculations.

Since the sensitivity analysis requires many calculations with parameter values varying around the optimum point, the probability is large that the DHW and SH demands cannot be fully covered by certain combisystem configurations and the respective penalties apply. It is because the combisystem optimized for given boundary conditions in particular for certain DHW and SH demand profiles, is actually fitted to these conditions in the sense that it is dimensioned to be able to deliver exactly an energy amount required to cover the peak demand. Already slight variations of system parameters might cause the penalty applied. To avoid too high distortion of the target function and, as a result, unexpected non-linearity or too sensitive parameters in all following calculations, the DHW and SH penalties (2.7), (2.8) are replaced with the less strict linear functions:

$$F_{pen,DHW} = \dot{m} \cdot c_p \cdot \Delta T_{DHW}/3600, \text{ [kWh]} \tag{4.9}$$

$$F_{pen,SH} = UA \cdot \Delta T_{SH}/1000, \text{ [kWh]} \quad (4.10)$$

In this way it is assumed that the amount of energy most probably missing only at times of peak consumption, is just as if delivered to the consumer by an external source. This simplification, in fact, may slightly promote the penalized configurations, but it surely helps to estimate the sensitivities more accurately.

The influence of all 18 optimization parameters and also 2 boundary condition parameters is investigated. Two variation ranges, "broad" and "narrow", both around the optimum point, are defined for each parameter. The "broad" range comprises about $[-50\%\,;\,+50\%]$ variation around the optimum for most parameters with some exceptions, and the "narrow" range is normally a "better" half of the "broad" one, where less penalty is anticipated. It is obvious that in the "broad" range containing the optimum in the middle, larger influence on the target function and more nonlinearity is expected for each parameter whereas in the "narrow" range the influence should be less and more linear.

Table 4.3 lists the parameters and corresponding variation ranges in which their influence is investigated by applied sensitivity methods.

Table 4.3: *Parameter variation ranges for calculation of parameter influence on solar energy costs F_{target} near optimum. "Broad" variation range stretches about $[-50\%\,;\,+50\%]$ around optimal parameter value whereas "narrow" range is a half of it*

Parameter	Notation	Variation ranges	
		broad	narrow
Optimization parameters			
1. Collector area, m^2	A_{col}	[7; 21]	[14; 21]
2. Store volume, m^3	V_{store}	[0.6; 1.8]	[1.2; 1.8]
3. Number of auxiliary nodes	N_{aux}	[4; 12]	[8; 12]
4. Store insulation thickness, m	D_{iso}	[0.1; 0.4]	[0.2; 0.3]
5. Pipe inner diameter, mm	D_{pipe}	[8; 20]	[10; 15]
6. Specific collector flow rate, kg/m^2h	m_{flow}	[5.5; 22]	[11; 16.5]
7. ΔT controller upper dead band, K	$\Delta T_{col,up}$	[2; 8]	[4; 6]
8. ΔT controller lower dead band, K	$\Delta T_{col,low}$	[2; 8]	[4; 6]
9. ΔT controller sensor pos. in store	$H_{col,sens}$	[0.10; 0.16]	[0.14; 0.21]
10. UA value of external solar HX, W/K	UA_{col}	[500; 2000]	[1000; 1500]
11. Collector inlet position in store	$H_{col,in}$	[0.4; 0.96]	[0.4; 0.8]
12. Space heating outlet position in store	$H_{SH,out}$	[0.035; 0.105]	[0.07; 0.105]
13. Space heating inlet position in store	$H_{SH,in}$	[0.15; 0.5]	[0.15; 0.3]
14. UA value of external DHW HX, W/K	UA_{DHW}	[3290; 9870]	[6580; 9870]

15. Set temperature of auxiliary heater, $°C$	$T_{aux,set}$	[42; 79]	[52; 78]
16. Auxiliary controller upper dead band, K	$\Delta T_{aux,up}$	[3.6; 14.4]	[7.2; 10.8]
17. Auxiliary controller lower dead band, K	$\Delta T_{aux,low}$	[1.1; 4.3]	[2.1; 3.2]
18. Collector slope,°	sl	[43; 79]	[53; 79]
Boundary condition parameters			
19. DHW demand multiplier	DHW	[0.5; 1.5]	[1.0; 1.5]
20. Collector price, Eur/m^2	$Price_{col}$	[150; 450]	[300; 450]

4.5.1. Parameter variations at optimum point

In the following, simple parameter variations are carried out at the optimum point. The parameters are varied "one at a turn", that is, all parameters but one are fixed to their optimal values and only this single parameter is varied in a corresponding range, mostly in $[-50\% ; +50\%]$.

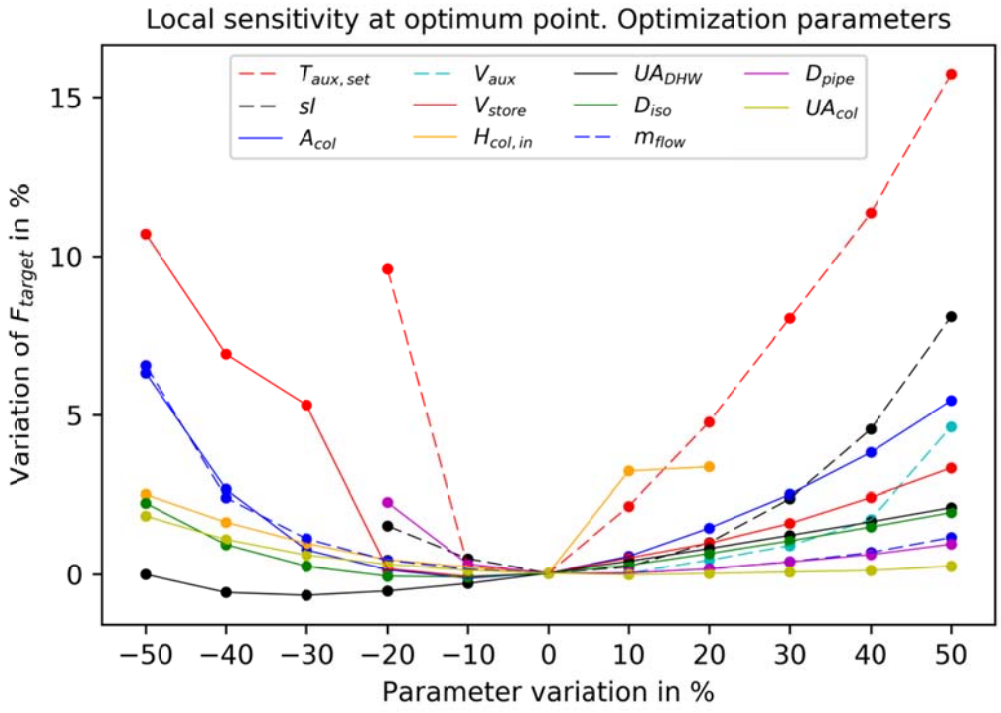

Figure 4.14: *Variations of optimization parameters at optimum point. Influence is significantly non-linear for "broad" variation range but rather linear in a "narrow" half range*

In Figure 4.14 variations of selected optimization parameter are presented. It is seen that variation of auxiliary set temperature $T_{aux,set}$ has the largest impact on the solar energy costs F_{target} : 50% increase of $T_{aux,set}$ causes 15% increase of F_{target}. Other influential parameters are the collector slope, collector area, store volume and auxiliary volume, height of the collector inlet in the store, etc. Lower and upper

dead bands of both collector and auxiliary heater controllers as well as the inlet and outlet positions of the space heating in the store have only a little influence on the target function when varied in corresponding ranges, and they are not shown in Figure 4.14. It is also easily seen that the influence is mostly nonlinear if the whole variation range is considered and rather linear for a half of the variation range [0% ; +50%].

In Figure 4.15 variation of collector price and DHW demand is shown together with variation of optimization parameters. Influence of these two parameters is significantly larger and more linear over the whole variation range than influence of the optimization parameters.

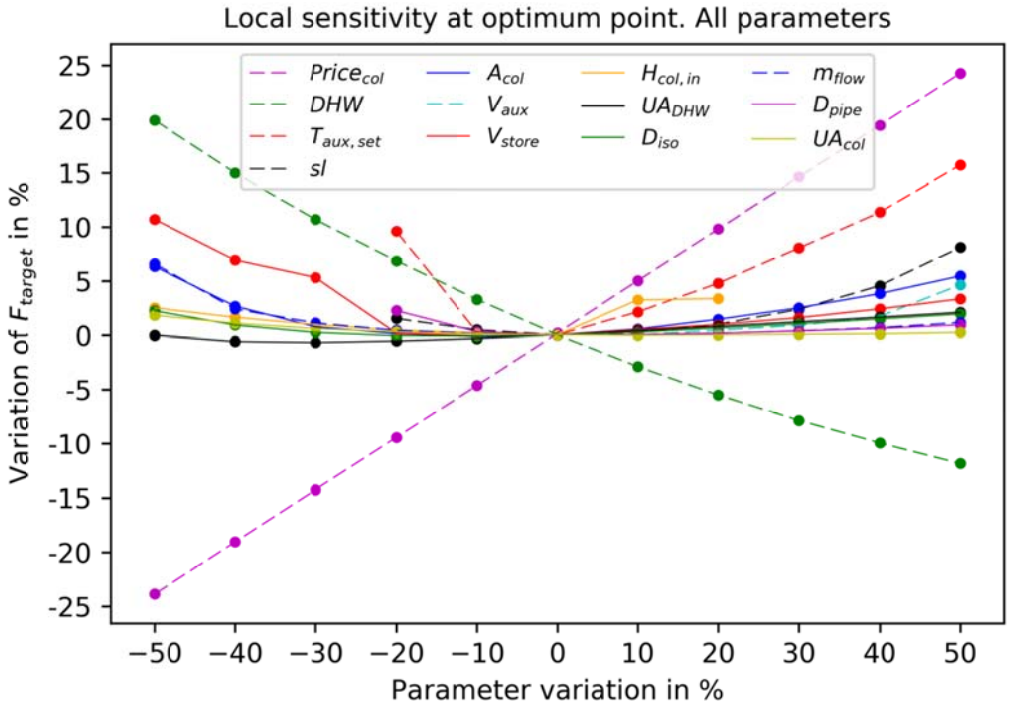

Figure 4.15: *Variations of all parameters from Table 4.3 at optimum point. Boundary condition parameters: collector price and DHW demand have significantly more influence on solar energy costs than optimization parameters in given ranges and their influence is linear over whole range*

It is obvious that the parameter variations at one point are too local. The influence of the investigated parameters showed by the variations is valid only for this selected point and it cannot be generalized on the whole parameter variation space because it might differ at other points of the space. From this reason the following global sensitivity methods are applied.

4.5.2. Results of MLR method

Parameter variations at the optimum point show that the effect of the parameters on the target function in the "narrow" variation range has mostly linear character. Although the variations are carried out only at one point and no information is available about the form of dependency at other points of the parameter space, the linear dependency may still be assumed and the MLR regression applied. The determination coefficient R^2 of the MLR model will either support or reject this assumption.

The "measured" data required as an input for the MLR are obtained as follows. First $n = 500$ parameter sets (combisystem configurations) are chosen by random sampling of the Latin Hypercube what gives the uniform distribution with respect to each parameter, and then the "measured" F_{target} is calculated by the TRNSYS simulation model for each combisystem configuration. The size n of the "measured" data has influence on the accuracy of the model, $n = 500$ is turned out to be fairly enough.

The MLR model is built on the simulated "measured" data. The estimates of the intercept b_0 and regression coefficients b_j of the corresponding combisytem parameter $x_j, j = 1,..,k$, as well as their 95% confidence intervals $[2.5\%; 97.5\%]$ and p – values showing the parameter significance level, are listed in Table 4.4.

Table 4.4: *Results of MLR method for all parameters varied in "narrow" variation space as in Table 4.3. Estimates of the intercept and regression coefficients* b_j, 95% *confidence intervals, corresponding p – values and significance levels are presented. Absolute and relative (with respect to optimum) variation of* $|\Delta F_{target}|$ *is shown due to* 55% *variation of corresponding parameters. Determination coefficient* R^2 *equals* 0.97

Paramater	b_j estimate	95% Confidence interval		p - value	Signifi-cance	$\lvert\Delta F_{target}\rvert$, Eur/kWh	$\lvert\Delta F_{target}\rvert$, % of opt.
		2.5%	97.5%				
0. Intercept	4.71e-03	-6.29e-03	1.57e-02	4.01e-01			
1. A_{col}, m^2	9.77e-04	8.40e-04	1.11e-03	< 2e-16	***	0.004	2.2
2. V_{store}, m^3	3.30e-03	1.63e-03	4.96e-03	1.19e-04	***	0.001	0.7
3. N_{aux}	9.87e-04	7.43e-04	1.23e-03	1.36e-14	***	0.002	1.3
4. D_{iso}, m	8.26e-03	-1.68e-03	1.82e-02	1.03e-01		-	-
5. D_{pipe}, mm	2.00e-04	-6.02e-06	4.06e-04	5.70e-02	.	0.001	0.3
6. m_{flow}, kg/m^2h	3.02e-04	1.29e-04	4.75e-04	6.59e-04	***	0.001	0.5

7. $\Delta T_{col,up}, K$	4.87e-04	-1.85e-05	9.92e-04	5.90e-02	.	0.001	0.3
8. $\Delta T_{col,low}, K$	-1.11e-04	-6.23e-04	4.01e-04	6.71e-01		-	-
9. $H_{col,sens}$	1.56e-03	-1.38e-02	1.69e-02	8.41e-01		-	-
10. $UA_{col}, W/K$	-3.50e-06	-5.45e-06	-1.56e-06	4.45e-04	***	0.001	0.6
11. $H_{col,in}$	-1.16e-02	-1.41e-02	-9.12e-03	<2e-16	***	0.003	1.5
12. $H_{SH,out}$	8.11e-03	-2.00e-02	3.62e-02	5.71e-01		-	-
13. $H_{SH,in}$	-6.19e-03	-1.29e-02	4.98e-04	6.96e-02	.	0.001	0.3
14. $UA_{DHW}, W/K$	9.35e-07	6.33e-07	1.24e-06	2.60e-09	***	0.002	1
15. $T_{aux,set}, °C$	1.09e-03	1.05e-03	1.13e-03	<2e-16	***	0.016	9.3
16. $\Delta T_{aux,up}, K$	-4.85e-04	-7.61e-04	-2.10e-04	5.88e-04	***	0.001	0.6
17. $\Delta T_{aux,low}, K$	-1.02e-04	-1.04e-03	8.37e-04	8.31e-01		-	-
18. $sl, °$	6.97e-04	6.59e-04	7.35e-04	<2e-16	***	0.01	6
19. DHW	-5.41e-02	-5.61e-02	-5.21e-02	<2e-16	***	0.015	8.9
20. $Price_{col}, Eur/m^2$	4.57e-04	4.48e-04	4.67e-04	<2e-16	***	0.025	15

The determination coefficient R^2 equals 0.97 meaning that 97% of the variance in measured data is explained by the MLR model. It justifies application of the MLR in the "narrow" parameter variation space. To give an example of the interpretation of the estimated regression coefficients, the coefficient $b_{20} = 4.57\text{e-}04$ for the collector price parameter $Price_{col}$ means that the increase by 1 Eur/m^2 of $Price_{col}$ causes 4.57e-04 Eur/kWh increase of the solar energy costs F_{target}. Significance level (see subsection 3.2.1) is depicted by $***$ for the estimates with $p-$values smaller than 0.001. The last two columns in Table 4.4 show the absolute and relative (comparing to the optimal F_{target}) change of the target function $|\Delta F_{target}|$, respectively, when the corresponding parameter varies over 55% of its "narrow" variation range as presented in Table 4.3. These values are calculated in order to compare with the results of the Morris method following in the next subsection.

The MLR method is also applied to the "broad" parameter variation space in order to check if the linearity assumption is still valid although it is not expected to be. Two broad MLRs models are constructed, the $MLR_{broad,all}$ model including all 20 parameters and $MLR_{broad,opt}$ including only 18 optimization parameters all varying in respective "broad" parameter ranges as listed in Table 4.3. Similarly, two narrow models $MLR_{narrow,all}$ (results already shown above in Table 4.4) and $MLR_{narrow,opt}$ are built. In Table 4.5 the determination coefficients R^2 are presented for all four models.

Table 4.5: *Determination coefficient R^2 for two "narrow" and two "broad" MLR models. Application of MLR is justified in "narrow" variation space only*

Model	Parameter space	Parameters	R^2
1. $MLR_{narrow,all}$	narrow	all	0.97
2. $MLR_{narrow,opt}$	narrow	only optimization	0.93
3. $MLR_{broad,all}$	broad	all	0.73
4. $MLR_{broad,opt}$	broad	only optimization	0.29

According to Table 4.5 the MLR models fit well the measured data for parameter variations in the "narrow" parameter space when either all 20 parameters or only 18 optimization parameters are considered. On the contrary, the "broad" MLR models are not satisfactory, due to significantly larger nonlinearity in the relationship between parameters and target function over the "broad" variation space. The $MLR_{broad,all}$ describes 73% of the measured target function variation, whereas the $MLR_{broad,opt}$ - only 29%. This difference is explained by strong linearity and large significance of the two boundary condition parameters present in $MLR_{broad,all}$.

The MLR models built for the $f_{sav,ext}$ as the target function might be also interesting to consider. The MLR model in "narrow" parameter space is briefly described in Appendix C.

4.5.3. Results of Morris method

Similarly as the MLR, the Morris method can be applied to calculate sensitivity measures of the target function with respect to variation of single parameters in a parameter space around the optimum.

The Morris method is applied to sensitivity estimation of the solar energy costs F_{target} in "narrow" and "broad" parameter variation ranges defined in Table 4.3. Settings of the method (see subsection 3.2.2) are chosen as follows: number of grid levels p is set to 10 and $\Delta = 5 \cdot 1/(p-1) \approx 0.55$ what means that the elementary effects are calculated by changing each parameter over 55% of its variation range. Number of trajectories, that is, at how many points elementary effects are evaluated for each parameter is set to 80. Since 20 elementary effects (1 effect per parameter) are calculated by each trajectory in cost of 21 evaluations of the target function, overall 1680 target function evaluations are needed for 20 parameters and 80

trajectories. The results of the Morris method are shown in Figures 4.16 and 4.17 for "narrow" and "broad" variation ranges, respectively.

On the left hand side of both figures the investigated parameters are presented in descending order regarding their Morris sensitivity measures μ^* - the mean values of the distributions G_i (distributions of absolute values of elementary effects, see subsection 3.2.2) for each parameter $i, i = 1,..,k$. The larger μ^* for the parameter the more influence it has on F_{target}. The values of μ^* can be recalculated into mean values of absolute change of F_{target} by simple relation $\left|\overline{\Delta F_{target}}\right| = \mu^* \cdot \Delta = \mu^* \cdot 0.55$ or in its relative change with respect to the optimal F_{target} which is shown on the second x - axis in Figures 4.16 and 4.17. The 95% confidence intervals of the mean values μ^* are shown by black lines for each parameter. It is seen that the confidence intervals are larger for the "broad" parameter variation range than for the "narrow" one.

In the left part of Figure 4.16 besides the Morris sensitivity measure, similar measure calculated from estimates of the regression coefficients (last column in Table 4.4) of the MLR method is shown in orange. Although being completely different the both methods deliver very similar results. It might be considered as a kind of justification of both of them.

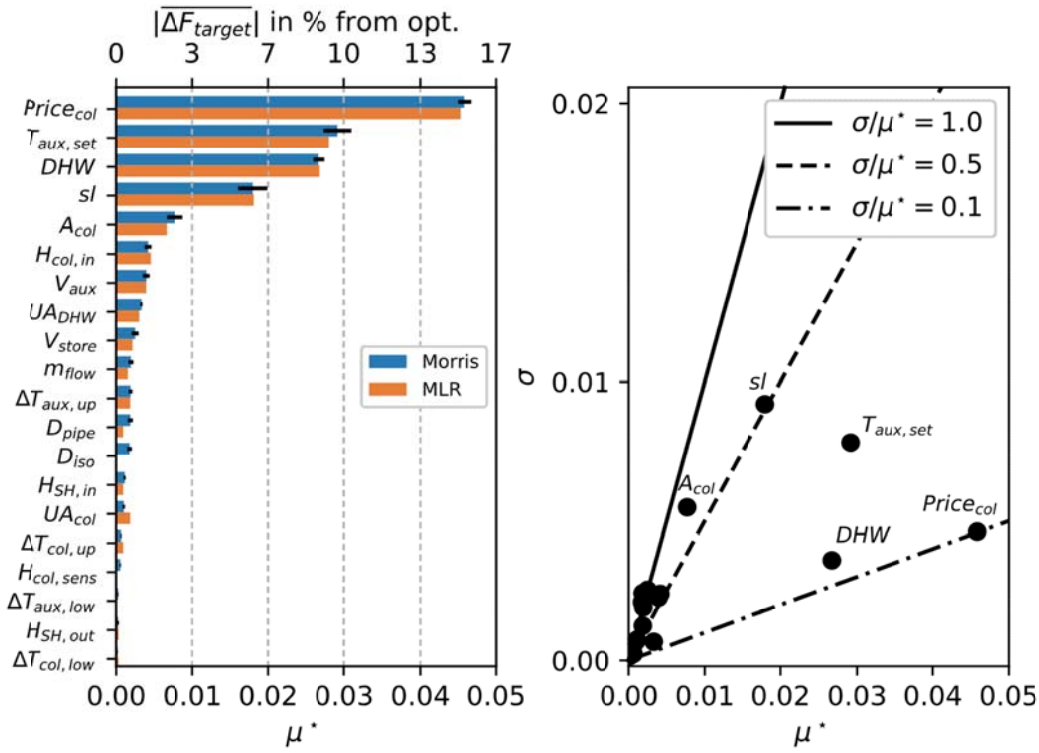

Figure 4.16: *Results of Morris method applied in "narrow" parameter variation space as in Table 4.3. In left figure Morris μ^* measure and recalculated $|\overline{\Delta F_{target}}|$ are shown in comparison with similar results obtained by MLR. Two methods show good compliance. Black lines show* 95% *confidence interval for obtained μ^*. In right figure coefficient of variation σ/μ^* shows ratio of nonlinear (σ) to linear (μ^*) effect of each parameter on solar energy costs*

On the right hand side of both figures the mean values μ^* are plotted against σ – the standard deviations of the distributions F_i. These plots show the ratio of linear and nonlinear effects for the investigated parameters. The smaller the ratio σ/μ^* (also called as the coefficient of variation) for the parameter is, more linear is its effect on the target function. In other words, the effect of parameters with smaller σ/μ^* is more homogeneous over the variation space whereas the parameters with larger σ/μ^* influence the target function differently strong (possibly their influence has different signs) at different points of the variation space. It is obvious that for the "broad" variation space the ratios σ/μ^* is larger than for the "narrow" one because more nonlinearity is expected for the "broad" space, what is also indicated by the MLR method from the previous subsection.

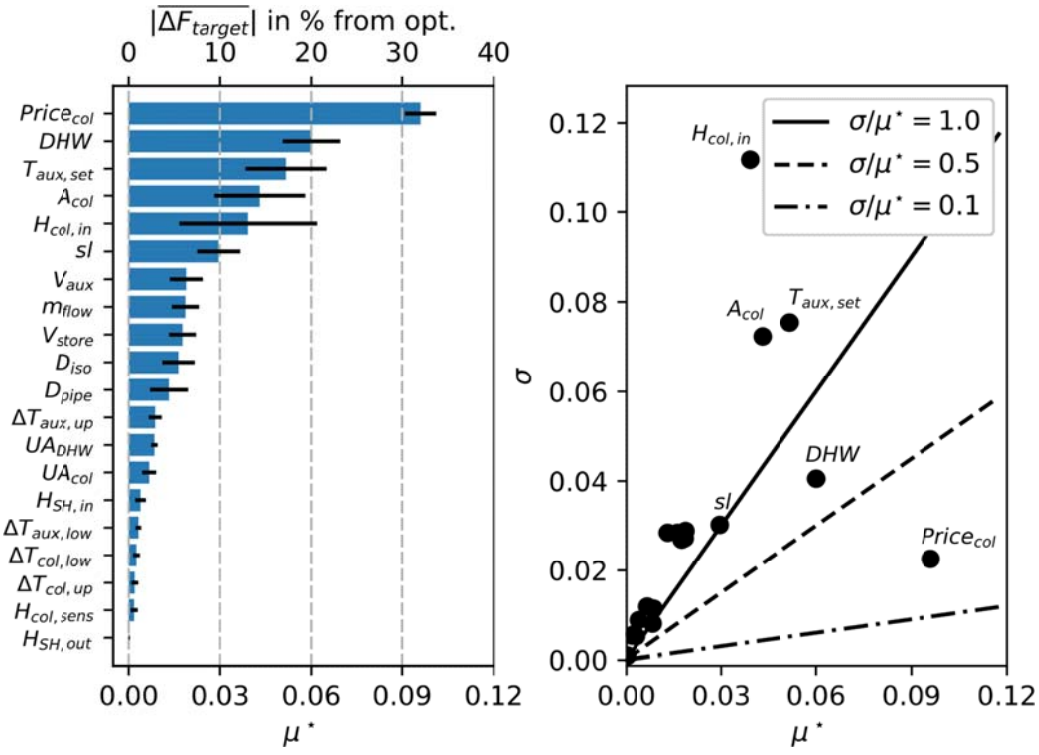

Figure 4.17: *Results of Morris method applied in "broad" parameter variation space as in Table 4.3. Larger* 95% *confidence intervals shown by black lines in left figure and larger coefficient of variation* σ/μ^* *indicate significantly higher nonlinearity of parameter effects in "broad" variation space than in "narrow" one shown in Figure 4.16*

According to Figures 4.16 and 4.17 the collector price denoted as $Price_{col}$ has the most significant effect on the target function F_{target} both in "broad" and "narrow" variation spaces. It has the most linear effect on F_{target} but not only linear. Even in "narrow" variation space its σ is not 0. It is explained by interaction of $Price_{col}$ with other parameters as it appears in F_{target} (4.1) not as a separate term but in multiplication with the collector area A_{col} divided by the whole energetic part – factor that is not constant over the parameter variation space. In Figure 4.18 sensitivity of only optimization parameters in "narrow" variation space is shown. In absence of $Price_{col}$ the collector area A_{col} becomes even less important most probably due to weaker interaction. In general the collector area A_{col} has rather negligible influence on the solar energy costs F_{target}. Although it has large effect both on the costs F_{cost} and on the saved final auxiliary energy $E_{ref} - E_{sol}$ of the solar combisystem, these two effects being in numerator and denominator of F_{target} (4.1) cancel each other. Sensitivity of the extended energy savings $f_{sav,ext}$ (almost the same as sensitivity of $E_{ref} - E_{sol}$) to the variation of the optimization

parameters is similar to those presented in Appendix C calculated by the MLR method

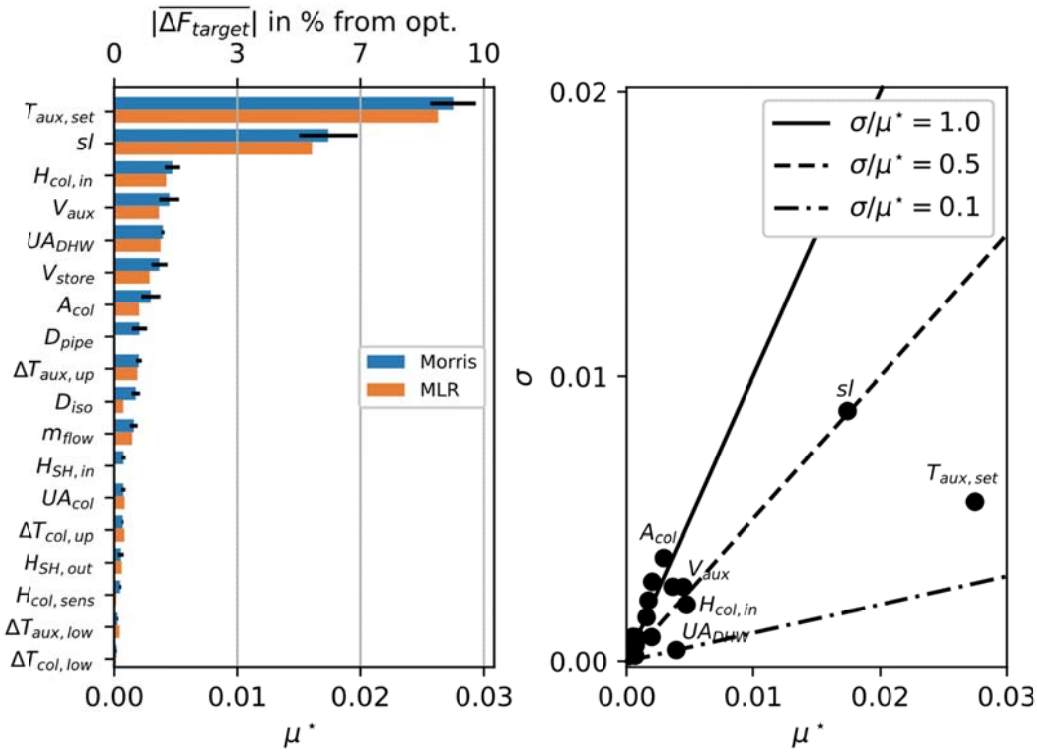

Figure 4.18: *Results of Morris method applied only to optimization parameters in "narrow" variation space as in Table 4.3. Influence of collector area A_{col} becomes even smaller in absence of $Price_{col}$ what shows significant interaction between them. Overall small influence of A_{col} is explained by cancelling of its effects in numerator and denominator of target function F_{target} (4.1)*

4.5.4. Results of FAST method

As already stated above, the Morris method is used to rank the parameters by their effect on the target function, that is, estimate this effect qualitatively. To quantify it more comprehensive sensitivity analysis methods as the FAST or Sobols' methods are to be applied (Saltelli, 2004). In fact, quantification is similar to that already received by determination coefficient R^2 of the MLR method showing how much variation in measured data is described by model. Significant difference is that the FAST method calculates how much variation in the target function is due to variation in a specific parameter. The mentioned methods are applicable to models with nonlinear relationship between the parameters and the target function. Hence, the FAST is applied to quantify parameter influence in "broad" variation space

Table 4.6 presents the main and total effects S_i and S_{Ti} as defined in (3.4) and (3.5), respectively, and calculated by the extended FAST method.

Table 4.6: *Main and total effects S_i and S_{Ti} calculated by extended FAST method*

Parameter	Main effect, S_i	Total effect, S_{Ti}
1. A_{col}, m^2	0.018	0.062
2. V_{store}, m^3	0.009	0.081
3. N_{aux}	0.014	0.088
4. D_{iso}, m	0.007	0.129
5. D_{pipe}, mm	0.003	0.018
6. $m_{flow}, kg/m^2h$	0.002	0.029
7. $\Delta T_{col,up}, K$	0	0.006
8. $\Delta T_{col,low}, K$	0	0.008
9. $H_{col,sens}$	0	0.003
10. $UA_{col}, W/K$	0.001	0.005
11. $H_{col,in}$	0.019	0.077
12. $H_{SH,out}$	0	0.005
13. $H_{SH,in}$	0	0.006
14. $UA_{DHW}, W/K$	0.002	0.009
15. $T_{aux,set}, °C$	0.079	0.124
16. $\Delta T_{aux,up}, K$	0	0.012
17. $\Delta T_{aux,low}, K$	0	0.006
18. $sl, °$	0.040	0.057
19. DHW	0.274	0.294
20. $Price_{col}, Eur/m^2$	0.411	0.428
Sum	0.882	1.447

According to Table 4.6 88% of variation in the solar energy costs F_{target} is explained by variation of all parameters. It is the quality measure of the FAST method same as the MLR determination coefficient R^2, showing that application of the method is successful. The MLR model applied in the same "broad" variation space shows "only" $R^2 = 0.73$ (see Table 4.5). Similarly to the Morris method and local parameter variations, the boundary condition parameters $Price_{col}$ and DHW have the largest influence on the solar energy cost F_{target} showed by the main

effects S_i of 41% and 27%, respectively, followed by $T_{aux,set}$ and sl with 8% and 4%. The results are also in accordance with ranking of the Morris method presented in Figure 4.17. Total effect indices S_{Ti} showing not only main effect of the parameters but also effect from interactions with other parameters are noticeably larger for some parameters than their main effects. This indicates more complex relations between these parameters and the target function.

4.5.5. Parallelization and reliability

Each sensitivity method applied to analysis of the solar thermal combisystem in the above subsections requires different amount of the input data in the form of the target function values "measured" at the specific points, that is, parameter values, which are also differently chosen by each method. The common to all methods is that the "measured" data are to be prepared before the method starts. In this sense they differ from the optimization methods which decide on the combisystem configurations to be calculated in the course of optimization. Since preparation of the "measured" data, that is, calculation of the target function, especially for computationally expensive models takes considerably more time than calculation of sensitivities by the method, all the parallelization potential is concentrated in possibility to perform the "measurements", in our case, the TRNSYS simulations, in parallel. If m computational kernels are available and $n, n \gg m$ independent simulations are to be carried out, then computation in parallel is approximately m times faster comparing to the usage of only one kernel.

The reliability of the results of sensitivity analysis presented in the above is only roughly checked. In the MLR method, 500 "measurements" are chosen for estimation of the regression coefficients. The method is also run with 1000 and 2000 "measurements" but without any significant difference in results. The Morris method turned out to be more sensitive to the number of input data, especially regarding ranking of less influential parameters. Here 1680 simulations are chosen as appropriate. The most computationally expensive method is the FAST with 10000 simulations needed to calculate indices of the first-order and total effects.

Calculation of the regression coefficients is carried out by R-Studio. The results of the Morris and FAST methods are obtained with using Sensitivity Analysis Library (SALib) (Herman and Usher, 2017) programmed in Python but also compared to own implementations of the methods written in Java programming language.

5. Dynamic optimization of solar thermal combisystems. Estimation of optimization potential of dynamic controller settings

In Chapter 4 optimization of the solar thermal combisystem in the planning process is carried out resulting in the configuration of the system which is optimal for the given one-year weather data and hot water consumption. It is called static (or design) optimization during which the main design parameters such as collector area, store volume, flow rates, etc., are determined. The values of these parameters stay constant during the simulation period (except for the flow rates which are zero when pumps do not run).

Optimization of solar thermal combisystems in operation or the so-called dynamic optimization implies that the system parameters being optimized are varying during the operation, usually with a given time resolution, f.e. on seasonal, daily or hourly basis. Apparently, only the operational parameters such as the controller settings or flow rates might be considered for dynamic optimization.

As it is shown in Chapter 4 and earlier in (Krause, 2003), the numerical optimization during the planning process can bring additional $> 10\%$ benefit in terms of the solar energy costs to a solar thermal system already appropriately designed by experienced engineers. Following (Krause, 2003) it seems that the further optimization of such systems in operation does not have much potential.

In this Chapter a systematic approach is proposed which enables estimation of the theoretical potential of the dynamic control settings optimization for solar heating combisystems designed for use in single- or multi-family houses by application of numerical optimization algorithm. Knowing this potential beforehand can help to decide if the smart dynamic controllers based on sophisticated predictive algorithms are worth to implement or not.

5.1. Idea of approach: splitting one-year optimization

The main challenge for any algorithm performing dynamic optimization are large number of optimization parameters which run into thousands already when only one control parameter is being adjusted on hourly basis. But even if the algorithm could deal with this number of parameters, the optimization would be unallowable long. For example, if five minutes are required to perform a single simulation of the

combisystem (what is usually a case for precise TRNSYS simulations with a 3 to 6 minute time step), then the optimization would take weeks or even months.

In an approach presented below long one-year optimization is split into many short ones (up to four days and in average with 15 parameters per optimization). Solving many short optimization problems is faster than optimizing the whole year at once as the optimization time increases faster than linearly with increasing the number of parameters. Such a splitting, however, is justified only if changing a single optimization parameter affects the system performance (mainly the store temperature profile) for a short time horizon usually not longer than a couple of days. Figure 5.1. shows three temperatures in the store (top part in red, middle - green and bottom - blue). Specific flow rate in the collector loop is set to 10 kg/hm^2 and it is switched from the low flow (10 kg/hm^2, solid lines) to high flow (30 kg/hm^2, dashed lines) on 14 April only. Flow rate in the store loop is adjusted as well according to equality of the capacity flow rates. Already after one day almost no change in the store temperatures caused by this local change in flow rates can be noticed.

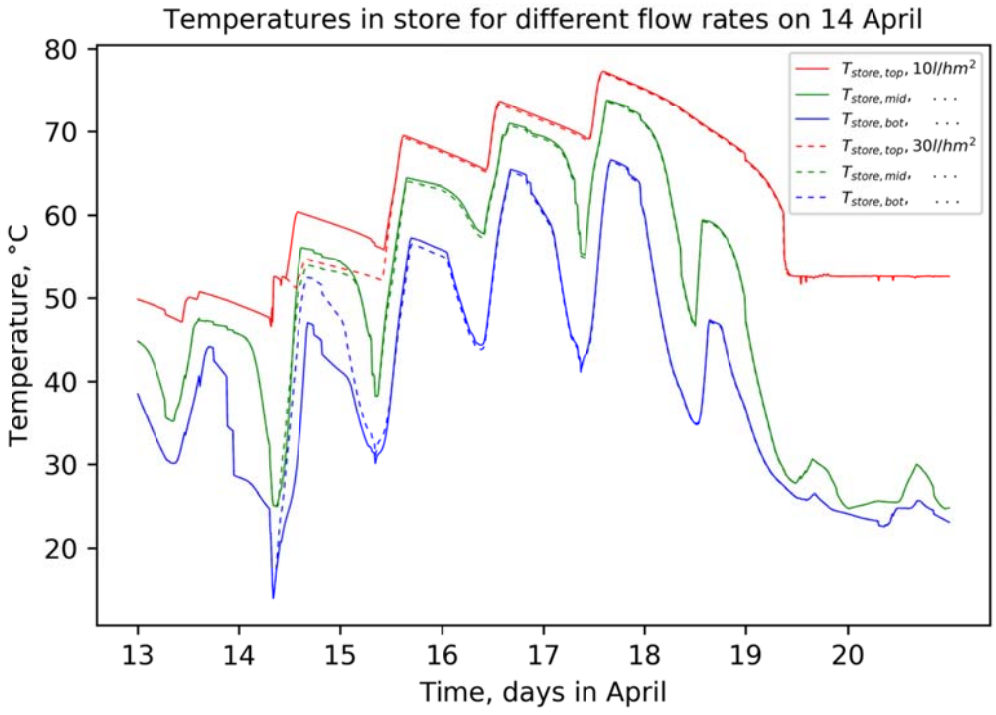

Figure 5.1: *Temperatures in store. Flow rates are changed from* 10 kg/hm^2 *(solid lines) to* 30 kg/hm^2 *(dashed lines) on 14 April only. Already after one day there is almost no influence on store temperatures*

5.2. Optimization of flow rate on hourly basis

The idea of splitting one-year optimization is applied to dynamic optimization of the slightly modified solar combisystem, similar to that shown in Figure 2.1 but with stratified charging of the store. The combisystem is optimized in order to get as much energy as possible from the collector into the storage tank and meanwhile minimize the energy consumed by the pumps. The target function is defined as follows:

$$\widehat{F}_{target} = Q_{sol} - 3W_{pumps} \tag{5.1}$$

Actually, the following function

$$\widehat{F}^{*}_{target} = Q_{aux} + 3W_{pumps} \tag{5.2}$$

should have been minimized, but it would not work with the idea of splitting optimization because of rather unpredictable time windows when the boiler heats up.

To maximize the target function $\widehat{F}_{target}$, the flow rate in the collector loop is adjusted on hourly basis but only on hours when the specific solar insolation is high enough ($> 200\ W/m^2$). The specific flow rate is varied in the range from 10 to 30 kg/hm^2. The flow rate in the store charging loop is calculated in the way that the capacity flow rates in the collector and store loops are equal.

As shown in Figure 5.1 the choice of the flow rate in the collector loop for a selected day (or hour) has almost no impact on the performance of the system (more precisely: on the temperature profile in the store) already a couple of days later. Thus, there is no reason to perform the whole year simulation of the system each time when the flow rate changes only during selected hours, and the idea of splitting optimization can be applied. It is suggested to split up the whole one-year optimization in many short ones with duration of up to four days. After each short four-day optimization, the temperature profile of the storage tank (temperatures of all store nodes), temperature of the air zone of the building, temperatures of the walls and fluxes through the walls are saved at the end of the first day being optimized and taken as the initial condition for the next optimization. Such simple splitting saves huge amount of computational time and, in this way, allows the one-year dynamic optimization to be completed in a reasonable time.

In Figure 5.2. two hourly optimizations with duration of four days each are schematically presented. The hours with solar insolation $> 200\ W/m^2$ for which the optimal flow rates are being determined are shown in grey color. In the

optimization 1, the optimal flow rates for days 1 – 4 are identified by maximizing the target function $\widehat{F}_{target}$ evaluated at the end of the day 4. After the optimization 1 is completed, the calculated flow rates only for the hours of day 1 are stored as optimal. Flow rates calculated for the hours of days 2 – 4 are further optimized in next optimizations. The temperature profile of the store, temperature of the air zone of the building, temperatures of the walls and fluxes are saved at the end of day 1 and are used to initialize the system at the beginning of day 2 in each simulation of the optimization 2. In this way "global" optimization proceeds each time optimizing four days in a row and after this short optimization is completed, it shifts one day and optimizes other four days. These steps are repeated until the end of the year is reached.

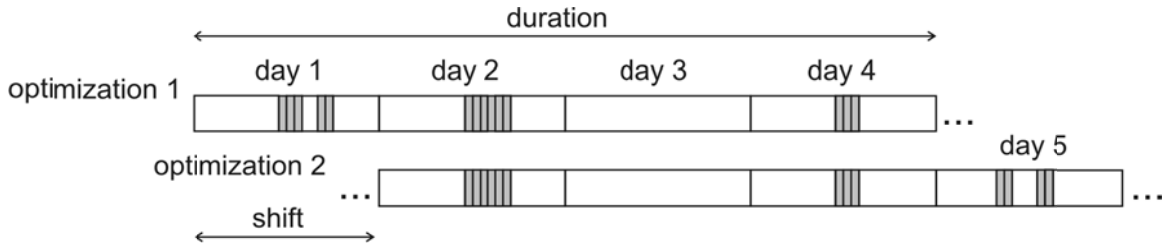

Figure 5.2: *Schematic presentation of two four-day optimizations. Hours with solar insolation* $> 200\ W/m^2$ *on which flow rates are optimized are shown in grey color. After optimization 1 is done optimal flow rates are saved for day 1. Store temperature profile and temperatures in building at the end of day 1 are taken as initial conditions for next optimization starting at day 2*

In each short optimization the target function $\widehat{F}_{target}$, calculated over the time interval of four days, is maximized. As mentioned above, minimization of the function $\widehat{F}^*_{target}$ would be more appropriate since it represents the final energy consumption of the system, but it would not work in the approach represented here. The backup heating may switch on by chance at the end of the fourth day, or just at the beginning of the fifth day. Evaluation of the target function $\widehat{F}^*_{target}$ based on Q_{aux} is misleading in these cases. Thus, it was decided to maximize the solar yield assuming that the more energy gets into the storage tank, less auxiliary energy is required, and the better is the system performance.

Choice of duration for each short optimization and how many days is the shift between two consequent optimizations are the questions which should be cleared in advance. Duration of the short optimization must be larger than the time interval within which the influence of the parameter variation occurred at the first day of optimization remains significant. Duration also depends on how the hourly

parameters influence the target function calculated at the end of the short optimization. If their influence is mostly linear and additive then the duration can be short, up to one-day. On the other hand if the parameters are involved in interactions and not only with their close neighbors but also with the parameters from the next days, then the optimization duration is to be longer. Short shift between two optimizations (with duration longer than the shift) seems to refine the optimization because most parameters are optimized more than once.

In the investigated case, the parameters (values of flow rates for specific hours) seem to be not involved in significant interactions; even short optimizations with one day duration and with one day shift (next optimization starts from the following day) provide almost the same results as presented four-day optimizations.

5.3. Potential of the dynamic flow rate optimization

The dynamic optimization of the fluid mass flow in the collector and storage loops is carried out by the binary (n-ary) search algorithm programmed in GenOpt (Generic optimization software) and described in Chapter 4. As a rule it is not as reliable in finding the global optimum as, for example, the genetic algorithm, but it is much faster. As shown above it seems to be reliable enough when applied to optimization of the solar combisystems. It is considered as an appropriate choice for the investigated case.

The dynamic flow rate optimization is applied to solar combisystem similar to that described in Chapter 2 (see Figure 2.1) but with stratified charging of the store.

The optimization results show that the extended fractional savings $f_{sav,ext}$ of the combisystem with hourly optimized flow rate are only 0.3 percent points larger than those of the reference with constant specific flow rate of $10\ kg/hm^2$ (35.92% versus 35.59%). It should be noted, however, that for the reference combisystem operated with high flow (constant specific flow rate of $30\ kg/hm^2$) $f_{sav,ext} = 34.49\%$. Thus, for this particular system, no significant improvement of the system performance can be expected by dynamically adjusting only the flow rates in collector and store loops.

5.4. Potential of boiler control optimization

Heating up the water and storing it causes thermal losses. It can be assumed that the system performance is the best if the boiler delivers to the store exactly the amount

of energy needed by the consumer at the specific moment. To estimate the potential of forecasting the consumption, that is, the optimization potential of the boiler control settings such as set temperature and control dead bands, one could proceed as above by adjusting these settings on the hourly basis. Here, however, another, simpler way is chosen.

The hydraulics of the investigated combisystem is modified to determine the theoretical optimization potential of boiler control settings. The boiler heating up the auxiliary volume inside the storage tank, is replaced by two electric instant heaters placed in tap water preparation and space heating loops, respectively (Figure 5.3). Such modification is expected to have several positive effects on the system performance. The store losses should decrease due to lower temperatures especially in the upper part of the tank. In summer, when stagnation of the system may occur, more store space is available for possible anti-stagnation control strategy (see Chapter 6) or, alternatively, the store can be made smaller and cheaper. The pump in the auxiliary loop is also obsolete.

For more consistent comparison, performance of the modified combisystem is compared to that of the reference combisystem (Figure 5.4) having the boiler "replaced" by electric instant heater being actually the same boiler controlled in the same way but with no standby and less electricity consumption of the auxiliary pump set to $15\ W$ (Figure 5.4). In the reference system the electricity consumption of the boiler is set to $9\ W$ when the boiler is idle and to $43\ W$ when it heats up. The heater turns on when temperature at the bottom of the auxiliary heated volume drops down to $50\ °C$ and turns off when it reaches $60\ °C$.

In the modified combisystem, the electric instant heater in the DHW loop turns on when the water coming from the store is colder than the set temperature of $45\ °C$. The instant heater in the space heating loop heats up the water coming from the store (when needed) to the set temperature received from the radiator. It should be noticed that the maximal heating rate of the electric heater in tap water preparation loop has to be increased to $25\ kW$ in order to fully fulfill the consumption demand.

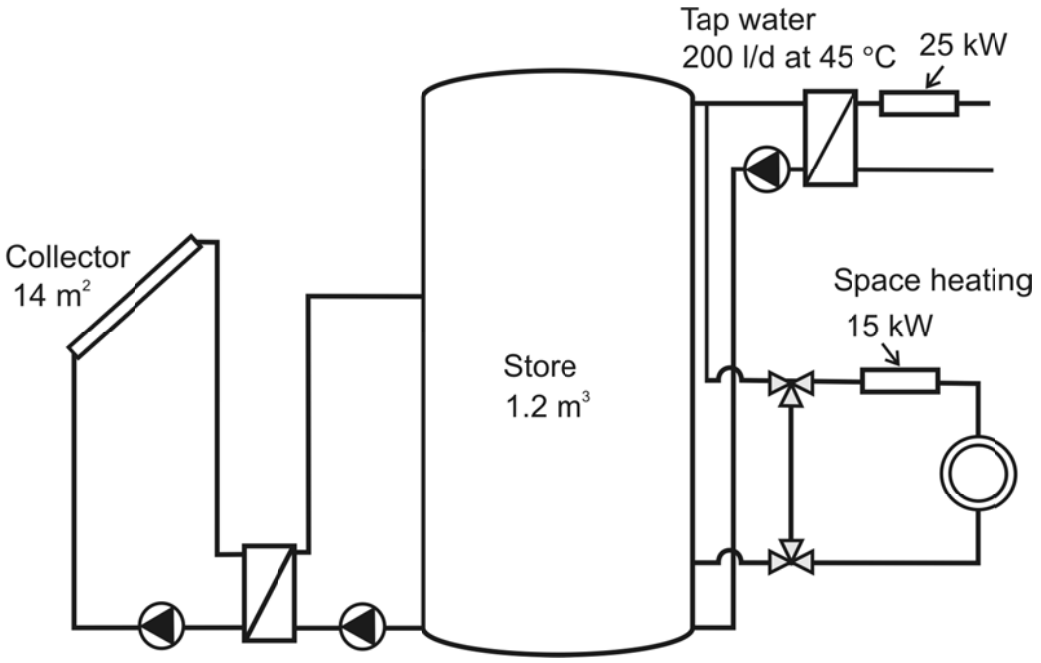

Figure 5.3: *Modified combisystem with two electrical instant heaters in tap water and space heating loops*

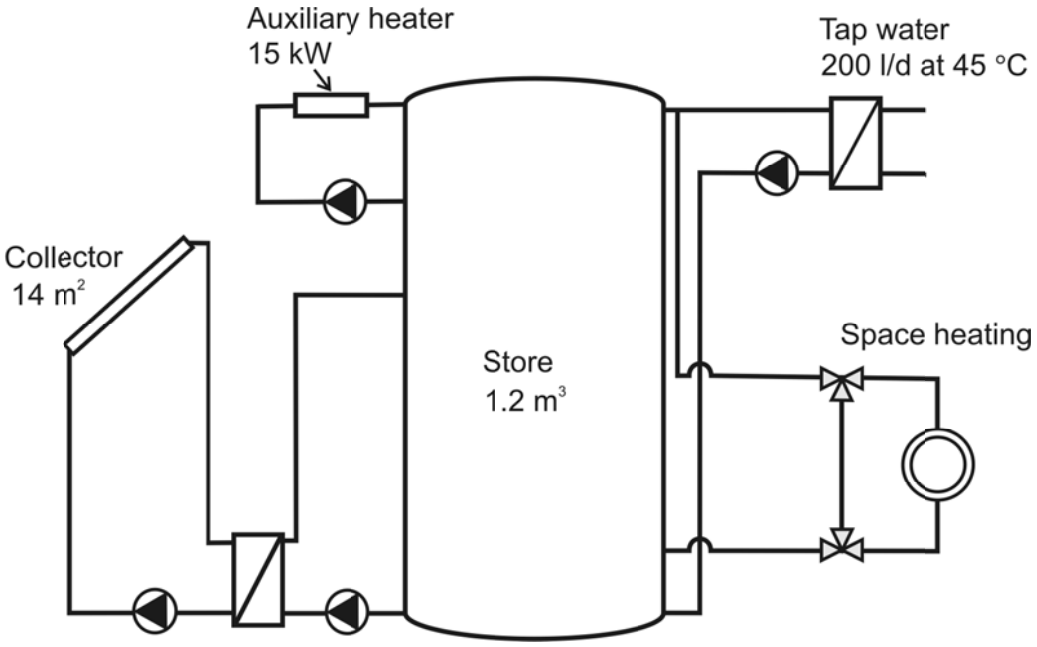

Figure 5.4: *Reference combisystem with electrical heater in the auxiliary heating loop*

The reference combisystem shown in Figure 5.4 and the modified combisystem with electric instant heaters built into domestic water preparation and space heating loops (Figure 5.3) are simulated in TRNSYS software. Table 5.1 shows the relevant energy quantities, performance factors and solar energy price for the both investigated combisystems as well as for the reference combisystem 0 from Figure 2.1 with $T_{set,aux} = 53°C$ and $T_{set,aux} = 70°C$. According to Table 5.1 the

combisystem 2 with heaters built in DHW and SH loops, has 1.85 percent points higher $f_{sav,ext}$ particularly due to smaller store losses, and, consequently, 0.87 $EurCent/kWh$ (around 5%) cheaper solar energy costs than the reference combisystem 1 with electrical heater inside the store. Performance of combisystem 2 is obviously even higher comparing to reference combisystem 0 having higher electricity consumption of the boiler (3.3 percent points in $f_{sav,ext}$ and 1.6 $EurCent/kWh$ (around 10%) in costs). If the boiler in reference combisystem 0 has not optimal (too high) set temperature $T_{set,aux} = 70°C$ (combisystem 0a in Table 5.1) then combisystem 2 is 5.8 percent point (3.1 $EurCent/kWh$ or 17% in costs) better. This last comparison shows the influence of set temperature of the boiler which is already shown to be significant in Chapter 4.

Table 5.1: *Optimization potential of boiler control settings. Performance of modified combisystem with two instant heaters in DHW and SH loops is shown along with that of three reference combisystems*

Combisystem	Auxiliary energy, kWh	Solar yield, kWh	Store losses, kWh	Electricity consumption, kWh	$f_{sav,therm}$	$f_{sav,ext}$	F_{target}, Eur/kWh
0. Reference combisystem with $T_{set,aux} = 53°C$	8084	4514	1216	274	0.3272	0.3054	0.1675
0a. Reference combisystem with $T_{set,aux} = 70°C$	8411	4319	1335	272	0.3003	0.2805	0.1824
1. Reference combisystem, Figure. 5.4	8084	4514	1216	186	0.3272	0.3202	0.1598
2. Modified combisystem with two instant heaters, Figure. 5.3	7885	4626	1112	173	0.3433	0.3387	0.1511

Although the modified combisystem 2 performs better than others, it must have more complicated controller instantly providing constant DHW temperature. The maximal heating rate of the instant electrical heater in the DHW loop is higher than that of the heater heating up the auxiliary volume in the reference system. On the other hand, the auxiliary pump is obsolete in the modified combisystem 2.

5.5. Conclusion

A simulation approach proposed above enables estimation of the theoretical potential of the dynamic control settings optimization for solar heating

combisystems. This approach can be used before improving the control settings of solar heating systems with help of sophisticated predictive algorithms to first estimate the theoretical potential of these improvements and then to decide if they are worth to implement or not.

Application of this approach to optimization of the flow rates in collector and store loops of a solar combisystem on hourly basis shows only 0.3 percent points of theoretically possible improvement in terms of the extended fractional savings $f_{sav,ext}$. On the other hand, optimization of the control settings of the auxiliary heater as shown by application of instant electrical heaters in DHW and SH loops, has more potential, but the controller must be more complicated and probably more expensive.

6. Control - based approach to avoid stagnation of solar heating systems

In the following Chapter a control - based anti - stagnation approach is proposed and numerically investigated. Practical implementation of the approach is described.

6.1. Stagnation of solar thermal systems. Brief overview and approaches

During the periods of high sun insolation and low hot water consumption, the probability that a solar heating system stagnate is high: the thermal store becomes filled with hot water and the exceed heat cannot be removed from the collector any more. When exposed to high temperatures, the heat transfer fluid in the collector loop may rapidly degrade, the produced excessive pressure may damage the solar thermal system components if the system is not properly built. The stagnation problem is even more harmful in climates with potential freezing periods where the propylene-glycol/water mixtures are typically used as the working fluid in the collector loop. Such mixtures are subject to deterioration at temperatures higher than 140°C and may become corrosive resulting in damages to the solar heating system components.

It is a common practice to switch off the pump in the collector loop when the temperature in the thermal store or at the collector outlet reaches the set thresholds. Most of the working fluid from the collector is pushed out by the steam into the expansion vessel and the residual evaporates in the collector. This helps to prevent damage to the system components such as the thermal store, pump and external heat exchanger. Emptying properties of the collectors are crucial for avoiding damages to the system components and deterioration of the working fluid at high stagnation temperatures. They also determine the maximum pressure strain which the system components must bear during stagnation.

In solar heating systems with too low flow rates in the collector, the stagnation may also happen on sunny days in spring and fall even when the thermal store can still accept energy but the temperature at the collector outlet is too high due to the low flow rate. Moreover, at low flow rates the partial stagnation can happen in the collector if it is not properly designed for the low flow operation.

Plenty of approaches have been developed to minimize the stagnation time of the solar heating systems. Most of them fall in one of the following three categories (see (Morhart, 2010)):

- stagnation-proof system concepts (drain-back concept with water as a working fluid, heat-pipe collectors)
- control strategies (switching mode for solar pump control, night time cooling)
- stagnation cooler (passive and active cooling, heat transfer to the swimming pool or ground)
- selective absorber coatings with the absorption coefficient as a function of the absorber temperature $\varepsilon = f(T_{absorber})$

In this study a control-based approach is presented and theoretically investigated in application to a solar heating system.

6.2. A control based approach. Main idea

To completely prevent stagnation of a solar heating system, a simple requirement must be fulfilled on a daily basis: the energy delivered by the collector must fit into the store. As the stores are usually well-insulated, even for a large specific store volume (large ratio between store volume and collector area) the stagnation may occur after several hot days in a row with minimal or no hot water consumption.

The control-based approach to avoid stagnation proposed in this Chapter starts with an attempt to minimize the energy produced by the collector during a day, that is, to get as little energy into the store as possible and, thus, have more space available for another sunny day. In order to achieve this, the performance of the thermal collector should be lowered what happens, for example, when it is operated at higher mean fluid temperature.

In Figure 6.1 the mean fluid temperature T_{mean} of the collector is shown for the two control strategies, the conventional ΔT strategy (dashed line) and the proposed anti-stagnation (constant $90°C$ collector output) strategy (solid line). The triangular dashed area built by these two lines gives a rough estimation of the potential of inefficient collector operation. The larger this area is, the less energy is produced by the collector operated in anti-stagnation mode comparing with the ΔT control strategy. It is also worth to mention that the quantity of energy produced by the collector when using proposed anti-stagnation control strategy is constant and it

does not depend on either the store size or its initial temperature. Of course it is only possible when input collector temperature can be hold constant, for example in systems charging the store via external heat exchanger.

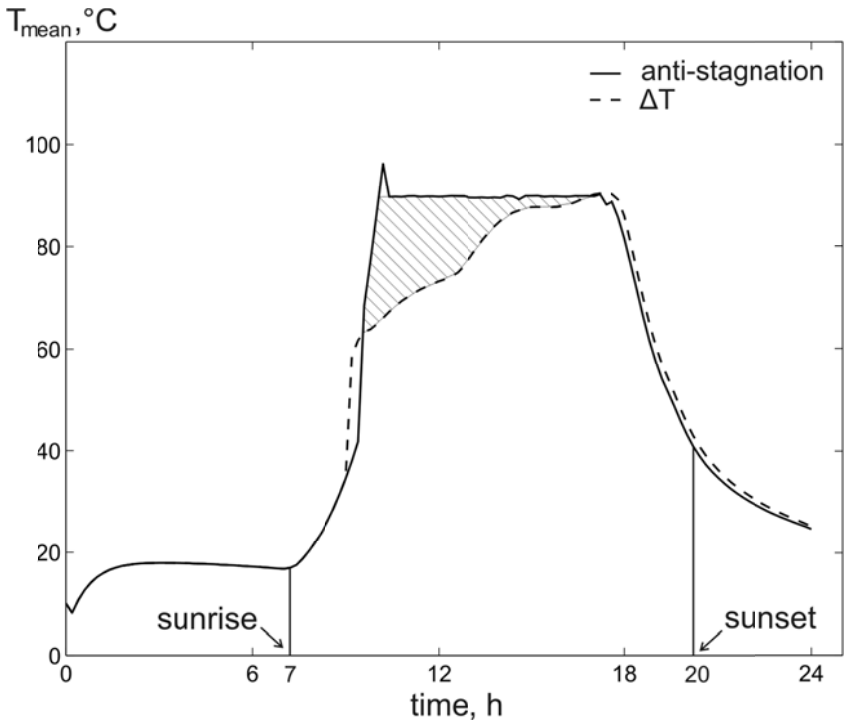

Figure 6.1: *Collector mean fluid temperature T_{mean} for anti-stagnation (solid line) and conventional ΔT(dashed line) control strategies. Dashed area shows the potential of inefficient collector operation*

As it was already shown in (Scheuren, 2008), inefficient collector operation alone is usually not enough to avoid stagnation. The stagnation may still happen a few hours later and can be even more dangerous. Thus, more store space is needed for the incoming energy and it could be provided, for example, by nightly cooling of the store. During the night, the hot water from the store can be cooled down through the collector as the ambient temperature is much cooler than the temperature in the store. The thermal collector is used then as a heat sink. The heat loss coefficient of the collector is a crucial factor for the performance of the night cooling and should be large enough. As shown below, the night cooling makes sense only for the solar thermal systems with not too good insulated flat plate collectors.

6.2.1. Suitable hydraulics

The proposed control-based approach of an inefficient collector operation coupled with the night cooling of the store can be directly applied to the solar heating systems with an external heat exchanger. The inefficient collector operation is

provided by adjusting the flow rates in the collector and store (primary and secondary) loops in an appropriate way.

Application to the heating systems with an internal heat exchanger seems more complicated as there is only one flow rate to adjust what might be not enough. Moreover, since the internal heat exchanger is usually placed in the lower one-third of the store, the night cooling requires additional pump for stirring the store a few times per night to enable cooling of the whole store.

6.3. Implementation of the approach

The proposed control-based strategy is applied to the reference solar combisystem of the IEA SHC Task 32 with an external heat exchanger similar to that described in Chapter 1 but with $40\,m^2$ of the flat plate collectors. The 5% propylene-glycol/water mixture is used as the heat transfer fluid in the collector loop. The specific heat transfer coefficient of the collector heat exchanger is set to $125\,W/Km^2$. The auxiliary heating volume is $200\,l$.

To safely operate the heating system close to the stagnation point, the following two requirements are to be met by the anti-stagnation control strategy:

a. relatively high constant specific flow rate (chosen at $27\,l/m^2h$) in the collector loop
b. the temperature T_{charge} at the HX output to the store does not exceed 95°C

The first requirement ensures that the fluid flows uniformly through the collector and there is no risk of the partial stagnation inside the collector. The second requirement prevents steam delivery to the store.

If the anti-stagnation control strategy is activated, the pump in the collector loop (primary pump) starts when the temperature T_{col} at the collector output rises up to 70°C in the morning and runs with the constant flow rate of $V_{pri} = 27\,l/m^2h$ (see Figure 6.2). The pump in the store loop (secondary pump) starts when the temperature T_{solar_F} at the entrance of the heat exchanger from the collector side reaches 95°C. It runs with a variable flow rate adjusted to keep the temperature T_{charge} at the heat exchanger output to the store close to 95°C. Such control strategy prevents the collector from overheating (the collector output temperature T_{col} does not exceed 100°C) and operates the collector at high mean fluid temperature, i.e. the collector efficiency is low.

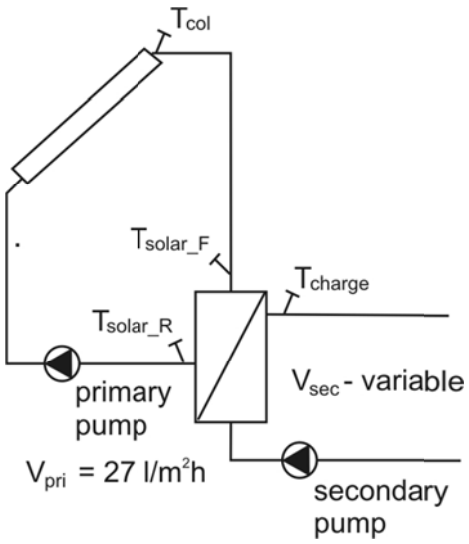

Figure 6.2: *Schematic representation of the temperature sensor positions for theoretical implementation of anti-stagnation control strategy*

In the evening when the sun does not heat up the collector, the night cooling mode turns on. The two pumps run with a constant flow rate of 27 l/m^2h and cool down the store through the collector as a heat sink. If the following day is expected to be very sunny and there will be no consumption, then the night cooling can be continued till early in the morning when the sun shines on the collector. Otherwise, the pumps should be turned off earlier providing that enough energy is left in the store to cover the possible consumption on the following day.

6.4. Results of theoretical implementation

6.4.1. Modeled weather conditions

The reference solar combisystem is simulated with application of the proposed anti-stagnation control strategy using the TRNSYS software. The extreme weather conditions are especially modeled for three different locations: Madrid, Zurich and Stockholm. The sunniest summer day is picked up from the statistical year for each location (Meteotest, 2016) and then the system is simulated for such ten days in a row. No heat consumption is assumed.

The aim of the simulation is to find the minimal V_{store}/A_{col} ratio at which the system still does not go into stagnation. In Table 6.1, the climate data and the minimal V_{store}/A_{col} calculated theoretically are given for the three chosen locations. The results show that even for such extreme modeled weather conditions

it is possible to completely avoid stagnation of the solar heating system with relatively small specific store volumes.

Table 6.1: *Minimal specific store volume V_{store}/A_{col} for three locations: Madrid, Zurich and Stockholm*

Location	Collector slope, °	Irradiation, kWh/m^2day	Ambient temperature, °C, T_{min} ; T_{max}	V_{store}/A_{col}, l/m^2
Madrid	35	7.36 (Aug, 18)	18.5; 35.5	68
Zurich	45	7.48 (Aug, 17)	15.9; 28.7	50
Stockholm	50	7.49 (Jul, 20)	15.2; 28.3	42,5

6.4.2. Method applicability range

To determine the applicability range of the proposed anti-stagnation control strategy to solar heating systems with different collector types, the collector loss coefficient U_{col} is varied in the range from 2.0 W/m^2K (evacuated tube collector) to 4.5 W/m^2K (poor isolated flat plate collector). For U_{col} between 2.0 and 2.5 W/m^2K the flow rate of the primary pump during the day and that of both pumps in the night must be gradually increased up to 70 l/m^2h. It is caused by good insulation of such a collector which does not allow to run the system all ten days in a row without stagnation at previously proposed 27 l/m^2h.

In Figure 6.3 the ratio $V_{store,min}/A_{col}$ versus U_{col} is shown for the location in Zurich. As seen from the figure, the minimal V_{store}/A_{col} grows exponentially with U_{col} decreasing, what means that the applicability of the proposed anti-stagnation is restricted to the flat plate collectors with U_{col} not smaller than 3.0 W/m^2K. The evacuated tube collectors and well-insulated flat plate collectors have still too good efficiency at around 90°C mean fluid temperature during the day. Furthermore, their heat losses are too low to sufficiently cool down the store in the night.

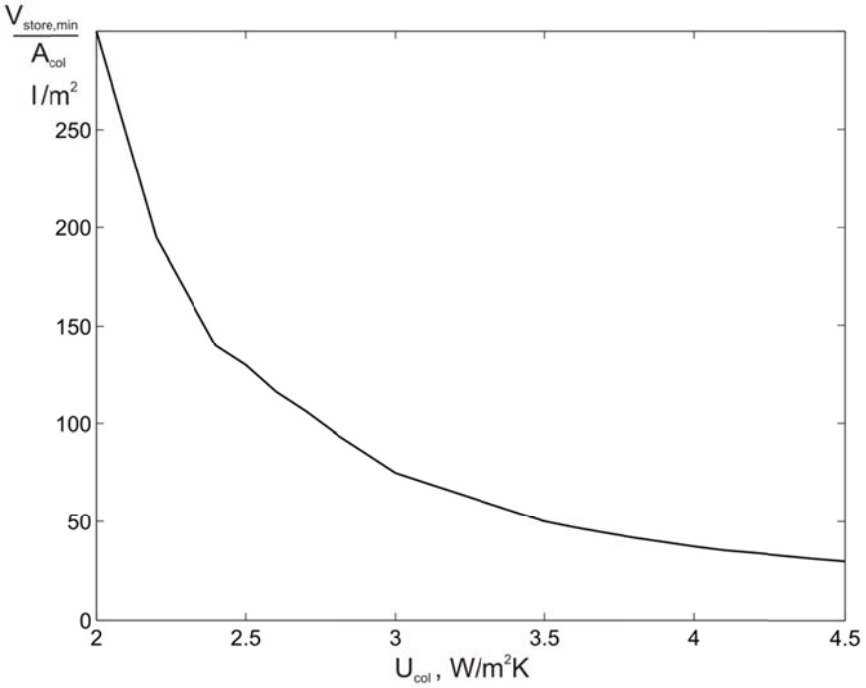

Figure 6.3: *Minimal specific store volume* $\boldsymbol{V_{store}/A_{col}}$ *versus collector thermal loss coefficient* $\boldsymbol{U_{col}}$ *for Zurich location*

6.4.3. Influence of the weather conditions

It is obvious that changes of weather conditions have influence on the minimal specific store volume. To estimate this influence, the variations of the global radiation H_t on horizontal plane, the ambient day and night temperatures, ($T_{amb,day}$ and $T_{\mathrm{amb,night}}$, respectively) are carried out for the modeled weather conditions in Madrid. Figure 6.4 shows nearly linear dependency of the minimal V_{store}/A_{col} on the global radiation H_t. Change of the global radiation in 5% leads to approximately 20% change of the minimal specific store volume.

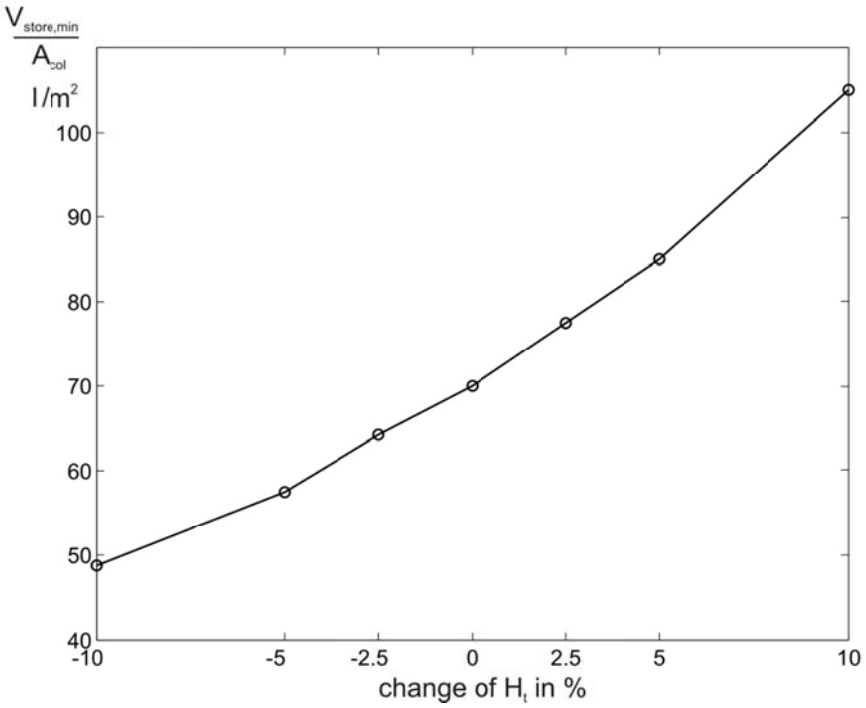

Figure 6.4: *Influence of global radiation H_t on minimal specific store volume V_{store}/A_{col} for Madrid location*

To investigate the variation of the ambient day and night temperatures ($T_{amb,day}$ and $T_{amb,night}$), the real ambient temperature is approximated by the sine curve. The modeled curve is varied in four different ways. First, day and night temperatures are changed independently, to show the influence of the ambient temperature on the inefficient collector operation and the night cooling separately. In two other variations the temperatures are changed simultaneously either in one direction (the sine curve is shifted up or down increasing or decreasing the average temperature) or in the opposite directions (the sine curve is deformed, contracted or stretched, preserving the average temperature). The latter variation is probably the most realistic one. It models the ambient temperature for the climate types starting with the maritime-like climate (small difference between day and night temperatures) and ending up by the continental one (hot day and quite cool night).

Figure 6.5 shows the simulation results of all four variations of the ambient temperature. As it was expected the shifting of the whole ambient temperature curve has the largest impact on the minimal specific store volume (solid line in Figure 6.5). Variation of only day temperature has approximately the same influence as that of the night temperature (dash-dotted and dotted lines, respectively). The least influential is the last variation that preserves the average temperature (dashed line).

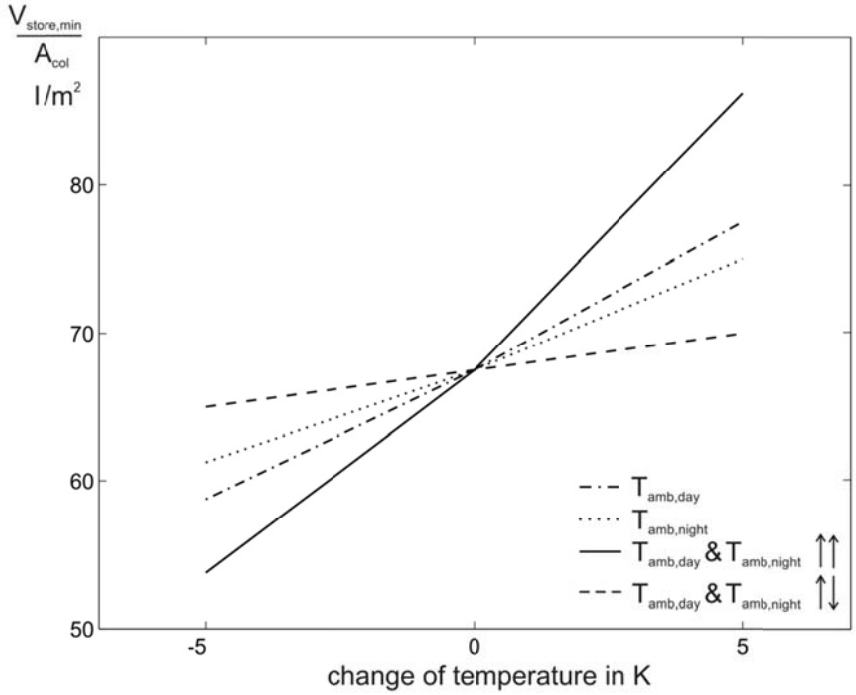

Figure 6.5: *Influence of ambient day and night temperatures on minimal specific store volume V_{store}/A_{col}. Dash-dotted and dotted lines show influence of changing only day and only night temperatures, respectively. Solid line describes influence of shifting both temperatures in one direction (both increasing or decreasing). Dashed line means streatching or contracting of temperature sine curve with preserving average temperature*

6.4.4. Influence of duration of night cooling period

Duration of the night cooling period is another important factor for the proposed anti-stagnation strategy. In principle, if no consumption is expected for the following day the night cooling period can be as long as possible, starting in the early evening, when the sun leaves the collector, and ending in the later morning when the rising sun shines on the collector again. For example, for the chosen Madrid weather condition (August 18) the maximum night cooling period is 14.8 hours. But if the hot water demand, larger than the auxiliary volume in the store, is expected on the next day, especially in the early morning, the night cooling must be stopped earlier in the morning or started later in the evening, thus, providing that enough energy is left in the store to fully cover the consumption on the next day. The similar is correct if the weather is expected not to be that shiny during the following day. The power consumed by the pumps could be then saved by making the night cooling period shorter.

In Figure 6.6 variations of the night cooling starting and ending times are presented for the modeled Madrid weather conditions and without hot water demand. It is easily seen that each half hour of the night cooling in the morning saves much more

storage space than half hour in the evening does. In other words, it is always better to start the night cooling as late in the evening as possible and to finish it just before the sun comes on the collector in the morning. This conclusion is trivial. It is explained by the lower ambient temperature in the morning and thus, more efficient night cooling.

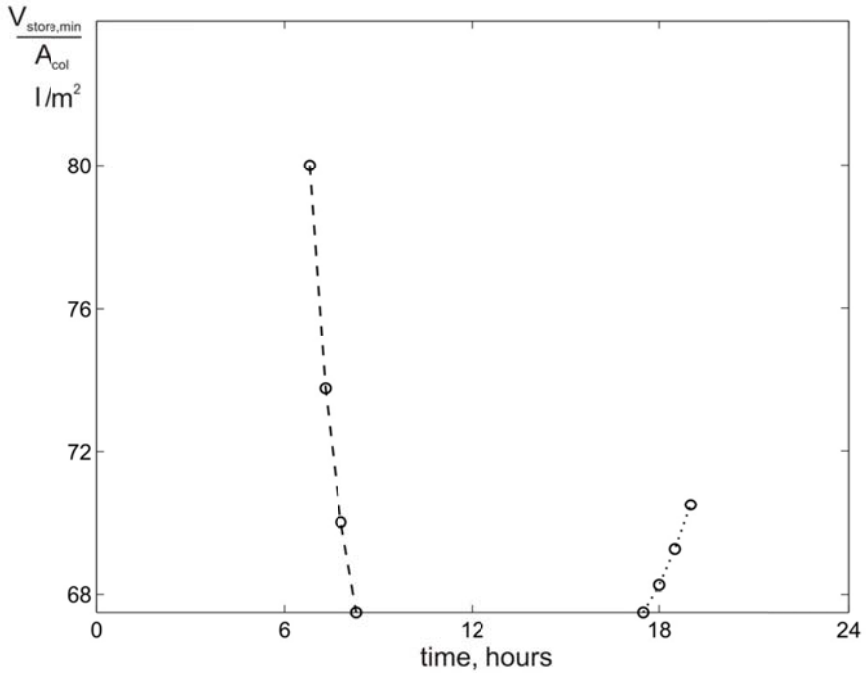

Figure 6.6*: Influence of duration of night cooling period on minimal specific store volume* V_{store}/A_{col} *. Dashed curve shows influence of stopping night cooling earlier in the morning whereas dotted curve shows effect of starting it later in the evening. Distance between two neighbour points depicted by circles is half an hour*

6.4.5. Electricity consumption of the pumps

In comparison with the usual ΔT control strategy, the proposed anti-stagnation strategy has larger power consumption of the pumps due to the night cooling of the store. For the most sunny day in Madrid the high efficient collector and store pumps consume 0.8 kWh and 0.2 kWh per night, respectively. During the night cooling the mass flows and thus the power consumption can be lowered by 50% resulting in only 10% increase of the minimal specific store volume. The pump power consumption during a day can be hardly compared with the usual ΔT control strategy as the solar heating system controlled by ΔT strategy usually stagnates earlier. If there were quite large hot water consumption and the ΔT strategy hold a day without stagnation, then the power consumption by the collector pump would be almost equal around 0.5 kWh/day for both strategies and the consumption by the store pumps would be 0.15 kWh for the ΔT strategy and 0.08 kWh for the anti-

stagnation strategy. This difference is explained by significantly lower flow rate in the store loop during a day for the anti-stagnation strategy.

6.4.6. Discussion

An important question to answer before the practical implementation of the proposed anti-stagnation control strategy is when to use this strategy and how to couple it with the usual ΔT control strategy. In the case when the residents leave for vacation for a couple of weeks in the summer it could be switched on manually (the so-called vacation modus of the controller). An automatic switching between the control strategies or automatic adjustment of the duration of night cooling period for the anti-stagnation strategy requires rough prediction of the weather and consumption profile on the following day. In other words, the controller should roughly know how much energy will come into the store next day, and how much consumption will take place. The weather conditions could be approximately estimated as average worst case conditions for the chosen location and season. A more precise weather forecast for the following day can be provided online by a nearby meteorological station. This feature must be programmed in the controller and the data transmission line must be reliable. The hot water consumption should be predicted or set to a fixed value by the consumer. Basing on these two predicted values, the weather conditions and consumption, it seems possible to control the heating system in such a way that no stagnation will take place in the summer and the hot water demand will be covered to 100 per cent.

6.5. Practical application of anti-stagnation control

The proposed and theoretically investigated anti-stagnation strategy was tested in field at two solar heating systems. In the following subsections the difficulties of practical implementation and possible solutions are discussed in more details.

6.5.1. Difficulties of implementation at Huett brewery

First field tests were carried out on solar heating system installed at the Huett brewery near Kassel (Germany). The schematics of the system is shown in the Figure 6.7. The solar heating system consists of 22 flat plate collectors with total aperture area of $155.5\,m^2$, external heat exchanger with specific UA-value of $130\,W/m^2K$ related to the collector aperture area and $10\,m^3$ solar store. Variable speed pumps are installed in primary and secondary solar loops. The solar heating

system charges the brewing water tank with variable water volume of maximum $50\ m^3$.

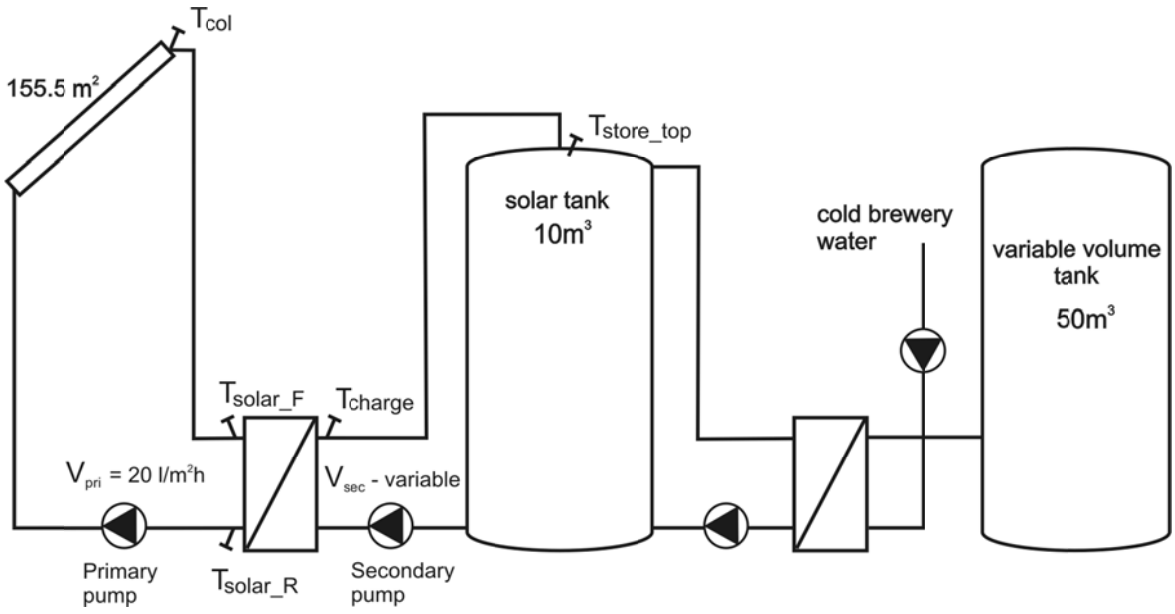

Figure 6.7*: Schematics of solar heating system at Huett brewery near Kassel (Germany) with positions of temperature sensors used for anti-stagnation approach*

The anti-stagnation algorithm is first programmed in the controller of the solar heating system with the following relevant settings:

Stagnation temperatures:

- $T_{col} > 130°C$
- $T_{solar\_F} > 103°C$
- $T_{store\_top} > 98°C$

If one of the temperature thresholds is reached, the primary and secondary pumps shut down.

Anti-stagnation algorithm settings:

- The primary pump turns on at $T_{col} > 75$°C and runs with the constant flow rate $V_{pri} = 20\ l/m^2h$. It shuts down at $T_{col} < 70$°C
- Speed of the secondary pump is varied by the PID controller to keep $T_{charge} = 80$°C. This temperature is chosen much lower than 95°C used in simulations in order to prevent store overheating due to possible temperature fluctuation occurring when using the PID controller.

The approach was monitored for several days. On the first testing day the secondary pump is started for test purpose already at $T_{charge} = 70$°C, indicated by the point P_1

in Figure 6.8. It is seen that just after starting the pump T_{charge} (brown curve) increases by around 10 K with no immediate effect on T_{col} (orange) and T_{solar_F} (light blue) temperatures. At the point P_2 the secondary pump is started at $T_{charge} = 80°C$ and only several minutes after this T_{solar_F} exceeds the stagnation threshold of 103°C and the system stagnates.

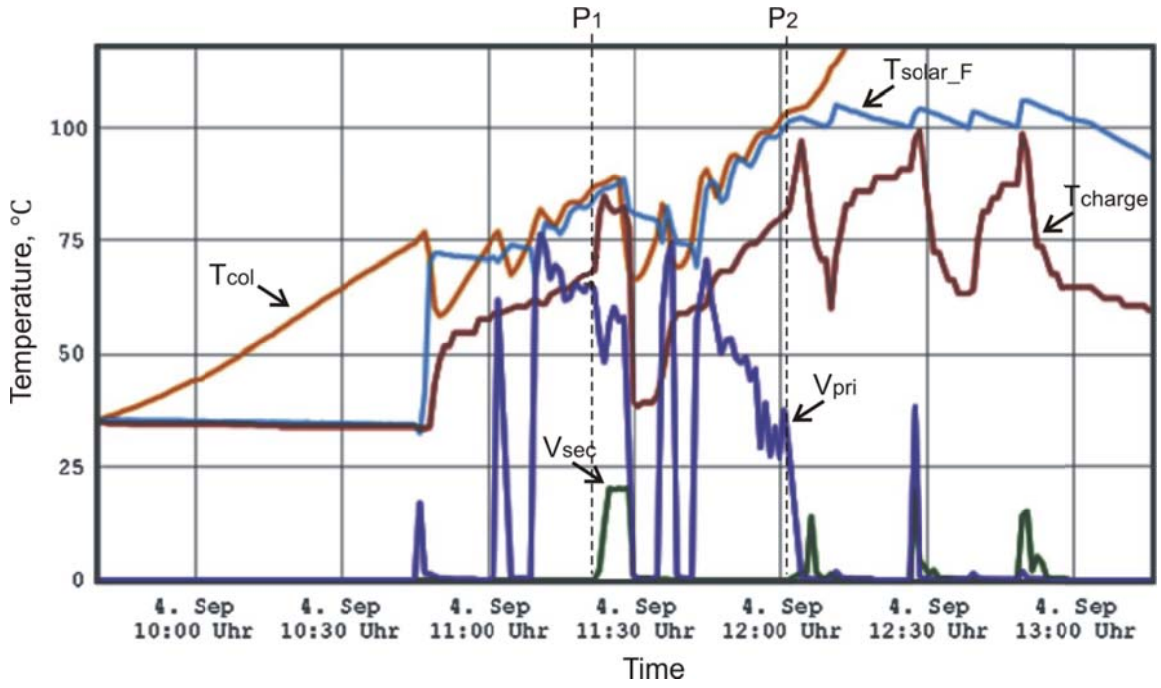

Figure 6.8: *Application of anti-stagnation approach to solar heating system at Huett brewery. First day shows it difficult to hold constant* $T_{charge} = 80°C$. *Point* P_1 *indicates test start of secondary pump and immediate increase of* T_{charge} *by* 10 K *followed by delayed decrease in* T_{solar_F} . *Point* P_2 *shows normal pump start, similar effect for* T_{charge} *and stagnation after only few minutes because of too high* T_{solar_F}

According to the measurements, two weak points of the approach are identified: difference between readings of two sensors T_{solar_F} and T_{charge} is more than 10 K when the secondary pump is not running and T_{charge} increases fast when the pump is turned on. But due to the capacity of the collector, T_{col} and T_{solar_F} respond too late to cooling down of T_{solar_R} and system stagnates. So, it is obvious that holding approximately constant $T_{charge} = 80°C$ is not possible by this control.

For the next day the behaviour of the secondary pump was changed as follows:

- Secondary pump turns on at $T_{solar\_R} > 85°C$ and runs with small speed until $T_{solar\_R} < 85°C$. If $T_{charge} > 80°C$ pump is managed by the PID controller keeping $T_{charge} = 80°C$.

In Figure 6.9 relevant temperatures and flow rates are shown for the second day. Due to modified control of the secondary pump, T_{charge} is hold around 80°C when the primary pump is on. The primary pump switches on and off according to T_{col} temperature. Last time it switches on at around 15: 48 and shortly after that (point P_1 in Figure 6.9) the system stagnate due to too high T_{solar_F}. It seems that the temperature sensor measuring T_{col} is improperly installed.

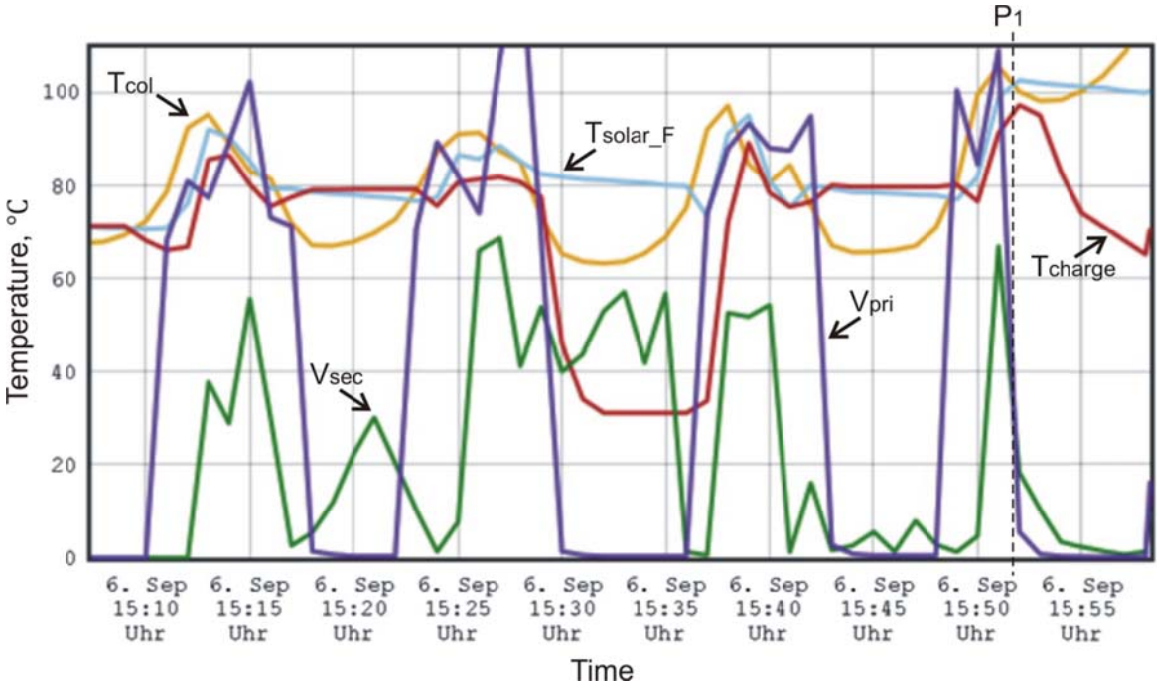

Figure 6.9*: Application of anti-stagnation approach to solar heating system at Huett brewery. Day two shows better control of $T_{charge} = 80°C$ due to modified control of secondary pump. But still system stagnates at point P_1. Primary pump starts too late most likely because improperly installed temperature sensor measuring T_{col}*

The secondary pump control was changed once more in order to keep T_{solar_F} constant at 80°C instead of T_{charge}. Figure 6.10 shows the influence of this modification. The system does not stagnate but T_{solar_F} shows relative large fluctuation around 80°C. It happens due to collector capacity. Variation of the flow rate of the secondary pump does not have immediate effect on the controlled T_{solar_F}. When secondary pump is started at $T_{solar\_F} = 80°C$ collector inlet temperature which is close to T_{solar_R} responses fast, but it takes around 5 minutes till it arrives at the collector output. At this time the PID controller being unable to hold T_{solar_F} (it keeps increasing), increases the flow rate of the secondary pump and cools down T_{solar_R} more than needed. After 5 minutes "cooled" fluid arrives at T_{solar_F}, PID controller switches off the secondary pump and waits until T_{solar_F} rises to 80°C to start the next loop.

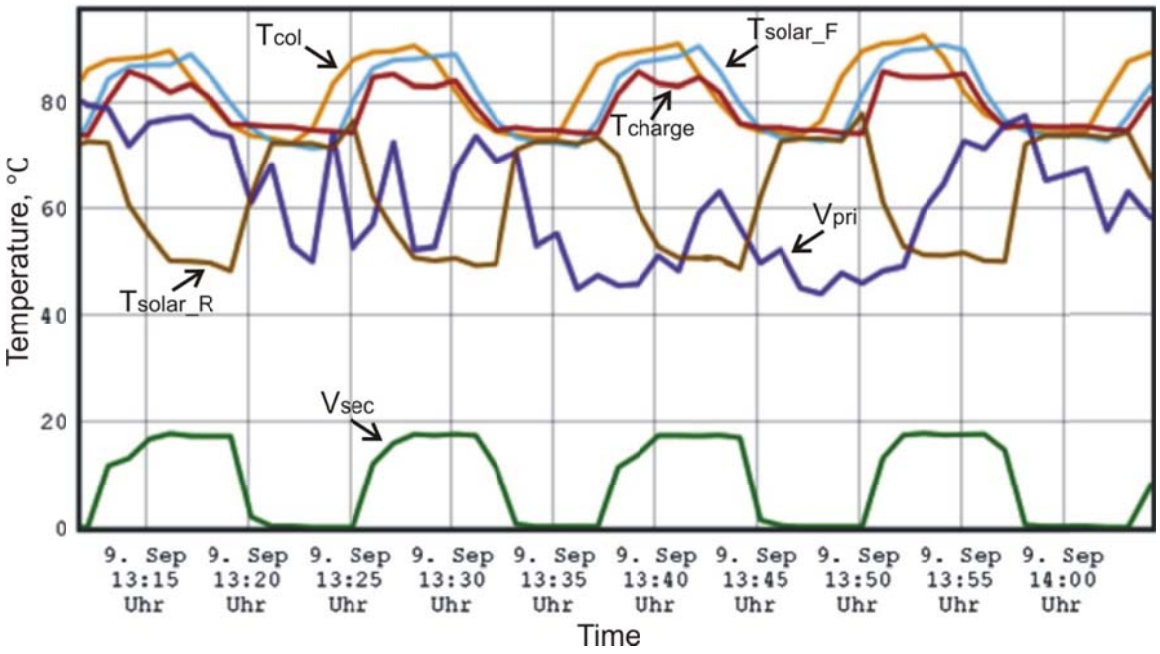

Figure 6.10: *Application of anti-stagnation approach to solar heating system at Huett brewery. Day three shows control of* $T_{solar\_F} = 80°C$ *on a sunny day. Primary pump stays on but secondary pump switches on and off due to capacity in pipes and collector*

It is obvious that neither T_{charge} nor T_{solar_F} can be hold constant in practical implementation by the PID controller varying the flow rate of the secondary pump by the proposed anti-stagnation strategy. The only temperature at the heat exchanger which can be hold constant by the PID controller is T_{solar_R} and, hence, the inlet temperature of the collector.

6.5.2. Modification. Implementation at Gartenstrasse

In the following the results of holding T_{solar_R} constant by varying secondary pump flow rate are shown for the solar thermal system for DHW preparation installed at the Gartenstrasse in Kassel (Germany). The collector field of 32 m^2 charges 2 m^3 store via external heat exchanger and stratification device.

In Figure 6.11 relevant temperatures and flow rates are shown when the flow rate of the secondary pump V_{sec} is varied by the PID controller so that $T_{solar\_R} = 75°C$ on a sunny day. It is seen that T_{solar_R} can be hold constant fairly well, with only $\pm 3K$ fluctuation at the beginning of the secondary pump operation and then with $\pm 1K$. At this T_{charge} can also be hold fairly constant with maximum at 83°C, maximum for T_{col} is 93°C.

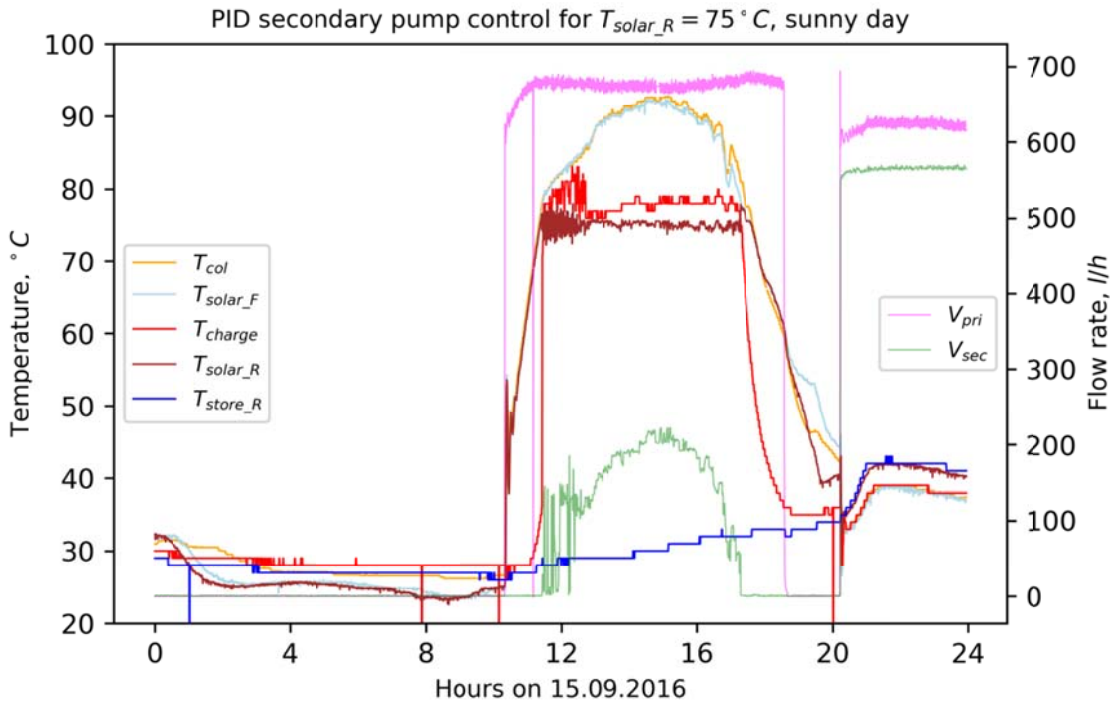

Figure 6.11: *Application of anti-stagnation approach to solar heating system in Gartenstrasse, Kassel on a sunny day.* $T_{solar\_R} = 75$°C *is hold very well (within at max* $\pm$3K*) by varying flow rate of secondary pump* V_{sec}

Figure 6.12 shows application on a partially cloudy day with high fluctuation of solar radiation. It is seen that secondary pump flow rate V_{sec} fluctuates significantly but T_{solar_R} can be still hold fairly constant, within at max $\pm$4.5K. However T_{charge} dependent on both T_{solar_F} and changing V_{sec} also fluctuates and has its maximum at 92°C, noticeably higher than on a sunny day. Maximum for T_{col} remains at 93°C.

To calculate potential of the daily inefficient collector operation for the measured solar heating system two sunny days with similar solar irradiation are chosen: 12 September with $G_t = 3.82\ kWh/m^2d$ and usual ΔT control and 15 September with $G_t = 4.02\ kWh/m^2d$ and anti-stagnation control. On these days the sum of energy incoming into store is calculated giving $Q_{store,in} = 73{,}93\ kWh/d$ for 12 September and $Q_{store,in} = 49{,}56\ kWh/d$ for 15 September what is around 33% less. For partly cloudy 14 September with $G_t = 3.46 kWh/m^2d$, $Q_{store,in} = 42{,}10\ kWh/d$.

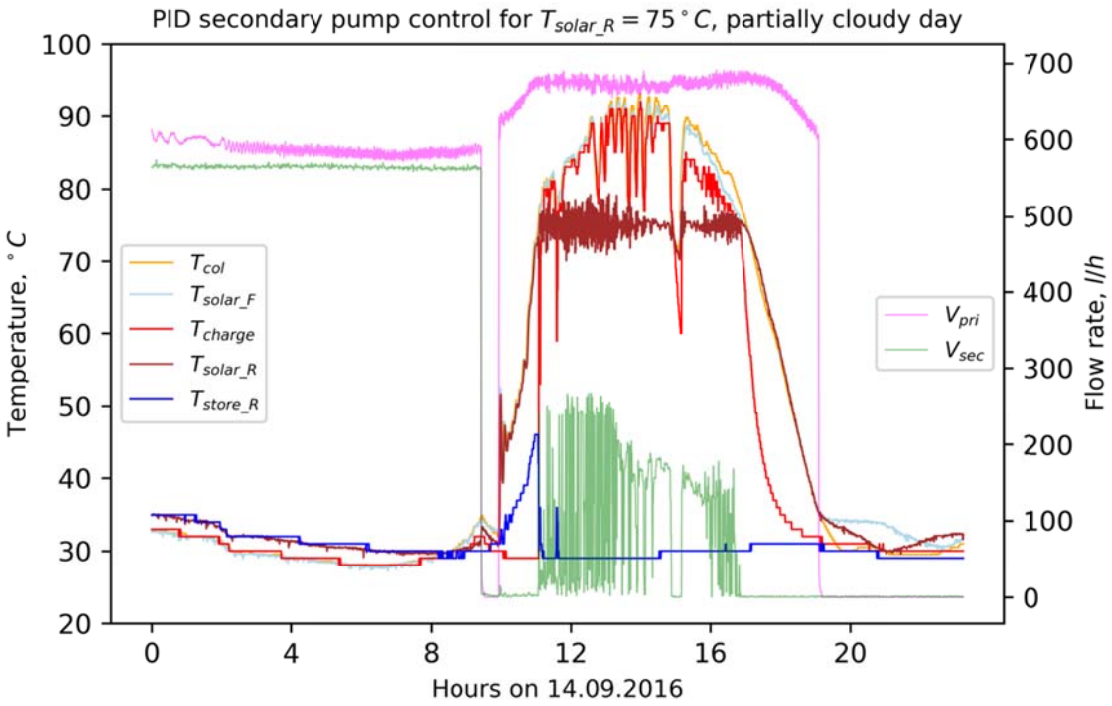

Figure 6.12: *Application of approach to solar heating system at Gartenstrasse, Kassel on a partly cloudy day. Flow rate of secondary pump V_{sec} fluctuates significantly but $T_{solar\_R} = 75°C$ is still hold fairly well (within at max $\pm 4.5K$) and none stagnation threshold is exceeded*

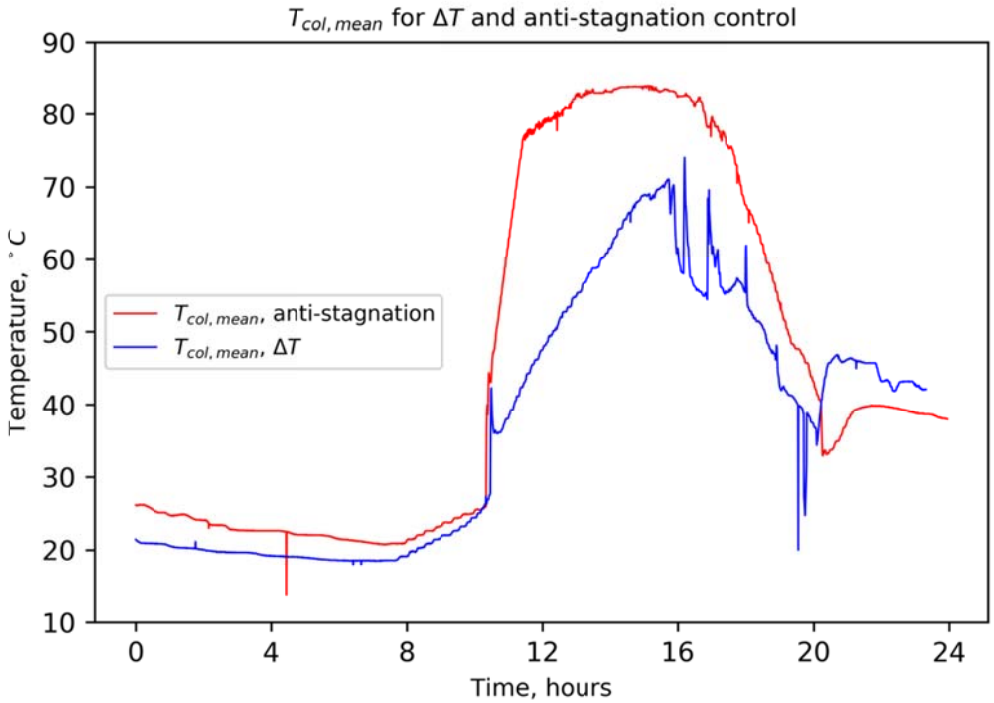

Figure 6.13: *Comparison of $T_{col,mean}$ for usual ΔT (on 12 September) and proposed anti-stagnation (on 15 September) control. During a day $T_{col,mean}$ for anti-stagnation control is significantly higher*

To conclude, the proposed anti-stagnation control strategy shows good theoretical potential. However in practical implementation it is especially sensitive to correct installation of relevant temperature sensors and proper settings of the PID controller because inefficient collector operation occurs at high collector output temperature close to stagnation threshold. Even small fluctuations in control might lead the solar heating system into stagnation. Successfully applied daily anti-stagnation control strategy shows more than 30% reduced energy flow to the store when compared to usual ΔT control.

7. Conclusion and outlook

In this thesis numerical optimization of the IEA Task 32 solar heating combisystem is carried out with regards to three different aspects: optimization of the combisystem in planning process, optimization in operation and anti-stagnation control-based approach. In all cases the main focus was on development of suitable methodology. In this chapter main results of the thesis are summarized and discussed.

7.1. Design optimization of solar combisystem. Application of sensitivity analysis methods

Basing on earlier research carried out at University of Kassel (Krause, 2003) which suggested application of heuristic approaches as evolutionary strategies or genetic methods to optimization of the combisystem in planning process, in this thesis a hybrid genetic CHC - binary (n-ary) search algorithm is proposed and tested with regards to computational efficiency and reliability. The method shows good performance: all optimizations started from different randomly choosen populations converge to nearly the same optimum ($\pm 2\%$). Local binary search algorithm used in the second stage of the hybrid algorithm to accelerate the convergence rate is shown to be able to avoid the local optimum. Good parallelization properties of the CHC algorithm allow up to n times acceleration where n is the population size when running either on the server or in distributed computational network with at least n available cores.

The proposed method is applied to optimization of the solar combisystem described in Chapter 1. For this first the target function as solar energy costs (costs of the combisystem divided by saved auxiliary final energy) is defined and then 18 parameters of solar combisystem which might have an influence on this target function are chosen for optimization within corresponding variation ranges. The combisystem is optimized for chosen extended fractional energy savings incorporated in target function as a constraint in form of additional penalty function term. In this way the IEA Task 32 solar combisystem was optimized for several extended fractional savings and the Pareto front in form of the optimal points connected to the curve: optimal solar energy costs vs. extended fractional savings is obtained. The minimal solar energy costs which can be reached for the combisystem at each given extended fractional savings or vice versa, the maximal

fractional savings for fixed energy costs can be easily determined from the Pareto front. It is shown that improvement of either around 13% in terms of costs or around 19 percent points in terms of energy savings is reachable comparing to the standard dimensioned IEA Task 32 solar combisystem. These figures are seen as potential of the numerical optimization for the combisystem in planning process.

Influence of the domestic hot water and space heating demand as well as the weather conditions (location of the combisystem) is investigated. Domestic hot water profile is proportionally changed $\pm 50\%$ (from initial $200\ l/d$ to $100\ l/d$ and $300\ l/d$) and Pareto fronts are constructed by optimizations. The solar energy costs increases by around 15% for 50% decrease in domestic hot water demand and it decreases by $5-8\%$ (depending on the point on the Pareto front) when demand grows by 50%. The combisystem optimized for standard $200\ l/d$ demand but used with -50% reduced demand ($100\ l/d$) is not significantly worse (only around $1-5\%$) from the combisystem initially optimized for the reduced demand.

Influence of space heating demand is analysed by changing the building envelope. The Pareto fronts for three buildings with $30, 60$ and $100\ kWh/m^2a$ of space heating demand differ less than in 5%. However, the optimal combisystem configurations for the same solar fractional savings differ significantly. For example, to reach $f_{sav,ext} = 0.50$ by the combisystem optimized for the SH demand of $30\ kWh/m^2a$, collector area of $20\ m^2$ is required, for $60\ kWh/m^2a$ - $38\ m^2$ and for $100\ kWh/m^2a$ - $57\ m^2$.

Influence of the location, that is, simultaneous change of the solar insolation and space heating shows that the minimal solar energy costs is nearly equal for the combisystems built in Stockholm and Zurich for $f_{sav,ext} < 0.35$; For higher $f_{sav,ext}$ up to 0.50 the comibsystem in Stockholm is up to 12% more expensive whereas the combisystem built in Madrid is around 40% cheaper. The combisystem optimized for Stockholm but built in Zurich is negligibly worse than that optimized for Zurich in terms of solar energy costs but obviously it has larger fractional savings than if it were built in Stockholm.

In Section 4.6 influence of variation of each optimization parameter as well as two boundary condition parameters on solar energy costs is accessed around the optimum point by application of three global sensitivity methods. First local sensitivity at optimum is estimated. All parameters are changed (mostly in $[-50\%; +50\%]$) one at a time showing that the both boundary condition

parameters: collector price and domestic hot water demand have the largest influence followed by the optimization parameters as boiler set temperature, slope, collector input height in store, collector area, store volume, etc.

To estimate the influence in larger parameter space over the optimum and to quantify it, three different sensitivity methods are applied in "narrow" and "broad" parameter spaces (Table 4.3). The MLR model built by multiple linear regression method basing on "measured" data calculated at random points of the "narrow" parameter space shows very good correspondence ($R^2 = 0.97$) to TRNSYS model in this parameter space. Being justified by high value of the determination coefficient, the model allows simple quantification of the parameter influence on the solar energy costs. For example, increase of the collector price by $1\ Eur/m^2$ causes $4.57\text{e-}04\ Eur/kWh$ increase in the solar energy costs or, in other interpretation, if the collector price is changed by around 25%, the solar energy costs is changed by around $0.025 Eur/kWh$ what is 15% from the optimum (Table 4.4). Two more MLR models are built: one including all parameters and another including only optimization parameters in "broad" parameter space. Both models show poor fit with $R^2 = 0.73$ and $R^2 = 0.29$, respectively. Large difference between two values of the determination coefficient is due to large linear influence of the boundary condition parameters: collector price and DHW load.

The qualitative sensitivity analysis method, the Morris method, based on calculation of measures μ^* and σ of the elementary effects ranks parameters by their importance. The variation coefficient σ/μ^* indicates if the parameter effect is mostly linear, that is nearly the same at different points of the parameter space (small values of σ/μ^*) or nonlinear, significantly different at different points. As expected in "narrow" parameter space the effect of the most parameters is linear, that is also shown by tight confidence ranges of the measure μ^* estimations. In "broad" variation space the effect of collector price remains mostly linear but effects of other significant parameters become nonlinear. Simple "quantification" of the effects shows good agreement between the MLR and Morris methods in "narrow" parameter space.

The extended FAST sensitivity method is applied to quantify the parameter influence in "broad" variation space. According to the method 88% of variation in solar energy price is explained by main effects of the parameters and method can be seen as justified. The collector price and DHW load have the largest influence on the solar energy price showed by the main effects S_i of 41% and 27%, respectively,

followed by $T_{aux,set}$ and sl with 8% and 4%. The results are also in accordance with ranking of the Morris method.

Although quite comprehensive study on design optimization of solar combisystem and sensitivity analysis around optimum is carried out, there are some minor weak points which remain open for future research. The combisystem cost function must be carefully defined by more precise and comprehensive market study than that carried out in this thesis. Installation expenses cannot be taken flat rate but must be differentiated depending on component sizes and installation peculiarities. Sensitivity analysis with respect to other boundary parameters as prices of store, heat exchanger, pipes, pumps, etc. as well as interest rate should be carried out.

7.2. Optimization of solar combisystem in operation

Dynamic optimization of the solar combisystem based on an idea to separate yearly optimization in many short ones is presented in Chapter 5. This approach is justified only when variation of the optimization parameter on a specific hour or day has influence on the system performance (target function) over a short time period only. The proposed approach is applied to estimate potential of the dynamic hourly adjustments of the flow rates in collector and store loops. The optimization results show only a negligible benefit of 0.3 per cent points in terms of the extended fractional energy savings when comparing to the constant (same over the year when the pumps are on) flow rate already optimized during the design optimization. Low optimization potential of dynamic flow rates adjustment indicates that application of a smart controller which varies the flow rates depending on weather forecast would be inefficient.

Potential of dynamic adjustment of the auxiliary heater control settings to the load profile is estimated in a different way. For this the boiler heating up the store auxiliary volume is replaced by two electrical instant heaters introduced into DHW and space heating loops. Simulation results show that comparing to reference 1 combisystem (see Table 5.1) 1.85 percent points higher $f_{sav,ext}$ due to smaller store losses and larger solar gains, is achievable. It means 0.87 $EurCent/kWh$ (around 5%) cheaper solar energy costs. If compared to the initial reference 0 combisystem with optimized constant $T_{set,aux} = 53°C$, the potential is even larger due to higher electricity consumption by the boiler (3.3 percent points in $f_{sav,ext}$ and 1.6 $EurCent/kWh$ (around 10%) in costs). If $T_{set,aux}$ is increased to 70°C for reference 0 combisystem then the dynamically optimized combisystem is 5.8

percent points in $f_{sav,ext}$ (3.1 $EurCent/kWh$ or 17% in costs) better. This last comparison shows the importance of auxiliary set temperature already stated in Chapter 4 by sensitivity methods.

The method of separating long year optimization in many short ones and its implementation for dynamic optimizations of solar thermal systems should be approved by further applications.

7.3. A control - based anti - stagnation approach

A control-based anti-stagnation approach is presented and theoretically investigated in Chapter 6. The proposed approach combines daily inefficient collector operation and nightly cooling. It is investigated theoretically basing on TRNSYS simulation. Minimal specific store volume required for stagnation-free operation for 10 sunniest days in a row without consumption is determined for three climate conditions. The method can be applied to solar thermal systems with external heat exchanger and collector with thermal loss coefficient larger than 3.0 W/m^2K. Influence of boundary conditions on minimal specific store volume is analysed. Change of the global radiation in 5% causes approximately 20% change of the minimal specific store volume. Influence of the ambient temperature variations (daily and nightly, simultaneous and in separate) and duration of night cooling is shown as well.

Difficulties of practical implementation of the approach are described when applied at Huett brewery (near Kassel, Germany). An approach cannot be applied as proposed due to collector capacity. Temperature at the inlet to the store could not be held at a fixed value. Large fluctuation occurs which lead to stagnation. The approach is sensitive to correct positioning of the relevant temperature sensors.

A modification of the approach which cannot ensure the theoretical potential but still provides good results is proposed. It turns to be reliable in application to solar heating system installed in Gartenstrasse in Kassel both on sunny and partially cloudy days. Inefficient daily collector operation shows 33% less energy incoming into the store in comparison to usual ΔT control.

The proposed approach should be further investigated. Nightly cooling must be practically implemented and the solar heating system analysed for several sunny days in a row without consumption. Influence of the PID controller settings on stability of the approach is to be estimated as well.

Nomenclature

Abbreviations

CHC	Cross generational elitist selection, Heterogeneous recombination by incest prevention and Cataclysmic mutation
CPU	Central processing unit
DHW	Domestic hot water
FAST	Fourier amplitude sensitivity test
GenOpt	Generic optimization program
HX	Heat exchanger
IAM	Incident angle modifier
IEA	International energy agency
HTC	High Throughput Computing
MLR	Multiple linear regression
PID	Proportional integral derivative
SA	Sensitivity analysis
SH	Space heating
SSE	Squared sum of errors
SSM	Sum of squares of the model
SSTO	Total sum of squares
TRNSYS	Transient system simulation program

Latin symbols

a_1	First order heat loss coefficient	W/m^2K
a_2	Second order heat loss coefficient	W/m^2K^2
A_{col}	Collector area	m^2
A_j, B_j	Fourier coefficients	$-$
A_{store}	Store surface area	m^2
b_j	Estimates of regression coefficients	$-$
C_{bri}	Specific heat capacity of brine	$kJ/(kgK)$
C_{wat}	Specific heat capacity of water	$kJ/(kgK)$
C_p	Specific heat capacity of water	$kJ/(kgK)$
d_i	Elementary effect	$-$
D	Variance	$-$
D_{iso}	Store insulation thickness	m
D_{pipe}	Pipe inner diameter	mm
$\Delta T_{aux,low}$	Auxiliary controller lower dead band	K
$\Delta T_{aux,up}$	Auxiliary controller upper dead band	K
$\Delta T_{col,low}$	ΔT controller lower dead band	K
$\Delta T_{col,up}$	ΔT controller upper dead band	K
e_i	Residuals	$-$
E_{sol}	Total energy consumption by solar combisystem	kWh
$E_{par,sol}$	Electricity consumption by solar combisystem	kWh
$E_{par,ref}$	Electricity consumption by reference system	kWh
E_{ref}	Total energy consumption by reference heating system	kWh
F_{cost}	Combisystem cost function with $r = 0.025$	Eur
F_{cost}^0	Combisystem cost function with $r = 0$	Eur
$F_{cost,cap}$	Capital costs	Eur
$F_{cost,contr}$	Combisystem cost function for contractor with $r = 0.025$	Eur
$F_{cost,contr}^0$	Combisystem cost function for contractor with $r = 0$	Eur
$F_{cost,disc}$	Discounter components costs	Eur
F_i	Distribution of elementary effects	$-$
$F_{penalty}$	Overall penalty function	$-$
$F_{pen,DHW}$	DHW penalty function	$-$

$F_{pen,SH}$	SH penalty function	$-$
F_{target}	Target function, solar energy costs	Eur/kWh
$f_{sav,ext}$	Extended fractional energy savings	$-$
$f_{sav,therm}$	Thermal fractional energy savings	$-$
f_{si}	Fractional savings indicator	$-$
G_i	Distribution of absolute values of elementary effects	$-$
G_i	Transformation functions in FAST method	$-$
$H_{col,in}$	Collector inlet position in store	$-$
$H_{col,sens}$	ΔT controller sensor position in store	$-$
$H_{SH,in}$	Space heating inlet position in store	$-$
$H_{SH,out}$	Space heating outlet position in store	$-$
$\widetilde{H}_{sol,p}$	Pressure drop in primary loop	m
$\widetilde{H}_{sol,s}$	Pressure drop in secondary loop	m
H_0	Null Hypothesis	$-$
Q_{DHW}	Domestic hot water demand	kWh
Q_{aux}	Auxiliary energy	kWh
$Q_{aux,pen}$	Auxiliary energy with penalty	kWh
$Q_{loss,ref}$	Store thermal losses of reference heating system	kWh
Q_{ref}	Energy consumption by reference heating system	kWh
Q_{SH}	Space heating demand	kWh
K^n	Unit hypercube	$-$
$L_{pipe,p}$	Pipe length in primary loop	m
$L_{pipe,s}$	Pipe length in secondary loop	m
m_{flow}	Specific collector flow rate	kg/m^2h
$\dot{m}_{pri}$	Mass flow rate in primary loop	kg/h
$\dot{m}_{sec}$	Mass flow rate in secondary loop	kg/h
N_{aux}	Number of auxiliary nodes	$-$
N_{max}	Maximum number of nodes in store	$-$
p	p-value	$-$
$Price_{col}$	Collector price	Eur/m^2
r	Interest factor	$-$
R^2	Determination coefficient	$-$

S_i	Main effects	$-$
S_{Ti}	Total effects	$-$
T_{air}	Air temperature of building zone	$℃$
$T_{\text{aux,set}}$	Boiler set temperature	$℃$
T_{col}	Collector output temperature	$℃$
$T_{\text{col,mean}}$	Mean collector temperature	$℃$
T_{DHW}	DHW temperature delivered to consumer	$℃$
UA_{col}	UA-value of collector heat exchanger	W/K
UA_{DHW}	UA-value of external DHW heat exchanger	W/K
V_{aux}	Auxiliary heating volume	m^3
V_{exp}	Expansion vessel volume	l
V_{pri}	Volume flow rate in primary loop	m^3/h
V_{sec}	Volume flow rate in secondary loop	m^3/h
V_{store}	Store volume	m^3
w_i	Frequency	$-$
W_{el}	Electricity consumption by solar combisystem	kWh
$W_{el,ref}$	Electricity consumption by reference heating system	kWh
x_i	Combisystem configuration	$-$
y_i	Measurements of target function	$-$
$\hat{y}_i$	Fit values of target function	$-$
$\overline{y}$	Mean of measured data	$-$

Greek symbols

β_j	Regression coefficients
ε_i	MLR model errors
η_0	Collector optical efficiency
Λ_j	Eigenfrequencies
μ	Mean of distribution F_i in Morris method
μ^*	Mean of distribution G_i in Morris method
σ	Standard deviation of distribution F_i in Morris method
Ω	Input space in Morris method

References

Bornatico, R., Pfeiffer, M., Witzig, A., Guzzella, L., 2012 Particle Swarm Optimization for the Optimal Sizing of a Solar Thermal Building Installation, Energy (41), 31-37

Campolongo, F., Cariboni, J., Saltelli, A., 2007 An effective screening design for sensitivity analysis of large models, Environmental Modelling & Software. Elsevier (22), 1509–1518

Cukier, R. I., Fortuin, C.M., Shuler, K. E., Petschek, A.G., and Schibly, J.H., 1973. Study of the Sensitivity of Coupled Reaction Systems to Uncertainties in Rate Coefficients. 1. Theory, The Journal of Chemical Physics (59), 3873–3878

Drück, H., 2006. MULTIPORT Store – Model for TRNSYS, Type 340 version 1.99F. Institut für Thermodynamik und Wärmetechnik (ITW), Universität Stuttgart, Germany

Eshelman, L., 1991 The CHC Adaptive Search Algorithm. Foundations of Genetic Algorithms, G. Rawlins, ed., 256-283

Fiedler, F., Bales, C., Persson, T., Thür, A., Design method for solar heating systems in combination with pellet boilers/stoves, EuroSun 2006, Glasgow, Scotland

Goldberg, D. E., 1998. Genetic Algorithms in Search, Optimization and Machine Learning, Addison Wesley Longman, Alabama, USA

Heimrath, R., Haller, M., 2007. Project Report A2 of Subtask A: The Reference Heating System, the Template Solar System. A technical report of Subtask A. Graz University of Technology, Graz, Austria

Heimrath, R., 2004. Simulation, Optimierung und Vergleich solarthermischer Anlagen zur Raumwärmeversorgung für Mehrfamilienhäuser, Dissertation am Institut für Wärmetechnik IWT der TU Graz, Graz

Herman, J., Usher, W., 2017. SALib: An open-source Python library for sensitivity analysis. Journal of Open Source Software, 2(9)

HTCondor, 2017. HTCondor Manual http://research.cs.wisc.edu/htcondor/manual/, Center for High Throughput Computing, University of Wisconsin–Madison, USA

Jordan, U., Vajen, K., 2005. DHWcalc: Program to generate Domestic Hot Water Profiles with Statistical Means for User Defined Conditions, Proc. ISES Solar World Congress, Orlando, USA

Klein, S. A., Beckman, W. A., Mitchell, J., Duffie, J. A., Duffie, N., 2009. TRNSYS 17: A Transient System Simulation Program. Solar Energy Laboratory, University of Wisconsin, Madison, USA

Krause, M., 2003. Optimierungsprozess für große solarintegrierte Wärmeversorgungs-anlagen, Dissertation, Kassel Universität, Kassel, Germany.

Kusyy, O., Vajen, K., Jordan, U., 2008. Application of sensitivity analysis to parameters of large solar water heating systems, EuroSun 2008, Lisbon, Portugal

Kusyy, O., Vajen, K., 2011. Theoretical investigation on a control-based approach to avoid stagnation of solar heating systems, Solar World Congress 2011, Kassel, Germany

Kusyy, O., Kuethe, S., Vajen, K., Jordan, U., 2010. Simulation-based optimization of a solar water heating system by a hybrid genetic – binary search algorithm, EuroSun 2010, Graz, Austria

Meteotest, 2016. Meteonorm Software ver. 7.2, http://www.meteonorm.com

Morhart, A., 2010. Stagnation: no standstill in the solar circuit. Sun&Wind Energy, 82-93.

Morris, M. D., 1991. Factorial Sampling Plans for Preliminary Computational Experiments, Technometrics (33), 161–174

Ng Cheng Hin, J., Zmeureanu, R., 2014. Optimization of a residential solar combisystem for minimum lifecycle cost, energy use and exergy destroyed. Solar Energy (100), 102–113.

Nocedal, J., Wright, R., 2006. Numerical Optimization, Springer, New York

Perers, B., Bales, C., 2002. A Solar Collector Model for TRNSYS Simulation and System Testing, A Report of IEA SHC Task 26 Solar Combisystems

Rey, A**.**, Zmeureanu, R., 2016. Multi-objective optimization of a residential solar thermal combisystem. Solar Energy (139), 622–632

Saltelli, A., 2004. Sensitivity analysis in practice. A guide to assessing scientific models, Wiley, Chichester, United Kingdom

Saltelli, A., Tarantola, S., and Chan, 1999. A quantitative model-independent method for global sensitivity analysis of model output, Technometrics (41), 39–56

Scheuren, J., 2008. Untersuchungen zum Stagnationsverhalten solarthermischer Kollektorfelder, Dissertation, Universität Kassel.

Streicher, W., Heimrath, R., 2002. SHC Task 26: Solar Combisystems, Subtask C

Wetter, M., 2008. GenOpt. Generic Optimization Program, User Manual v.2.1.0, https://simulationresearch.lbl.gov/GO/download/manual-2-1-0.pdf, Lawrence Berkeley National Laboratory, University of California, USA

Wilhelms, C., Küthe, S., Heinzen, R., Vajen, K., Jordan, U., 2008. Neue Methoden zur grafischen Modellierung komplexer thermodynamischer Systeme in Trnsys Simulation Studio, Proc. BAUSIM

Zass, K., Jordan, U., Vajen, K., 2007. Influence of different charge and discharge strategies on the performance of medium-sized solar combisystems, Proc. ISES Solar World Conference, Beijing, China

Appendix

A. Price functions of solar combisystem components

Price functions $F_{cost,disc}(C_i)$ for capital cost calculation (4.7) for each main solar combisystem component $C_i, i = 1, \dots, N$ based on online discounter offers. All prices are in Euro and include German value-added tax (VAT) of 19%

Collector: $$-0.66 \cdot \left(\frac{A_{col}}{m^2}\right)^2 + 200 \cdot \frac{A_{col}}{m^2} + 0.75 \quad (A.1)$$

Collector pipes: $$\left(0.005 \cdot \left(\frac{D_{pipe}}{mm}\right)^2 + 0.19 \cdot \frac{D_{pipe}}{mm} + 1.2\right) \cdot 2 \cdot \frac{L_{pipe,p}}{m} \quad (A.2)$$

Expansion vessel: $$0.008 \cdot \left(\frac{V_{exp}}{l}\right)^2 + 0.35 \cdot \frac{V_{exp}}{l} + 13.67 \quad (A.3)$$

Collector pump: $$8.77 \cdot \left(\frac{\dot{V}_{pri}}{m^3/h}\right)^2 + 2.47 \cdot \frac{\dot{V}_{pri}}{m^3/h} \cdot \frac{\widetilde{H}_{sol,p}}{m} + 37.92 \cdot \frac{\dot{V}_{pri}}{m^3/h} + 91.43 \quad (A.4)$$

Solar HX: $$0.145 \cdot \frac{UA_{col}}{W/K} - 10.51 \cdot \frac{m_{flow}}{l/m^2 h} + 323 \quad (A.5)$$

DHW HX: $$0.043 \cdot \frac{UA_{DHW}}{W/K} + 48.5 \quad (A.6)$$

Store charge pump: $$8.77 \cdot \left(\frac{\dot{V}_{sec}}{m^3/h}\right)^2 + 2.47 \cdot \frac{\dot{V}_{sec}}{m^3/h} \cdot \frac{\widetilde{H}_{sol,s}}{m} + 37.92 \cdot \frac{\dot{V}_{sec}}{m^3/h} + 91.43 \quad (A.7)$$

Store: $$\begin{cases} 399.5 \cdot \frac{V_{store}}{m^3} + 244.3, & V_{store} \le 2m^3 \\ 171.3 \cdot \left(\frac{V_{store}}{m^3}\right)^2 + 1689 \cdot \frac{V_{store}}{m^3} - 1682, & V_{store} > 2m^3 \end{cases} \quad (A.8)$$

Store insulation: $$A_{store} \cdot \left(54.89 \cdot \left(\frac{A_{store}}{m^2}\right)^{-0.794} + 24.56\right) \cdot \frac{\left(1 - 0.7^{\frac{D_{iso}}{m}/0.1}\right)}{0.3} \quad (A.9)$$

Cellar pipes: $$\left(0.005 \cdot \left(\frac{D_{pipe}}{mm}\right)^2 + 0.19 \cdot \frac{D_{pipe}}{mm} + 1.2\right) \cdot 2 \cdot \frac{L_{pipe,s}}{m} \quad (A.10)$$

Controller: $$300 \quad (A.11)$$

Other parts: $$300 + 10 \cdot \frac{A_{col}}{m^2} \quad (A.12)$$

B. Influence of boundary conditions on optimization results (Tables with results)

Table B.1: *Optimization results for DHW demand* -50% $(100\ l/d)$ *presented by red curve in Figure* 4.11*. First column shows properties of base case Task 32 combisystem*

	base case Task 32	opt2, $c = 0.40$	opt3, $c = 0.45$	opt4, $c = 0.50$	opt5, $c = 0.60$
Optimization parameters					
Collector area, m^2	20	25	31	39	58
Store volume, m^3	2	1.8	2	2	2.9
Auxiliary volume, m^3	0.2	0.1	0.14	0.12	0.22
Store insulation, m	0.15	0.2	0.2	0.2	0.2
Pipe inner diameter, mm	13	14	14	16	18
Specific flow rate, kg/m^2h	15	12	11	11	10
ΔT upper dead band, K	7	7	8	5	5.5
ΔT lower dead band, K	4	1	0.5	0.5	0.5
ΔT sensor pos. in store, %	0.1	0.09	0.11	0.13	0.13
UA of solar HX, W/K	2100	1900	1900	3100	4000
UA of DHW HX, W/K	5333	3480	3480	3480	4100
Coll. inlet pos. in store, %	0.4	0.84	0.81	0.81	0.84
SH outlet pos. in store, %	0.96	0.95	0.93	0.94	0.93
SH inlet pos. in store, %	0.15	0.15	0.2	0.18	0.18
Set temp. of aux. heater, $°C$	63	50	48	49	46
Aux. upper dead band, K	8	6.4	4	5.6	5.6
Aux. lower dead band, K	2	2.6	2.1	3.1	2.8
Collector slope,°	45	59	60	62	64
Energy quantities, MWh/a					
Aux. energy demand, Q_{aux}	7.82	5.98	5.5	4.96	3.87
Solar yield, (kWh/m^2a)	5.89(294)	5.65(225)	6.31(203)	6.92(177)	8.53(147)
Store losses	2.3	1.69	1.85	1.91	2.38
Ref. store losses, $Q_{loss,ref}$	0.64	0.64	0.64	0.64	0.64
SH demand, Q_{SH}	8.46	8.45	8.45	8.45	8.45
DHW demand, Q_{DHW}	2.93	1.46	1.46	1.46	1.46
Ref. demand, E_{ref}	14.72	12.97	12.98	12.97	12.98
Ref. el. demand, $E_{par,ref}$	0.23	0.22	0.22	0.22	0.22
Solar demand, E_{sol}	9.88	7.7	7.12	6.49	5.2
Solar el. demand, $E_{par,sol}$	0.27	0.26	0.26	0.26	0.25
Capital costs, $kEur$ (Eur/m^2)					
End user $F_{cost,cap}$	13.3(663)	14.9(594)	17.0(548)	19.8(506)	26.8(461)
Contractor $F_{cost,cap}$	8.9(442)	9.9(396)	11.3(365)	13.2(337)	17.9(307)
Target function (Annuity costs), Eur/kWh, (Eur/a)					
End user, interest rate 2.5% F_{target}, (F_{cost})	**0.196**, (951)	**0.202**, (1064)	**0.208**, (1217)	**0.218**, (1415)	**0.247**, (1920)
End user, own capital F^0_{target}, (F^0_{cost})	0.158, (763)	0.162, (854)	0.167, (977)	0.175, (1136)	0.198, (1541)
Contractor, int. rate 2.5% $F_{target,contr}$, $(F_{cost,contr})$	0.131, (634)	0.135, (709)	0.139, (811)	0.146, (943)	0.165, (1280)
Contractor, own capital $F^0_{target,contr}$, $(F^0_{cost,contr})$	0.105, (509)	0.108, (569)	0.111, (651)	0.117, (757)	0.132, (1027)
Contractor, own cap., no tax $\hat{F}^0_{target,contr}$, $(\hat{F}^0_{cost,contr})$	0.088, (427)	0.091, (478)	0.094, (547)	0.098, (636)	0.111, (863)
Extended fractional energy savings					
$f_{sav,ext}$	**0.329**	**0.406**	**0.451**	**0.5**	**0.6**

Table B.2: *Optimization results for DHW demand* $+50\%$ $(300\ l/d)$ *presented by green curve in Figure* 4.11. *First column shows properties of base case Task 32 combisystem*

	base case Task 32	opt1, $c = 0.30$	opt2, $c = 0.35$	opt3, $c = 0.40$	opt4, $c = 0.50$	opt5, $c = 0.60$
Optimization parameters						
Collector area, m^2	20	13	20	24	39	55
Store volume, m^3	2	1.2	1.3	1.8	2	3
Auxiliary volume, m^3	0.2	0.16	0.14	0.14	0.24	0.2
Store insulation, m	0.15	0.25	0.2	0.25	0.3	0.3
Pipe inner diameter, mm	13	10	12	12	14	18
Specific flow rate, kg/m^2h	15	11	9	8	7	10
ΔT upper dead band, K	7	4	7.5	4	4	9
ΔT lower dead band, K	4	0.5	1.7	3.5	1	1
ΔT sensor pos. in store, %	0.1	0.2	0.13	0.18	0.16	0.15
UA of solar HX, W/K	2100	1300	1600	1600	3100	4300
UA of DHW HX, W/K	5333	8440	7820	7200	9060	10300
Coll. inlet pos. in store, %	0.4	0.74	0.81	0.77	0.77	0.87
SH outlet pos. in store, %	0.96	0.93	0.9	0.93	0.89	0.94
SH inlet pos. in store, %	0.15	0.26	0.3	0.28	0.26	0.23
Set temp. of aux. heater, $°C$	63	66	66	67	61	63
Aux. upper dead band, K	8	15.2	13.6	13.6	14.4	16
Aux. lower dead band, K	2	4	4	3.3	2.4	3.5
Collector slope,°	45	52	57	56	60	64
Energy quantities, MWh/a						
Aux. energy demand, Q_{aux}	7.82	9.17	8.36	7.76	6.36	5.06
Solar yield, (kWh/m^2a)	5.89(294)	4.72(363)	5.81(290)	6.46(269)	7.90(202)	9.57(174)
Store losses	2.3	1.04	1.31	1.34	1.36	1.68
Ref. store losses, $Q_{loss,ref}$	0.64	0.64	0.64	0.64	0.64	0.64
SH demand, Q_{SH}	8.46	8.45	8.45	8.45	8.45	8.47
DHW demand, Q_{DHW}	2.93	4.39	4.39	4.39	4.39	4.39
Ref. demand, E_{ref}	14.72	16.45	16.45	16.45	16.45	16.47
Ref. el. demand, $E_{par,ref}$	0.23	0.23	0.23	0.23	0.23	0.23
Solar demand, E_{sol}	9.88	11.51	10.58	9.86	8.21	6.65
Solar el. demand, $E_{par,sol}$	0.27	0.28	0.28	0.27	0.27	0.26
Capital costs, $kEur$ (Eur/m^2)						
End user $F_{cost,cap}$	13.3(663)	10.6(813)	12.9(647)	15.0(625)	20.7(530)	27.4(497)
Contractor $F_{cost,cap}$	8.9(442)	7.1(542)	8.6(431)	10.0(416)	13.8(353)	18.2(331)
Target function (Annuity costs), Eur/kWh, (Eur/a)						
End user, interest rate 2.5% F_{target}, (F_{cost})	**0.196**, (951)	**0.158**, (927)	**0.163**, (1075)	**0.180**, (1483)	**0.201**, (1960)	**0.154**, (758)
End user, own capital F^0_{target}, (F^0_{cost})	0.158, (763)	0.127, (744)	0.131, (863)	0.144, (1190)	0.161, (1573)	0.123, (608)
Contractor, int. rate 2.5% $F_{target,contr}$, $(F_{cost,contr})$	0.131, (634)	0.105, (618)	0.109, (717)	0.120, (988)	0.134, (1307)	0.102, (505)
Contractor, own capital $F^0_{target,contr}$, $(F^0_{cost,contr})$	0.105, (509)	0.085, (496)	0.087, (575)	0.096, (793)	0.108, (1049)	0.082, (405)
Contractor, own cap., no tax $\hat{F}^0_{target,contr}$, $(\hat{F}^0_{cost,contr})$	0.088, (427)	0.071, (417)	0.073, (483)	0.081, (667)	0.090, (881)	0.069, (340)
Extended fractional energy savings						
$f_{sav,ext}$	**0.329**	**0.3**	**0.357**	**0.401**	**0.501**	**0.596**

Table B.3: *Optimization results for SH demand* $30\,kWh/m^2a$ *presented by green curve in Figure* 4.12*. First column shows properties of base case Task 32 combisystem*

	base case Task 32	opt2, $c = 0.30$	opt3, $c = 0.40$	opt4, $c = 0.50$	opt5, $c = 0.60$
Optimization parameters					
Collector area, m^2	20	9	13	20	32
Store volume, m^3	2	0.77	1.17	1.57	2
Auxiliary volume, m^3	0.2	0.14	0.14	0.26	0.16
Store insulation, m	0.15	0.2	0.2	0.25	0.2
Pipe inner diameter, mm	13	14	10	10	14
Specific flow rate, kg/m^2h	15	36	13	8	9
ΔT upper dead band, K	7	4	6.5	4	8
ΔT lower dead band, K	4	1.4	1.2	4	0.7
ΔT sensor pos. in store, %	0.1	0.2	0.13	0.16	0.15
UA of solar HX, W/K	2100	1000	1000	1300	2200
UA of DHW HX, W/K	5333	5340	5340	5960	7200
Coll. inlet pos. in store, %	0.4	0.45	0.74	0.77	0.77
SH outlet pos. in store, %	0.96	0.91	0.89	0.84	0.93
SH inlet pos. in store, %	0.15	0.3	0.18	0.3	0.26
Set temp. of aux. heater, $°C$	63	55	56	51	51
Aux. upper dead band, K	8	8	12	9.6	8
Aux. lower dead band, K	2	0.7	3.5	3.8	2.4
Collector slope,°	45	53	59	61	61
Energy quantities, MWh/a					
Aux. energy demand, Q_{aux}	7.82	4.88	4.26	3.52	2.73
Solar yield, (kWh/m^2a)	5.89(294)	3.16(351)	4.05(311)	4.87(243)	6.24(194)
Store losses	2.3	0.99	1.25	1.32	1.87
Ref. store losses, $Q_{loss,ref}$	0.64	0.64	0.64	0.64	0.64
SH demand, Q_{SH}	8.46	4.12	4.12	4.12	4.12
DHW demand, Q_{DHW}	2.93	2.93	2.93	2.93	2.93
Ref. demand, E_{ref}	14.72	9.54	9.53	9.54	9.54
Ref. el. demand, $E_{par,ref}$	0.23	0.2	0.2	0.2	0.2
Solar demand, E_{sol}	9.88	6.38	5.65	4.76	3.82
Solar el. demand, $E_{par,sol}$	0.27	0.24	0.24	0.24	0.23
Capital costs, $kEur$ (Eur/m^2)					
End user $F_{cost,cap}$	13.3(663)	7.8(865)	10.0(768)	13.3(662)	17.7(552)
Contractor $F_{cost,cap}$	8.9(442)	5.2(576)	6.7(512)	8.8(441)	11.8(368)
Target function (Annuity costs), Eur/kWh, (Eur/a)					
End user, interest rate 2.5% F_{target}, (F_{cost})	**0.196**, (951)	**0.177**, (558)	**0.185**, (716)	**0.199**, (950)	**0.222**, (1266)
End user, own capital F^0_{target}, (F^0_{cost})	0.158, (763)	0.142, (447)	0.148, (575)	0.160, (762)	0.178, (1016)
Contractor, int. rate 2.5% $F_{target,contr}$, $(F_{cost,contr})$	0.131, (634)	0.118, (372)	0.123, (477)	0.133, (633)	0.148, (844)
Contractor, own capital $F^0_{target,contr}$, $(F^0_{cost,contr})$	0.105, (509)	0.095, (298)	0.099, (383)	0.107, (508)	0.119, (677)
Contractor, own cap., no tax $\hat{F}^0_{target,contr}$, $(\hat{F}^0_{cost,contr})$	0.088, (427)	0.079, (250)	0.083, (322)	0.090, (427)	0.100, (569)
Extended fractional energy savings					
$f_{sav,ext}$	**0.329**	**0.331**	**0.407**	**0.501**	**0.6**

Table B.4: *Optimization results for SH demand* $100\ kWh/m^2a$ *presented by red curve in Figure* 4.12*. First column shows properties of base case Task 32 combisystem*

	base case Task 32	opt2, $c = 0.0$	opt3, $c = 0.30$	opt4, $c = 0.35$	opt5, $c = 0.50$
Optimization parameters					
Collector area, m^2	20	14	24	34	57
Store volume, m^3	2	1.1	1.83	2	5
Auxiliary volume, m^3	0.2	0.12	0.12	0.1	0.13
Store insulation, m	0.15	0.2	0.25	0.2	0.25
Pipe inner diameter, mm	13	10	14	14	16
Specific flow rate, kg/m^2h	15	12	12	12	10
ΔT upper dead band, K	7	4	5.5	5	4
ΔT lower dead band, K	4	4	4	0.5	1.9
ΔT sensor pos. in store, %	0.1	0.15	0.07	0.13	0.13
UA of solar HX, W/K	2100	1300	1600	2200	4900
UA of DHW HX, W/K	5333	4720	5960	5340	5960
Coll. inlet pos. in store, %	0.4	0.84	0.87	0.87	0.9
SH outlet pos. in store, %	0.96	0.91	0.97	0.97	0.99
SH inlet pos. in store, %	0.15	0.3	0.3	0.26	0.26
Set temp. of aux. heater, $°C$	63	56	54	61	59
Aux. upper dead band, K	8	12	7.2	16	15.2
Aux. lower dead band, K	2	2.6	2.8	2.4	2.8
Collector slope,°	45	51	52	58	59
Energy quantities, MWh/a					
Aux. energy demand, Q_{aux}	7.82	13.48	11.99	11.09	8.42
Solar yield, (kWh/m^2a)	5.89(294)	4.63(330)	6.35(264)	7.67(225)	11.1(193)
Store losses	2.3	1.18	1.38	1.79	2.45
Ref. store losses, $Q_{loss,ref}$	0.64	0.64	0.64	0.64	0.64
SH demand, Q_{SH}	8.46	14	14	14.01	14.01
DHW demand, Q_{DHW}	2.93	2.93	2.93	2.93	2.93
Ref. demand, E_{ref}	14.72	21.3	21.3	21.31	21.32
Ref. el. demand, $E_{par,ref}$	0.23	0.25	0.25	0.25	0.25
Solar demand, E_{sol}	9.88	16.62	14.86	13.79	10.65
Solar el. demand, $E_{par,sol}$	0.27	0.3	0.29	0.29	0.29
Capital costs, $kEur$ (Eur/m^2)					
End user $F_{cost,cap}$	13.3(663)	10.3(737)	14.9(622)	18.1(533)	29.1(509)
Contractor $F_{cost,cap}$	8.9(442)	6.9(491)	10.0(414)	12.1(355)	19.4(339)
Target function (Annuity costs), Eur/kWh, (Eur/a)					
End user, interest rate 2.5% F_{target}, (F_{cost})	**0.196**, (951)	**0.158**, (739)	**0.166**, (1070)	**0.173**, (1300)	**0.195**, (2082)
End user, own capital F^0_{target}, (F^0_{cost})	0.158, (763)	0.127, (593)	0.133, (859)	0.139, (1044)	0.157, (1671)
Contractor, int. rate 2.5% $F_{target,contr}$, $(F_{cost,contr})$	0.131, (634)	0.105, (493)	0.111, (713)	0.115, (867)	0.130, (1388)
Contractor, own capital $F^0_{target,contr}$, $(F^0_{cost,contr})$	0.105, (509)	0.085, (395)	0.089, (572)	0.093, (696)	0.104, (1114)
Contractor, own cap., no tax $\hat{F}^0_{target,contr}$, $(\hat{F}^0_{cost,contr})$	0.088, (427)	0.071, (332)	0.075, (481)	0.078, (584)	0.088, (936)
Extended fractional energy savings					
$f_{sav,ext}$	**0.329**	**0.22**	**0.303**	**0.353**	**0.5**

Table B.5: *Optimization results for Stockholm (SE) presented by green curve in Figure* 4.13. *First column shows properties of base case Task 32 combisystem located in Zurich (CH)*

	base case Task 32	opt1, $c = 0.25$	opt2, $c = 0.30$	opt3, $c = 0.35$	opt4, $c = 0.40$	opt5, $c = 0.50$
Optimization parameters						
Collector area, m^2	20	16	22	30	41	60
Store volume, m^3	2	1.2	1.5	1.9	2	5
Auxiliary volume, m^3	0.2	0.14	0.14	0.14	0.14	0.26
Store insulation, m	0.15	0.2	0.2	0.2	0.2	0.25
Pipe inner diameter, mm	13	12	12	14	14	18
Specific flow rate, kg/m^2h	15	11	9	9	10	10
ΔT upper dead band, K	7	6.5	8.5	10	11.5	6.5
ΔT lower dead band, K	4	0.7	1	2.4	1.9	0.5
ΔT sensor pos. in store, %	0.1	0.13	0.15	0.05	0.05	0.11
UA of solar HX, W/K	2100	1000	1600	2200	3100	3700
UA of DHW HX, W/K	5333	4720	5340	5340	5340	5960
Coll. inlet pos. in store, %	0.4	0.81	0.87	0.74	0.81	0.9
SH outlet pos. in store, %	0.96	0.89	0.92	0.93	0.95	0.95
SH inlet pos. in store, %	0.15	0.3	0.3	0.24	0.2	0.24
Set temp. of aux. heater, $°C$	63	58	55	58	55	51
Aux. upper dead band, K	8	13.6	9.6	14.4	12	9.6
Aux. lower dead band, K	2	2.8	3.5	4	2.8	3.3
Collector slope,°	45	64	66	70	71	75
Energy quantities, MWh/a						
Aux. energy demand, Q_{aux}	7.82	11.73	10.91	10.11	9.28	7.64
Solar yield, (kWh/m^2a)	5.89(294)	4.81(300)	5.78(262)	6.87(228)	7.82(190)	10.1(168)
Store losses	2.3	1.23	1.38	1.67	1.79	2.4
Ref. store losses, $Q_{loss,ref}$	0.64	0.64	0.64	0.64	0.64	0.64
SH demand, Q_{SH}	8.46	12.41	12.41	12.42	12.41	12.42
DHW demand, Q_{DHW}	2.93	2.93	2.93	2.93	2.93	2.93
Ref. demand, E_{ref}	14.72	19.41	19.42	19.43	19.42	19.43
Ref. el. demand, $E_{par,ref}$	0.23	0.25	0.25	0.25	0.25	0.25
Solar demand, E_{sol}	9.88	14.54	13.57	12.61	11.64	9.7
Solar el. demand, $E_{par,sol}$	0.27	0.29	0.29	0.29	0.28	0.28
Capital costs, $kEur$ (Eur/m^2)						
End user $F_{cost,cap}$	13.3(663)	11.0(690)	13.6(619)	16.8(560)	20.5(499)	29.5(491)
Contractor $F_{cost,cap}$	8.9(442)	7.4(460)	9.1(413)	11.2(373)	13.7(332)	19.7(327)
Target function (Annuity costs), Eur/kWh, (Eur/a)						
End user, interest rate 2.5% F_{target}, (F_{cost})	**0.196**, (951)	**0.162**, (791)	**0.167**, (977)	**0.177**, (1204)	**0.189**, (1467)	**0.217**, (2114)
End user, own capital F^0_{target}, (F^0_{cost})	0.158, (763)	0.130, (635)	0.134, (784)	0.142, (966)	0.151, (1178)	0.174, (1697)
Contractor, int. rate 2.5% $F_{target,contr}$, ($F_{cost,contr}$)	0.131, (634)	0.108, (527)	0.111, (651)	0.118, (803)	0.126, (978)	0.145, (1409)
Contractor, own capital $F^0_{target,contr}$, ($F^0_{cost,contr}$)	0.105, (509)	0.087, (423)	0.089, (522)	0.095, (644)	0.101, (785)	0.116, (1131)
Contractor, own cap., no tax $\hat{F}^0_{target,contr}$, ($\hat{F}^0_{cost,contr}$)	0.088, (427)	0.073, (356)	0.075, (439)	0.079, (541)	0.085, (659)	0.098, (950)
Extended fractional energy savings						
$f_{sav,ext}$	**0.329**	**0.251**	**0.301**	**0.351**	**0.401**	**0.501**

Table B.6: *Optimization results for Madrid (ES) presented by red curve in Figure* 4.13. *First column shows properties of base case Task 32 combisystem located in Zurich (CH)*

	base case Task 32	opt1, $c = 0.0$	opt2, $c = 0.60$
Optimization parameters			
Collector area, m^2	20	9	18
Store volume, m^3	2	0.8	1.5
Auxiliary volume, m^3	0.2	0.12	0.12
Store insulation, m	0.15	0.15	0.15
Pipe inner diameter, mm	13	14	12
Specific flow rate, kg/m^2h	15	36	10
ΔT upper dead band, K	7	4	5
ΔT lower dead band, K	4	0.5	1.9
ΔT sensor pos. in store, %	0.1	0.24	0.13
UA of solar HX, W/K	2100	1000	1300
UA of DHW HX, W/K	5333	4100	5340
Coll. inlet pos. in store, %	0.4	0.71	0.87
SH outlet pos. in store, %	0.96	0.97	0.95
SH inlet pos. in store, %	0.15	0.27	0.18
Set temp. of aux. heater, $°C$	63	59	57
Aux. upper dead band, K	8	10.4	12
Aux. lower dead band, K	2	3.5	2.8
Collector slope,°	45	54	58
Energy quantities, MWh/a			
Aux. energy demand, Q_{aux}	7.82	5.29	3.43
Solar yield, (kWh/m^2a)	5.89(294)	5.25(583)	7.69(427)
Store losses	2.3	1.63	2.19
Ref. store losses, $Q_{loss,ref}$	0.64	0.64	0.64
SH demand, Q_{SH}	8.46	5.96	5.96
DHW demand, Q_{DHW}	2.93	2.93	2.93
Ref. demand, E_{ref}	14.72	11.7	11.7
Ref. el. demand, $E_{par,ref}$	0.23	0.2	0.2
Solar demand, E_{sol}	9.88	6.88	4.67
Solar el. demand, $E_{par,sol}$	0.27	0.26	0.25
Capital costs, $kEur$ (Eur/m^2)			
End user $F_{cost,cap}$	13.3(663)	7.5(836)	11.9(663)
Contractor $F_{cost,cap}$	8.9(442)	5.0(557)	8.0(442)
Target function (Annuity costs), Eur/kWh, (Eur/a)			
End user, interest rate 2.5% F_{target}, (F_{cost})	**0.196**, (951)	**0.112**, (539)	**0.122**, (855)
End user, own capital F^0_{target}, (F^0_{cost})	0.158, (763)	0.090, (433)	0.098, (686)
Contractor, int. rate 2.5% $F_{target,contr}$, $(F_{cost,contr})$	0.131, (634)	0.075, (359)	0.081, (570)
Contractor, own capital $F^0_{target,contr}$, $(F^0_{cost,contr})$	0.105, (509)	0.060, (288)	0.065, (457)
Contractor, own cap., no tax $\hat{F}^0_{target,contr}$, $(\hat{F}^0_{cost,contr})$	0.088, (427)	0.050, (242)	0.055, (384)
Extended fractional energy savings			
$f_{sav,ext}$	**0.329**	**0.412**	**0.601**

C. MLR model for $f_{sav,ext}$ in "narrow" parameter space

Table C.1: *Results of MLR method for $f_{sav,ext}$ in "narrow" variation space as in Table 4.3. Estimates of the intercept and regression coefficients b_j, 95% confidence interval, corresponding p – values and significance levels are presented. Absolute and relative (with respect to optimum) variation in $|\Delta F_{target}|$ is shown due to 55% variation in corresponding parameters. Determination coefficient R^2 equals* 0.98

Paramater	b_j estimate	95% Confidence interval		p - value	Signifi-cance	$\lvert\Delta F_{target}\rvert$, Eur/kWh	$\lvert\Delta F_{target}\rvert$, % of opt.
		2.5%	97.5%				
0. Intercept	2.84E-01	2.72E-01	2.96E-01	<2e-16	***		
1. A_{col}, m^2	8.45E-03	8.29E-03	8.60E-03	<2e-16	***	0.033	10.7
2. V_{store}, m^3	1.94E-02	1.76E-02	2.12E-02	<2e-16	***	0.006	2.1
3. N_{aux}	-1.42E-03	-1.69E-03	-1.15E-03	<2e-16	***	0.003	1.0
4. D_{iso}, m	9.43E-02	8.34E-02	1.05E-01	<2e-16	***	0.005	1.7
5. D_{pipe}, mm	-2.40E-04	-4.67E-04	-1.32E-05	0.04	*.	0.001	0.2
6. m_{flow}, kg/m^2h	-6.36E-04	-8.26E-04	-4.46E-04	1.31e-10	***	0.002	0.6
7. $\Delta T_{col,up}$, K	-6.19E-04	-1.17E-03	-6.28E-05	0.03	.*	0.001	0.2
8. $\Delta T_{col,low}$, K	9.50E-05	-4.69E-04	6.59E-04	0.7		0.000	0.0
9. $H_{col,sens}$	-4.06E-03	-2.09E-02	1.28E-02	0.6		0.000	0.0
10. UA_{col}, W/K	9.91E-06	7.77E-06	1.21E-05	<2e-16	***	0.003	0.9
11. $H_{col,in}$	1.86E-02	1.58E-02	2.13E-02	<2e-16	***	0.004	1.3
12. $H_{SH,out}$	-1.63E-02	-4.72E-02	1.46E-02	0.3		0.000	0.1
13. $H_{SH,in}$	1.31E-02	5.69E-03	2.04E-02	0.0	***.	0.001	0.4
14. UA_{DHW}, W/K	2.26E-07	-1.07E-07	5.59E-07	0.2		0.000	0.1
15. $T_{aux,set}$, $°C$	-1.69E-03	-1.73E-03	-1.65E-03	<2e-16	***	0.024	7.9
16. $\Delta T_{aux,up}$, K	5.57E-04	2.54E-04	8.61E-04	0.0	***	0.001	0.4
17. $\Delta T_{aux,low}$, K	-1.38E-04	-1.17E-03	8.95E-04	0.8		0.000	0.0
18. sl, °	-1.07E-03	-1.11E-03	-1.03E-03	<2e-16	***	0.015	5.0
19. DHW	1.31E-02	1.09E-02	1.52E-02	<2e-16	***	0.004	1.2
20. $Price_{col}$, Eur/m^2	-6.78E-06	-1.74E-05	3.81E-06	0.208774		0.000	0.1